

Globular cluster formation with multiple stellar populations: A comprehensive overview of a star-cloud interaction scenario

Kenji Bekki^{1*} and Madeleine McKenzie^{2†}

¹*ICRAR M468 The University of Western Australia 35 Stirling Hwy, Crawley Western Australia 6009, Australia*

²*Carnegie Science institution, 813 Santa Barbara Street, Pasadena, CA 91101, USA*

Accepted, Received 2005 February 20; in original form

ABSTRACT

We present a new scenario of globular cluster (GC) formation with multiple stellar populations (MPs) in which both the first and second populations (1P and 2P, respectively) of stars form from giant molecular clouds (GMCs) polluted by asymptotic giant branch (AGB) stars within and around the GMCs. Unlike previous GC formation scenarios with AGB stars being the primary polluters, the new scenario alleviates tensions with the mass-budget and dilution-timing problems. The principal results based on idealized analytic models of the formation scenario are as follows. The observed fraction of 1P stars and the helium abundance spreads between the 1P and 2P as a function of GC masses can be well reproduced. The modelled GCs show O–Na, C–N, and Mg–Al anticorrelations and Si–Al, ²⁵Mg/Mg, ²⁶Mg/Mg correlations, which are qualitatively similar to observations. The observed Mg–K anticorrelation can be reproduced, only if super-AGB stars make a significant contribution to chemical enrichment within GMCs. The lack of correlations of Li abundances with [Na/Fe] and [Al/Fe] can be reproduced, only if about 20% of the polluting AGB stars produce Li-rich ejecta, which disfavours scenarios with polluters incapable of Li production. Iron-complex, Type-II GCs with two distinct populations having different chemical abundances of *s*-process elements can be formed through merging of two GCs formed from two GMCs within a host dwarf galaxy at different epochs. The new scenario predicts young massive clusters formed in galaxy environments with surface star formation rate densities well below $1M_{\odot} \text{ yr}^{-1} \text{ kpc}^{-2}$ are unlikely to evolve into GCs with MPs. It also predicts low ¹²C/¹³C ratios of 2P (≈ 5), a [Na/Fe]–[F/Fe] anticorrelation, and P-rich star formation with [P/Fe] > 0.5 and [N/Fe] > 0.5. These predictions are tested against more than 30 observed properties of GCs with MPs, representing one of the most comprehensive observational benchmarks against a specific GC formation scenario to date.

Key words: globular clusters:general – galaxies:star clusters – stars:formation – stars:AGB and post-AGB

1 INTRODUCTION

Globular cluster (GC) formation represents a crucial cross-road between stellar nucleosynthesis, star formation feedback, and galaxy evolution. For instance, mass-loss processes within star-forming gas clouds dictate whether newly born clusters remain tightly bound as GCs or ultimately disintegrate (e.g., Hills 1980; Geyer & Burkert 2001; Baumgardt

& Kroupa 2007). Furthermore, a remarkably high pressure of interstellar medium in galaxies ($P \geq 10^5 \text{ k}_B$) is a necessary condition for GC formation within isolated and merging galaxies (e.g., Elmegreen & Efremov 1997; Bekki et al. 2002; Pfeffer et al. 2024). The observed correlations and anticorrelations between chemical abundances of various elements in GCs, such as C–N anticorrelations (e.g., Norris & Cottrell 1979; Suntzeff 1981; Lardo et al. 2014), O–Na anticorrelations (e.g., Kraft et al. 1993; Gratton et al. 2001; Carretta et al. 2009a,b, C09a, C09b), and Mg–K anticorrelations (e.g., Mucciarelli et al. 2012; Alvarez Garay et al. 2022, 2025) can

* E-mail: kenji.bekki@uwa.edu.au

† NASA Hubble Fellow

be used to provide theoretical constraints on the possible nucleosynthetic sites producing these elements (e.g., Ventura et al. 2012, V12; Iliadis et al. 2016, I16).

One of the most remarkable breakthroughs in GC research over the last 25 years is that almost all of the Galactic GCs harbor more than one stellar population (i.e., multiple stellar populations, “MPs”; Bedin et al. 2004; Piotto et al. 2005; see Gratton, Sneden, & Carretta 2004 and Gratton et al. 2019, G19 for reviews). Spectroscopic studies of GC stars have also revealed anticorrelations between light elements, such as O-Na, C-N, and Mg-Al anticorrelations (e.g., Ramirez & Cohen 2002; C09a; Yong et al. 2009; Nataf et al. 2019; Mészáros et al. 2020; ME20). It is commonly assumed that GC stars with chemical abundances similar to those of the Galactic halo field stars with similar metallicities are “first generation” of “first population” stars (referred to as “1P” from now on) formed earlier whereas Na-rich (O-depleted etc) stars are “second generation” or “second population” stars (2P) formed later. Consequently, numerous observational and theoretical studies have been conducted to reveal the physical properties of 1P and 2P stars of the Galactic GCs (see G19; Bastian & Lardo 2019, BL19 for recent reviews on this issue).

The physical properties of GCs hosting MPs, as revealed by these observations, have provided valuable constraints on the GC formation scenarios. For example, the fraction of 1P stars is observed to be anticorrelated with the present-day and initial GC masses (e.g., C09a; Milone & Marino 2022, MM22), which implies that 2P formation is more efficient in more massive GCs. Clusters exhibiting MPs are broadly divided into two categories (e.g., Marino et al. 2015; Milone et al. 2017), Type I and II, depending on whether they have large [Fe/H] spreads of more than 0.05 dex (Type II) or not (Type I), and Fe-rich stars in Type II GCs also have significantly enhanced abundances of *s*-process elements (“*s*-rich” population). The observed abundance patterns of these *s*-rich populations are thought to be consistent with pollution by low-mass AGB stars (e.g., Shingles et al. 2014; McKenzie et al. 2022, 2024). Because existing theories of cluster formation have yet to fully explain this diverse array of empirical properties, this paper addresses these phenomena in a comprehensive manner.

The most popular scenario for globular cluster (GC) formation with MPs posits that 2P stars form from pristine gas mixed with (diluted by) gaseous ejecta from “polluters” originating from the 1P. Several candidate polluters have been proposed, such as Asymptotic Giant Branch (AGB) stars (e.g., Cottrell & Da Costa 1981; D’Antona & Caloi 2004), massive stars (e.g., Prantzos & Charbonnel 2006), fast-rotating massive stars (e.g., Decressin et al. 2007), supermassive stars (e.g., Denissenkov & Hartwick 2014), very massive stars (e.g., Gieles et al. 2025), and massive interacting binaries (e.g., de Mink et al. 2009; Bastian et al. 2013; Nguyen & Sills 2024).

Among the GC formation frameworks involving these polluters, the “AGB scenario”—where massive AGB stars ($m \geq 4 M_{\odot}$) act as the primary polluters—has been the most extensively investigated using one-zone chemical evolution models or idealized analytical ones (e.g., Fenner et al. 2004; Conroy & Spergel 2010; D’Ercole et al. 2010, D10) and numerical simulations of cluster formation (e.g., D’Ercole et al. 2008, D08; Bekki 2010, 2011, 2019a; Calura et al.

Table 1. Description of physical meanings for symbols often used in the present study. A symbol with “0” in its subscript means the initial value of a physical property. For example, $M_{\text{gc},0}$ is the initial stellar mass of a GC at its birth (M_{gc} is the present-day one). Likewise, $F_{1\text{P},0}$, which is not shown in this table, is the initial 1P fraction. 1P and 2P instead of FG (1G) and SG (2G) are used to represent first and second populations of stars formed within GCs just for convenience in the present study.

Symbol	Physical meaning
M_{gc}	GC mass
$M_{\text{gc},0}$	Initial GC mass
$M_{1\text{P}}$	Total mass of 1P stars
$M_{2\text{P}}$	Total mass of 2P stars
M_{gmc}	Initial GMC mass
M_{g}	Total mass of pristine gas (within a GMC)
M_{agb}	Total mass of AGB stars (around a GMC)
M_{ej}	Total mass of AGB ejecta
M_{o}	Original mass required to form a GC with MPs
M_{ns}	Total mass of new stars around/within a GMC
t_{life}	GMC lifetime
$F_{1\text{P}}$	1P fraction ($= M_{1\text{P}}/M_{\text{gc}}$)
$F_{2\text{P}}$	2P fraction ($= 1 - F_{1\text{P}}$)
F_{dil}	Dilution factor ($= M_{\text{g}}/M_{\text{ej}}$)
F_{b}	Mass budget factor ($= M_{\text{o}}/M_{\text{gc}}$)
R_{s}	Mass ratio of new stars to GMC mass
ρ_{agb}	Mass density of AGB stars
$\rho_{\text{agb,th}}$	Threshold ρ_{agb} for GCs with MPs
Σ_{agb}	Surface mass density of AGB stars
Σ_{SFR}	Star formation rate (SFR) surface density
$\Sigma_{\text{SFR,th}}$	Threshold Σ_{SFR} for GCs with MPs
δY	Helium abundance difference between 1P and 2P
α	IMF slope
ϵ_{sf}	Star formation efficiency
m_{agb}	Total mass of an AGB star
$m_{\text{agb,l}}$	Lower mass cut-off of polluting AGB stars
$m_{\text{agb,u}}$	Higher mass cut-off of polluting AGB stars

2019; McKenzie & Bekki 2021a,b; Lacchin et al. 2022, 2026; Yaghoobi et al. 2022).

The AGB framework, referred to here as the “classic AGB scenario” for convenience, assumes that: (i) original GCs initially consist entirely of 1P stars, and (ii) pristine gas later mixes with the gaseous ejecta of these 1P AGB stars to ultimately form the 2P population (e.g., D08). These previous investigations have provided specific, verifiable predictions regarding differences in binary star fractions (e.g., Vesperini et al. 2011), spatial distributions (e.g., Bekki 2011; Vesperini et al. 2013, 2021; Mastrobuono-Battisti et al. 2021), and global rotation or anisotropy in stellar velocity dispersions (e.g., Bekki 2010; Mastrobuono-Battisti et al. 2016) between the 1P and 2P stars of GCs.

Bekki et al. (2007, B07) demonstrated that if GCs form from the interstellar gas of host dwarf galaxies that has been enriched by the field AGB stars of those hosts, they can naturally display internal star-to-star abundance variations. In their models, both 1P and 2P stars can form during a continuous star-formation event, which bypasses the requirement for the exceptionally massive initial stellar systems invoked by the classic AGB scenario.

Using high-resolution simulations of dwarf galaxies containing GCs, Maxwell et al. (2014) first demonstrated that if GCs are located within the central regions of dwarf galaxies, they can accrete both pristine interstellar gas and gaseous ejecta from field AGB stars. This processed material subse-

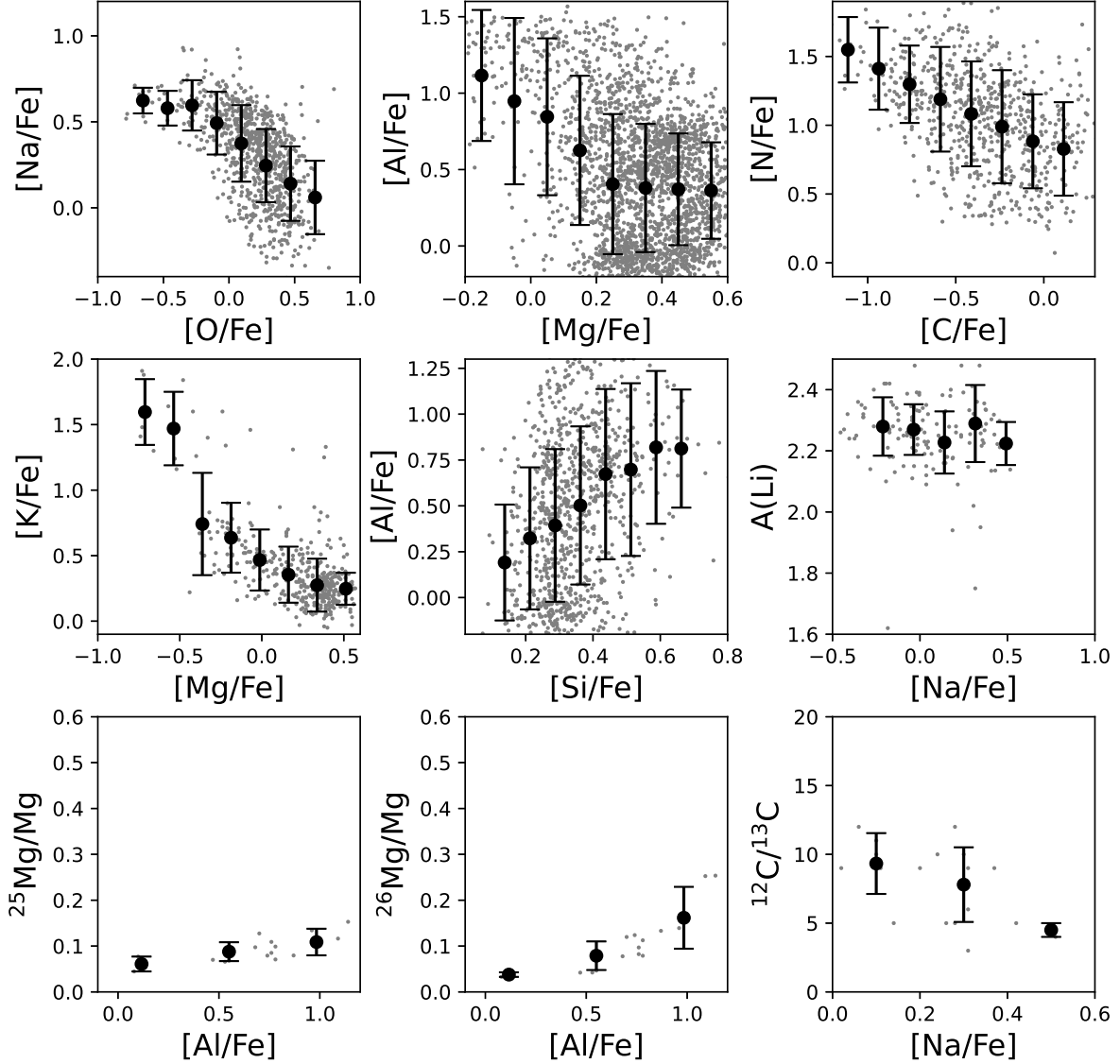


Figure 1. Observed correlations and anticorrelations between various chemical abundances of GC stars that this paper discusses in the context of the SCI scenario. The mean and 1σ dispersion of chemical abundances at different abundance bins are shown by filled circles and error bars, respectively. The details of these observational data sets are given in the main text. *These are suggested to be the nine benchmark tests for any theory of GC formation in this paper.*

quently triggers a secondary episode of star formation from the accreted gas, yielding multiple populations. These two pioneering studies clearly demonstrated that field AGB stars can play a vital role in the formation of GCs with MPs.

Nonetheless, the classic AGB scenario faces two potentially severe challenges. The first is that the primordial stellar systems, consisting initially of only 1P stars, must be at least ≈ 10 times more massive than the present-day GC masses (widely known as the “mass-budget problem”). Us-

ing N -body simulations tracking the long-term dynamical evolution of Galactic GCs, Webb & Leigh (2015) demonstrated that: (i) proto-GCs can typically be a factor of 4.5 more massive than present-day GCs, and (ii) the initial masses of at least three specific GCs were up to 10 times larger than their current masses.

Recent studies exploring the potential initial masses of GCs have also shown that the mass fractions of 1P and 2P stars lost from clusters can be highly diverse (e.g., Leitinger

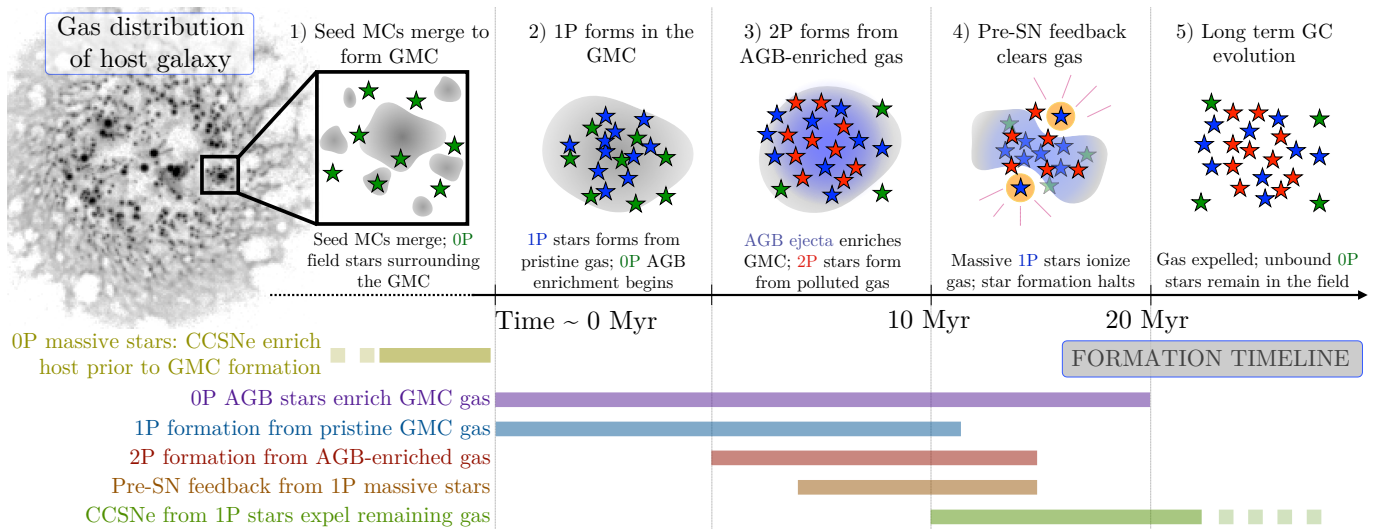


Figure 2. An illustration of the SCI scenario. In this scenario, seed small molecular clouds (MCs) can grow through merging and accretion of other small MCs to become a GMC (Step 1). New stars (“1P”) can form during this growth, and the growing GMC can be also polluted by pre-existing field stars (“0P”) within and around GMCs (2). As star formation accelerates within the GMC, new stars (“2P”) start to form from the polluted (thus enriched) gas (3). Soon after the formation of a cluster of massive stars ($m > 10M_{\odot}$), their strong stellar feedback ionizes the gas and subsequently truncates further star formation and expel all remaining gas from the GMC (4). Finally, a massive star cluster (SC) with MPs forms, which can be later identified as a GC with MPs. Thus, MPs can be formed before stellar feedback effects (winds and core collapse supernovae, CCSNe) of clusters of massive stars completely destroy SC-hosting GMCs: the chemical enrichment timescale of a GMC corresponds to the lifetime (t_{life}). Although this paper focuses exclusively on the chemical enrichment by pre-existing intermediate-mass stars, other stars can possibly enrich GMCs. For example, if ONe novae pollute forming GMCs, then stars formed from pristine gas mixed with nova ejecta can have rather high $[P/Fe]$ (> 1), which can be observed as P-rich stars. Mergers between neutron stars (NSs) around GMCs can introduce large scatters in the chemical abundances of r -process elements within GMCs. The number densities of pre-existing intermediate-mass stars within and around GMCs can determine whether or not SCs can finally have MPs in the scenario. GMCs in the present-day galaxies are unlikely to host SCs with MPs due to very low densities of pre-existing stars around and within them.

et al. 2023). Therefore, the mass-budget problem might not be an insurmountable issue for the classic AGB framework.

The second challenge is the dilution timing problem: the dilution of AGB ejecta by pristine gas must occur at the exact epoch when massive AGB stars are actively shedding their stellar winds into the intracluster environments. This problem has yet to be fully resolved, although recent hydrodynamical simulations of GC formation and evolution demonstrate that GCs can efficiently accrete interstellar gas (McKenzie & Bekki 2021a), and that secondary star formation from AGB ejecta mixed with accreting gas can successfully take place within pre-existing GCs (e.g., Calura et al. 2019).

If star-forming giant molecular clouds (GMCs) encounter nearby field AGB stars or intermediate-age SCs, the dilution of AGB ejecta with pristine gas immediately following wind ejection becomes inevitable. Furthermore, if GMCs assemble through the accretion and merger of small, low-mass molecular clouds (e.g., Kobayashi et al. 2017), and if these small precursor clouds already harbor low- and intermediate-mass stars—akin to populations observed in environments like the Taurus Molecular Cloud (e.g., Cohen & Kuhl 1979)—the resulting GMC will naturally contain AGB stars within and around its volume.

Consequently, new star clusters (SCs) forming inside GMCs polluted by AGB stars will display distinct chemical abundances dictated by the local degree of enrichment. This AGB–GMC interaction naturally resolves the dilution tim-

ing problem inherent to the classic AGB scenario, although the detailed mechanism of star formation from pristine GMC gas mixed with AGB winds warrants further investigation.

Because the AGB stars polluting a GMC originate from older stellar generations formed earlier within the host galaxy, their collective mass can be substantially larger than that of the newborn GC inside the cloud. Since most of these polluting stars are not gravitationally bound to the GMC (or the newborn cluster), they disperse into the field after the GMC is disrupted by stellar feedback. As a result, this framework avoids the mass-budget problem entirely. This GC formation model, based on the physical interaction between GMCs and stellar populations (specifically intermediate-mass AGB stars here), is termed the “star-cloud interaction (SCI) scenario” to clearly distinguish it from the classic AGB framework. Within the framework presented here, we adopt the definition that stellar systems only qualify as GCs if they host MPs arising from the chemical enrichment processes described above. Massive stellar systems that form through similar pathways, but in environments where the number density of AGB stars falls below a threshold value for MP formation, and therefore lack MPs, are designated as star clusters (SCs) rather than GCs.

The primary objective of this study is to present a comprehensive overview of the SCI scenario by exploring the results of idealized analytical models. We focus specifically on: (i) the correlations of present-day GC masses (M_{GC}) with the number fractions of 1P stars (F_{1P}) and internal helium

abundance spreads (δY); (ii) the correlations and anticorrelations among various light-element abundances (e.g., the O–Na and Mg–K anticorrelations); (iii) the varying degrees of lithium depletion across different clusters; (iv) the physical origin of the Type I and Type II GC dichotomy; and (v) the potential minimum metallicity threshold ($[\text{Fe}/\text{H}]_{\text{min}}$) required for the formation of GCs with MPs.

Fig. 1 summarizes the nine observed chemical abundance relations whose physical origins are investigated in detail using this new scenario. Because this work relies on analytical modeling rather than full numerical hydrodynamics, we do not address the observed structural and kinematic differences between 1P and 2P stars, even though such properties are vital for testing cluster formation theories. These crucial structural and kinematic aspects will be addressed in future papers.

The plan of this paper is organized as follows. In §2, we present the overview of the SCI scenario and explain its advantages over the classic model in accounting for various empirical properties of GCs. We describe the analytical framework capable of predicting the properties of GCs across different mass regimes (M_{gc}) in §3. The primary results and their underlying physical mechanisms are presented in §4. The broader physical implications of these findings for observational studies of GCs with MPs in both the local and high-redshift universe are discussed in §5. Finally, we summarize our key conclusions and model predictions in §6.

2 OVERVIEW OF THE NEW SCENARIO

2.1 New scenario

2.1.1 AGB stars within and around GMCs as polluters

Harris & Pudritz (1994) first discussed how GCs are formed from high-density cores of supergiant molecular clouds (“SGMCs”) to explain the observed properties of GCs, such as GC numbers as a function of GC masses. We also consider that GCs can be formed from GMCs in gas-rich dwarf galaxies in the SCI scenario. Massive gas clouds that can form GCs with typically $[\text{Fe}/\text{H}] \approx -1.6$ could not be rich in molecular hydrogen due to the low metallicity and dust abundances of the clouds. Nevertheless, we use the term “GMCs” for GC-forming gas clouds just for convenience in this paper. In the new scenario, star formation is assumed to continue within GMCs during their lifetimes (t_{life}), which can typically be $[1\text{--}3] \times 10^7$ yr (e.g., Kawamura et al. 2009; Kruijssen et al. 2019; Chevance et al. 2020). Clusters of massive stars with masses (m) of more than $10M_{\odot}$ are assumed to quench star formation through their pre-supernova (pre-SN) feedback effect soon after their formation (e.g., Kim et al. 2021). Thus, it is assumed in the scenario that gaseous ejecta from very massive and supermassive stars, fast-rotating massive interacting binaries, and colliding stars cannot be converted into new stars after the pre-SN feedback effect starts to clear GMC gas.

Various stellar sources surrounding GMCs, such as AGB and super AGB stars (sAGB), CO and ONe novae, CCSNe, Type Ia supernovae (SNIa), etc., can possibly interact with GMCs to eventually influence the chemical and dynamical evolution of GMCs through their stellar winds and feedback effects. We here focus exclusively on interac-

tions between AGB stars and GMCs among various star-cloud interactions. AGB and sAGB stars with masses (m_{agb}) ranging from $\approx 4M_{\odot}$ to $\approx 10M_{\odot}$ are assumed to be the major polluters that can enrich the pristine gas of growing GMCs in the new scenario. The lower and upper mass cutoffs of m_{agb} ($m_{\text{agb,l}}$ and $m_{\text{agb,u}}$, respectively) could be different in GMCs with different physical properties. Hydrodynamical interactions of the much less energetic winds from these AGB stars with GMCs can cause efficient mixing with (and dilution of) the pristine gas of the GMCs to form new (2P) stars from the mixed gas.

In present-day luminous star-forming galaxies, ρ_{agb} is too low for AGB-GMC interactions to significantly alter GMC chemical abundances. However, the new scenario assumes that ρ_{agb} can be high enough to alter the original chemical abundances of GMCs in forming compact dwarf galaxies. An outcome of this scenario is that massive star clusters formed in galaxies with lower ρ_{agb} do not form MPs. Fig. 2 illustrates the key ingredients of the new scenario, and Table 1 summarizes the physical meanings of the symbols often used in discussing the scenario. We can make a rough estimation of the ρ_{agb} required for GC formation with MPs ($\rho_{\text{agb,th}}$) as follows. We first assume that (i) 2P stars are formed from AGB ejecta mixed with GMC gas, (ii) the total mass of 2P stars ($M_{2\text{P}}$) is a significant fraction of the total mass (M_{gc}), and (iii) all young massive AGB stars approaching within GMC sizes (R_{gmc}) can pollute GMCs within GMC lifetimes (t_{life}). The present-day fraction of 2P stars ($F_{2\text{P}}$) in a GC is a key parameter in this $\rho_{\text{agb,th}}$:

$$F_{2\text{P}} = \frac{M_{2\text{P}}}{M_{\text{gc}}}. \quad (1)$$

We assume that a GMC can capture stellar winds from AGB stars within a cylindrical volume of $\pi R_{\text{gmc}}^2 v_{\text{gmc}} t_{\text{life}}$, where v_{gmc} is the 3D velocity of the GMC. The total mass of AGB ejecta (M_{ej}) mixed with the pristine gas of a GMC is therefore estimated as follows:

$$M_{\text{ej}} = \pi f_{\text{ej}} R_{\text{gmc}}^2 v_{\text{gmc}} t_{\text{form}} \rho_{\text{agb}}, \quad (2)$$

where f_{ej} is the mass fraction of AGB ejecta in AGB stars. We here consider that a fraction (f_{lost}) of the initial GC mass ($M_{\text{gc,i}}$) can be lost due to internal two-body relaxation effects and external tidal stripping. If AGB ejecta mixed with pristine gas with a total mass of M_{g} is converted into new stars with a star formation efficiency (ϵ_{sf}), then M_{ej} can be related to M_{gc} as follows:

$$F_{2\text{P}} M_{\text{gc}} = \epsilon_{\text{sf}} (1 + F_{\text{dil}}) (1 - f_{\text{lost}}) M_{\text{ej}}, \quad (3)$$

where F_{dil} is the ratio of pristine gas mass to AGB ejecta mass (the “dilution factor”) and is defined as:

$$F_{\text{dil}} = \frac{M_{\text{g}}}{M_{\text{ej}}}. \quad (4)$$

Therefore, $F_{2\text{P}}$ depends on multiple parameters including ρ_{agb} :

$$F_{2\text{P}} = \frac{\pi \epsilon_{\text{sf}} (1 + F_{\text{dil}}) (1 - f_{\text{lost}}) f_{\text{ej}} R_{\text{gmc}}^2 v_{\text{gmc}} t_{\text{life}} \rho_{\text{agb}}}{M_{\text{gc}}}. \quad (5)$$

Thus, it is possible that $F_{2\text{P}} \approx 0$ in GMCs formed within galaxies with very low ρ_{agb} . Using the above equations, the threshold $\rho_{\text{agb,th}}$ can be derived for a given set of these variables (e.g., M_{gc}):

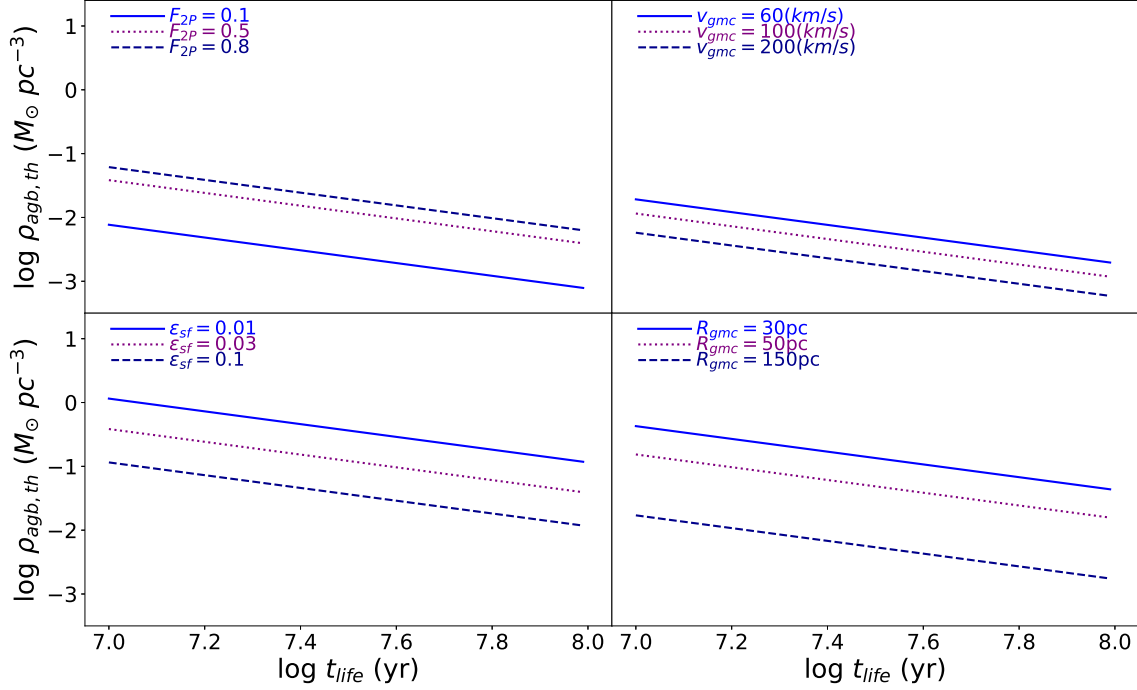


Figure 3. Threshold mass densities of AGB stars ($\rho_{\text{agb,th}}$) above which GCs with MPs can finally form from GMCs in gas-rich galaxies as a function of GMC lifetimes (t_{life}) for different model parameters: dependence on F_{2P} in the upper left panel, on v_{gmc} in the upper right, on ϵ_{sf} in the lower left, and on R_{gmc} in the lower right).

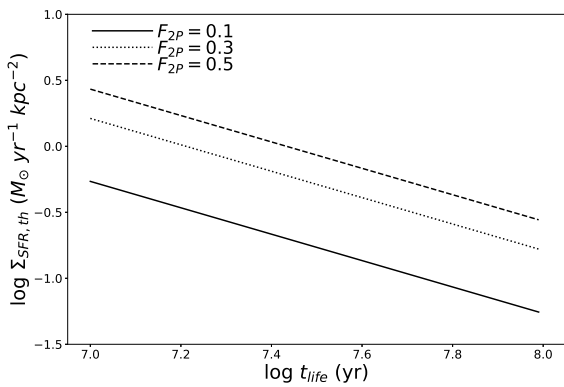


Figure 4. Threshold SFR densities ($\Sigma_{\text{SFR,th}}$) above which GCs with MPs can finally form from GMCs in gas-rich galaxies as a function of t_{life} for $F_{2P}=0.1$ (solid), 0.3 (dotted), and 0.5 (dashed). Clearly, $\Sigma_{\text{SFR,th}}$ should be higher for higher F_2 for a given t_{life} .

$$\rho_{\text{agb,th}} = \frac{F_{2P} M_{\text{gc}}}{\pi \epsilon_{\text{sf}} f_{\text{ej}} R_{\text{gmc}}^2 v_{\text{gmc}} t_{\text{life}} (1 + F_{\text{dil}}) (1 - f_{\text{lost}})}. \quad (6)$$

Thus, $\rho_{\text{agb,th}}$ depends both on GMC properties (e.g., R_{gmc}) and galactic dynamical parameters (e.g., v_{gmc}). For example,

$$\rho_{\text{agb,th}} = 2.0 \times 10^{-2} M_{\odot} \text{pc}^{-3}, \quad (7)$$

for a fiducial set of variables: $M_{\text{gc}} = 2 \times 10^5 M_{\odot}$, $F_{2P} = 0.5$, $\epsilon_{\text{sf}} = 0.3$, $F_{\text{dil}} = 0.5$, $f_{\text{lost}} = 0.5$, $f_{\text{ej}} = 0.9$, $R_{\text{gmc}} = 100$ pc, $v_{\text{gmc}} = 30 \text{ km s}^{-1}$, and $t_{\text{life}} = 2 \times 10^7$ yr. As shown in Fig. 3, $\rho_{\text{agb,th}}$ depends on the parameters of GCs, GMCs, and their host galaxies. It is clear that $\rho_{\text{agb,th}}$ is larger for shorter t_{life} , larger F_{2P} , higher v_{gmc} , lower ϵ_{sf} , and smaller R_{gmc} . Fig. 3 clearly demonstrates that galaxies need to have more than $10^{-3} M_{\odot} \text{pc}^{-3}$ for their SCs to have MPs. If a luminous disk galaxy like our own Milky Way (MW) has a disk radius (R_{d}) of 15 kpc, a disk thickness (z_{d}) of 0.2 kpc, a SFR of $1 M_{\odot} \text{yr}^{-1}$, and an AGB mass fraction (f_{agb}) of 0.085 among all stars, then the mean ρ_{agb} of the galaxy is only $6 \times 10^{-5} M_{\odot} \text{pc}^{-3}$, which is too low for the galaxy's SCs to have MPs. A LMC-type dwarf galaxy with $R_{\text{d}} = 5$ kpc, $z_{\text{d}} = 0.2$ kpc, and SFR = $0.1 M_{\odot} \text{yr}^{-1}$ can have only $8 \times 10^{-5} M_{\odot} \text{pc}^{-3}$. Even if the SFRs of these galaxies are enhanced by a factor of 10, ρ_{agb} would still be less than $10^{-3} M_{\odot} \text{pc}^{-3}$. These low ρ_{agb} values imply that the present-day MW and LMC are highly unlikely to have SCs with MPs. This $\rho_{\text{agb,th}}$ is currently unable to be derived directly from the observed surface brightness and colors of a star-forming galaxy. We accordingly consider that the surface density of a star formation rate (Σ_{SFR}) in a star-forming galaxy can be used to discuss whether its massive young star clusters

(SCs) can possess MPs. If all young stars are formed in the thin disk of a galaxy, then the surface mass density of young AGB stars with masses ranging from $4M_{\odot}$ to $10M_{\odot}$ can be approximated using Σ_{SFR} :

$$\Sigma_{\text{agb}} = f_{\text{agb}} t_{\text{agb}} \Sigma_{\text{SFR}}, \quad (8)$$

where f_{agb} is the mass fraction of the AGB stars and t_{agb} is a timescale within which all stars with $4 \leq m/M_{\odot} \leq 10$ can evolve into AGB phases. Although the SFR of a galaxy could rapidly change on a timescale of an order of 10^8 yr, we here ignore such time variations. Using $\Sigma_{\text{agb}} = z_{\text{d}} \rho_{\text{agb}}$ (where z_{d} is the disk thickness of a galaxy) and the above two equations, the threshold SFR density ($\Sigma_{\text{SFR,th}}$) over which GCs with MPs can be formed in a galaxy can be estimated:

$$\Sigma_{\text{SFR,th}} = \frac{F_{2\text{P}} M_{\text{gc}} z_{\text{d}}}{\pi \epsilon_{\text{sf}} f_{\text{ej}} f_{\text{agb}} R_{\text{gmc}}^2 v_{\text{gmc}} t_{\text{life}} t_{\text{agb}} (1 + F_{\text{dil}}) (1 - f_{\text{lost}})}. \quad (9)$$

This $\Sigma_{\text{SFR,th}}$ in units of $M_{\odot} \text{ kpc}^{-2} \text{ yr}^{-1}$ can be expressed as a function of the physical parameters of GCs as follows:

$$\Sigma_{\text{SFR,th}} = 1.4 \left(\frac{M_{\text{gc}}}{2 \times 10^5 M_{\odot}} \right) \left(\frac{\epsilon_{\text{sf}}}{0.3} \right)^{-1} \left(\frac{1 + F_{\text{dil}}}{1.5} \right)^{-1} \left(\frac{1 - f_{\text{lost}}}{0.5} \right)^{-1} \quad (10)$$

for $F_{2\text{P}} = 0.5$, $f_{\text{agb}} = 0.1$, $R_{\text{gmc}} = 100$ pc, $v_{\text{gmc}} = 30$ km s^{-1} , $t_{\text{life}} = 2 \times 10^7$ yr, $t_{\text{agb}} = 10^8$ yr, and $z_{\text{d}} = 300$ pc. Like $\rho_{\text{agb,th}}$, this $\Sigma_{\text{SFR,th}}$ depends on multiple model parameters in a complicated way, the details of which we do not discuss in this paper. One example of these parameter dependencies is shown in Fig. 4, describing a higher $\Sigma_{\text{SFR,th}}$ for a larger $F_{2\text{P}}$. Since f_{agb} depends strongly on the power-law slope and the upper and lower mass cutoffs of the stellar initial mass function (IMF) in dwarf galaxies, $\Sigma_{\text{SFR,th}}$ also depends on the IMF (e.g., lower $\Sigma_{\text{SFR,th}}$ for a more top-heavy IMF). It would be safe to claim that $\Sigma_{\text{SFR,th}}$ should be as high as $\approx 1 M_{\odot} \text{ kpc}^{-2} \text{ yr}^{-1}$ in GC formation with $F_{2\text{P}} \approx 0.5$ from GMCs with typical t_{life} . $\Sigma_{\text{SFR,th}}$ can be used to assess whether young massive SCs in galaxies can have MPs or not, as discussed later in §5.

2.1.2 Physical properties of GC-hosting GMCs

Recent theoretical studies of GMC formation and evolution have demonstrated that (i) massive GMCs ($\geq 10^6 M_{\odot}$) can form through continuous gas accretion and the merging of other GMCs, (ii) the formation timescales can be longer than 10^7 yr, and (iii) collisions or merging of massive GMCs can trigger massive star formation and enhance star formation efficiencies (e.g., Kobayashi et al. 2017). The longer t_{life} ($> 10^7$ yr) is a crucial condition required for the chemical enrichment of GMCs by AGB stars in the SCI scenario. The bursty star formation during GMC formation triggered by GMC collisions can correspond to 2P formation in the scenario and also explain the high SFEs required for bound cluster formation (e.g., Baumgardt & Kroupa 2007).

Low-mass GMCs in the Galaxy, such as the Taurus Molecular Cloud, are observed to form preferentially low- and intermediate-mass stars (e.g., Cohen & Kuhi 1979). Accordingly, the accretion and merging of such low-mass GMCs dominated by low- and intermediate-mass stars can be a key physical process for massive GMCs hosting GCs. If a large number of pre-existing intermediate-mass stars from low-mass GMCs can eventually become centrally concentrated

within a GC-forming GMC, then they can pollute the central region of the GMC to a much larger extent after they enter into AGB phases. The observed extreme 2P population with a rather large [Na/Fe] in GCs could be due to chemical enrichment by clusters of pre-existing AGB stars in the central regions of GC-forming GMCs.

Grasha et al. (2019) investigated the distances (R) of SCs of various ages (T_{age}) from GMCs in M51. From this, they derived the T_{age} distributions of SCs within three spatial zones: $R \leq R_{\text{gmc}}$, $R_{\text{gmc}} < R \leq 2R_{\text{gmc}}$, and $2R_{\text{gmc}} < R \leq 3R_{\text{gmc}}$ (see their Fig. 8). Although they found a high fraction (≈ 0.4) of young SCs ($T_{\text{age}} \approx 10^6$ yr) within $R \leq R_{\text{gmc}}$, there is a noticeable trend of increasing SC numbers with age for $T_{\text{age}} > 10^7$ yr across all three investigated areas around the GMCs. The peak around $T_{\text{age}} = 2 \times 10^8$ yr is particularly intriguing, suggesting that GMCs could potentially be influenced by stellar winds originating from these intermediate-age SCs. However, the seemingly low spatial densities of SCs around GMCs in M51 (e.g., 129 SCs around 112 GMCs for $R \leq R_{\text{gmc}}$) indicate that these GMCs cannot be significantly enriched chemically by nearby intermediate-age SCs; consequently, new SCs MPs cannot form from them. Conversely, these observations also imply that intermediate-age stars within SCs could enrich nearby GMCs to a greater extent in environments where the densities of such stars are substantially higher, providing supportive observational evidence for the SCI scenario.

2.1.3 Type II GC formation via GC merging

Carretta et al. (2010) proposed that NGC 1851 was formed from the merging of two SCs to have two different populations with a [Fe/H] spread of 0.08 dex. Lee (2015) also proposed that the observed chemical abundance patterns of M22 can be nicely explained by the merging of two GCs within their host dwarf galaxy. Using one-zone chemical evolution models of dwarf galaxies, Bekki & Tsujimoto (2016, BT16) demonstrated that two GCs formed from two distinct GMCs at different epochs within their host dwarf galaxy can have different [Fe/H] and s -process element abundances. These two merge together later within their host dwarf galaxy to form a new GC with two distinct [Fe/H] and s -process element abundances (e.g., [Ba/Fe]) due to the lower velocity dispersion of stars in the host dwarf; the new GC can be classified as a Type II GC (BT16). This merger scenario can nicely explain not only the two distinct s -poor and s -rich populations observed in some Type II GCs (e.g., M22; Marino et al. 2015) but also the mass-budget problem in s -rich populations, as discussed later in §5.

The mass ratio (m_2) of the two merging GCs can possibly determine the mass fractions of Fe-rich and s -rich populations in these GCs. It would be possible that the two merging GCs can merge with other very small SCs ($m_2 \ll 0.1$) before or after their merging; however, the chemical fingerprint of such minor merger events might be hard to find observationally. Our recent numerical simulations of GC formation in gas-rich galaxy mergers have shown that massive nuclear SCs can be formed through multiple merging between a number of SCs with different ages and [Fe/H] (Matsui et al. 2025). If these nuclear SCs are stripped from their host galaxies to become complex GC-like objects like ω Centauri, then they should show wide [Fe/H] spreads. Thus, in this GC

merger scenario, pair merging can create Type II GCs with two distinct *s*-poor and *s*-rich populations, whereas multiple merging can lead to the formation of nuclear SCs that finally become massive GCs with wide age and [Fe/H] spreads like M54 and ω Centauri. Lower mass AGBs (1-3 M_{\odot}), which are not viewed as the dominant driver of MP formation, can be responsible for establishing the *s*-process differences in Type II GCs, thus it is expected that there is some [Fe/H] enhancement due to galactic chemical evolution between the formation of *s*-poor and *s*-rich populations.

2.2 Solutions for the potential problems of the classic AGB scenarios

2.2.1 The mass budget problem

If 2P stars in a GC are formed from gas ejected from polluters that evolved from 1P stars of the original GC, then the total mass (M_o) of the original GC can be inferred from the present-day GC mass (M_{gc}), the chemical abundances of 2P stars, and the chemical yields of the polluters (e.g., Bekki & Norris 2006). We here define the mass budget factor as follows:

$$F_b = \frac{M_o}{M_{gc}}. \quad (11)$$

This F_b needs to be rather large (> 10) to explain the observed fractions of 2P stars in GCs for a canonical IMF (the so-called mass budget problem). In the classic AGB scenario, the progenitor systems are assumed to be GC-like objects that are considerably more massive than present day GCs, which exacerbates rather than alleviates the problem. In the SCI scenario, massive progenitors are not required as any AGB stars passing through or near a growing GMC can enrich the pristine gas. The total mass of polluting AGB stars, which depends on the broader field star population of the host galaxy, can naturally exceed M_{gc} without invoking an unrealistically large stellar mass. The mass-budget problem is therefore not a fundamental concern within our new framework.

2.2.2 Timing of dilution by pristine gas

The classic AGB scenario needs to assume that the right amount of pristine gas is accreted onto existing GCs through some physical mechanisms (e.g., Bondi-type gas accretion) just when intermediate-mass stars enter into AGB phases (e.g., D10). It also needs to fine-tune the time evolution of gas accretion rates in order to dilute AGB ejecta to the right degree and thereby reproduce well the observed anticorrelations between light elements (e.g., D10). While the ejection of pristine gas from intermediate mass close binaries and subsequent mixing with AGB ejecta has been proposed as a workaround within the classic AGB framework (e.g., Vanbeveren 2012; Bekki 2023), a comprehensive solution is yet to emerge. In the SCI scenario, however, this issue does not pose any challenges as stellar winds from AGB stars directly mix with the pristine gas of the surrounding GMC immediately following ejection, making the precise timing of gas accretion onto an existing cluster less crucial.

2.2.3 Feedback effects from delayed CCSNe and type Ia SNe

The classic AGB scenario does not have the “supernova avoidance problem”, which would be one of the serious problems in other scenarios (e.g., Renzini et al. 2015), because chemical pollution of pristine gas by AGB stars can proceed after CCSNe have exploded. However, delayed CCSNe (e.g., Zapartas et al. 2017) and prompt Type Ia SNe could possibly expel pristine gas and AGB ejecta within GC-forming gas clouds due to their explosive energy in the scenario. Although the dynamical influences of Type Ia SNe on the intra-cluster gas of GCs have been investigated using hydrodynamical simulations of forming GCs (e.g., Lacchin et al. 2026), previous theoretical studies have not investigated whether intra-cluster gas can be completely expelled by the feedback effects of delayed CCSNe. Since delayed CCSNe explosions can start to occur ~ 40 Myr after the initial bursty formation of stars in GC formation (e.g., Zapartas et al. 2007), they can synchronize the gas ejection from massive AGB stars. Therefore, it would be likely that delayed CCSNe expel all AGB ejecta and intracluster gas from GCs to completely truncate secondary star formation, representing a serious challenge for the classic AGB scenario that has yet to be fully addressed.

If AGB ejecta can be retained even after mixing with ejecta from delayed CCSNe, new 2P stars formed from AGB ejecta might have significantly larger [Fe/H] than 1P stars. No such [Fe/H] enhancement is observed in Type I GCs. Therefore, it is a pressing issue for the classic AGB scenario to investigate how delayed CCSNe influence the formation processes and the chemical abundances of 2P stars. This possibly serious problem in the classic AGB scenario can be avoided in the new scenario, because the chemical enrichment of GMCs by AGB stars is completed well before the onset of CCSN and delayed CCSN explosions. Gaseous ejecta from these SNe can enrich the ISM of GC-hosting dwarf galaxies, if the gas can be trapped by the gravitational potentials of the galaxies. Gaseous ejecta from low-mass AGB stars ($m \leq 3M_{\odot}$) formed within GCs would be immune to these feedback effects of delayed CCSNe; however, they are highly likely to be influenced by the feedback effects of numerous SNIa. It is thus possible that AGB ejecta after GC formation can all be expelled from GCs in the SCI scenario.

2.2.4 Star formation suppression by existing stars

Many previous simulations based on the classic AGB scenario assumed that secondary star formation from AGB ejecta retained in young SCs is possible from high-density gas (e.g., Bekki 2010). However, these simulations did not investigate how existing stars in young massive SCs (i.e., GC progenitors) influence the collapsing protostellar cores due to limitations in the spatial resolution of the simulations. Bobrick et al. (2025) have recently shown that secondary star formation directly from retained AGB ejecta can be severely suppressed (or even not possible) due to multiple disruptive encounters of protostellar cores with existing stars in young massive SCs. Bekki (2019b) also demonstrated that the interaction of small clouds with existing stars and the deep gravitational potential of SCs combine to severely suppress

the formation of more massive stars ($m > 10M_{\odot}$). So it is currently not so clear whether secondary star formation from retained AGB ejecta is really possible in dense stellar systems. The SCI scenario does not have such a potential problem in secondary star formation, because all stellar populations form during the assembly and evolution of the parent GMC, prior to its dispersal by stellar feedback, rendering secondary star formation within an already-formed cluster unnecessary.

3 ANALYTIC MODELS

3.1 A model for mass-dependent GC properties

Fig. 2 briefly summarizes several key points of the analytic model for the new scenario. In the new GC formation scenario, a present-day GC consists of (i) stellar populations formed from pristine gas (“1P”), (ii) those formed from the gas of a GC-forming GMC chemically polluted by surrounding AGB stars (“2P”), and (iii) stars that pre-dated before 1P and 2P formation. Our recent simulations of GC formation from GMCs have already shown that GMCs can have a “precursor population” (or “0P”) of stars that were gravitationally trapped by GMCs (McKenzie & Bekki 2021b). These 0P stars of a GC have chemical abundance patterns of the field stars of their host galaxy, so their abundances can be quite distinct from those of the 1P and 2P stars of the GC. For example, their metallicities can be slightly lower than those of the 1P and 2P stars of the GC due to their earlier formation epochs.

If these stars can continue to be gravitationally trapped by GCs until the present, they are highly likely to be observed in the outer parts of GCs (i.e., stellar halos). It is thus an important observational question whether such 0P stars with a peculiar chemical abundance pattern can be found in the outer parts of GCs. Although pre-existing AGB stars chemically pollute a GC-forming GMC, the present-day GC might have lost most of these stars due to long-term stripping processes. Our previous numerical simulations of GC formation showed that only a small fraction of field stars in dwarf galaxies can be gravitationally trapped by GCs (Bekki & Yong 2012; BY12). Accordingly, the total GC mass is as follows:

$$M_{\text{gc}} = M_{1\text{P}} + M_{2\text{P}} + M_{\text{s}}, \quad (12)$$

where M_{s} is the total mass of the pre-existing stars gravitationally trapped by GMCs and could be much smaller than $M_{1\text{P}}$ and $M_{2\text{P}}$. The present-day 1P fraction is therefore defined as follows:

$$F_{1\text{P}} = \frac{M_{1\text{P}}}{M_{\text{gc}}}. \quad (13)$$

The pre-existing stars could have chemical abundances similar to those of GMCs because they are formed only slightly before GMC formation. If we distinguish between these stars based on their chemical abundances, and not on their formation epochs, 1P and the pre-existing stars have similar chemical abundances so that they can be observationally identified as ‘1P’. The total mass of observationally identified 1P stars is therefore the sum of $M_{1\text{P}}$ and M_{s} . We suggest that pre-existing stars could be observed as loosely bound stellar halos around GCs. The initial GC masses ($M_{\text{gc},i}$) should

be significantly larger than M_{gc} , firstly because M_{gc} is the total mass of low-mass stars ($m \leq 0.8M_{\odot}$), and secondly because GCs can lose their stars through internal dynamical evolution and tidal stripping.

$$M_{\text{gc}} = (1 - f_{\text{lost}})M_{\text{gc},0}, \quad (14)$$

where f_{lost} is the fraction of initial stars that are lost from a GC. This f_{lost} depends on f_{low} and f_{strip} , where f_{low} is the fraction of low-mass stars with $0.1 \leq m/M_{\odot} \leq 0.8M_{\odot}$ and f_{strip} is the fraction of stripped stars. Although these f_{low} and f_{strip} could be different in different GCs, we use a fixed $f_{\text{lost}} = 0.5$ for all stellar populations. The original gas mass (M_{o}) required for the formation of a GC is calculated for a given star formation efficiency (ϵ_{sf}):

$$M_{\text{o}} = \frac{M_{\text{gc},0}}{\epsilon_{\text{sf}}} \quad (15)$$

If all stars in GCs are formed from the gas of GMCs, then M_{o} can be the total mass of the GMC (M_{gmc}). If $M_{\text{gc}} = 2 \times 10^5 M_{\odot}$, $f_{\text{lost}} = 0.75$, and $\epsilon_{\text{sf}} = 0.1$ are adopted, then $M_{\text{gmc}} = 8 \times 10^6 M_{\odot}$ is expected; this would be a conservative value due to the adopted high ϵ_{sf} .

Since 2P stars are formed from AGB ejecta “diluted” by (i.e., mixed with) pristine GMC gas, the fraction of 2P stars ($F_{2\text{P}}$) is determined by the dilution factor ($F_{\text{dil}} = \frac{M_{\text{g}}}{M_{\text{ej}}}$). We here adopt the following linear relation between F_{dil} and the initial fraction of 2P stars ($F_{2\text{P},i}$):

$$F_{2\text{P},0} = a_{\text{dil}}F_{\text{dil}} + b_{\text{dil}}, \quad (16)$$

where $a_{\text{dil}} = -0.1$ and $b_{\text{dil}} = 1.0$. Appendix B describes how the above relation is derived for $0 \leq F_{\text{dil}} \leq 10$. The initial 1P fraction ($F_{1\text{P},i}$) can be simply derived from $F_{2\text{P}}$ ($F_{1\text{P},0} = 1 - F_{2\text{P},0}$). It should be noted here that this $F_{1\text{P},0}$ can be different from $F_{1\text{P}}$ due to the long-term dynamical evolution of GCs. Since it is assumed that pre-existing stars can chemically pollute GMCs, M_{ej} is estimated as follows:

$$M_{\text{ej}} = f_{\text{agb}}f_{\text{ej}}M_{\text{s},0}, \quad (17)$$

where f_{agb} is the mass fraction of intermediate-mass stars among all new stars, f_{ej} is the mass fraction of AGB ejecta in AGB stars, and $M_{\text{s},0}$ is the total mass of new stars that can interact with a GMC during the GMC’s lifetime. In order to estimate f_{agb} , we adopt the following power-law function for the IMF of stars:

$$\Psi(m) = C_{\text{imf}}m^{-\alpha}, \quad (18)$$

where m is the initial mass of a star and α is the power-law slope. The IMF with $\alpha = 2.35$ corresponds to the canonical Salpeter IMF (Salpeter 1955). The normalization factor C_{imf} is determined by α , m_{l} (lower mass cutoff), and m_{u} (upper mass cutoff). We assume that m_{l} and m_{u} are fixed at $0.1M_{\odot}$ and $50M_{\odot}$, respectively, for all models. The lower and upper mass cutoffs for AGB (sAGB) stars that can chemically enrich GMCs are referred to as $m_{\text{agb},\text{l}}$ and $m_{\text{agb},\text{u}}$, respectively. We adopt $m_{\text{agb},\text{l}} = 4M_{\odot}$ and $m_{\text{agb},\text{u}} = 10M_{\odot}$, unless specified. We adopt $f_{\text{ej}} = 0.9$ as a fiducial value, though these depend on stellar masses and the IMF slope (e.g., Weidemann 2000). We also adopt $f_{\text{agb}} = 0.12$, which is reasonable for the standard Salpeter IMF with $\alpha = 2.35$. Only a very small fraction of existing stars polluting a GMC can be trapped by the GMC and subsequently by its new SC (BY12):

$$M_s = f_{\text{trap}} M_{s,0}, \quad (19)$$

where we adopt $f_{\text{trap}} = 0.01$ as a fiducial value. The ratio of $M_{s,0}$ to M_{gmc} is a crucial parameter that determines the chemical enrichment processes within GMCs in the new scenario:

$$M_{s,0} = R_s M_{\text{gmc}}. \quad (20)$$

Physically, R_s represents the mass fraction of new stars (including intermediate-mass stars) residing within and around a GMC relative to the total GMC mass, integrated over the GMC lifetime. A larger R_s therefore implies a higher local density of AGB stars available to pollute the GMC gas, and consequently a more chemically enriched 2P population. In order to understand how R_s depends on M_{gmc} , we have performed new hydrodynamical simulations of disk galaxies with a revised model of molecular gas formation on dust grains; the details of the simulation and the model for GMC formation are briefly described in Appendix A.

In particular, we have investigated the total mass of newly formed stars (M_{ns}) with ages ranging from 0.02 Gyr to 0.1 Gyr around each GMC in simulated galaxies at different time steps, and found that M_{ns} depends strongly on M_{gmc} in a simulated compact dwarf disk galaxy with many star-forming GMCs (see Appendix A for the results). Based on these results, we adopt the following relation between R_s and M_{gmc} :

$$R_s = a_s \log\left(\frac{M_{\text{gmc}}}{10^7 M_\odot}\right) + b_s, \quad (21)$$

where a_s and b_s are set to be 0.15 and 0.01, respectively. This $R_s - M_{\text{gmc}}$ relation can depend on galactic properties such as their sizes and masses, as demonstrated by our galaxy-scale simulations. We adopt a reasonable and realistic assumption that only a fraction of GMC gas is mixed with AGB ejecta to form new stars:

$$M_g = f_g M_{\text{gmc}}, \quad (22)$$

where f_g is a parameter that controls M_g and thus F_{dil} for a given M_{ej} . Since pristine gas polluted by AGB stars is converted into new 2P stars, the initial total mass of 2P stars ($M_{2P,0}$) is estimated as follows:

$$M_{2P,0} = F_{2P,0} M_{\text{gmc}} (R_s f_{\text{agb}} f_{\text{ej}} + f_g). \quad (23)$$

Significant fractions of these initial 2P stars can be lost due to long-term dynamical processes and stellar mass loss; we estimate the present-day total mass of 2P stars as follows:

$$M_{2P} = (1 - f_{\text{lost}}) M_{2P,0}, \quad (24)$$

where $f_{\text{lost}} = 0.75$ is adopted, though f_{lost} could be different between initial 1P and 2P stars. In the present scenario, 1P stars can be formed before and after chemical enrichment by AGB stars. Therefore, the initial total mass of 1P stars ($M_{1P,0}$) is a function of multiple model parameters:

$$M_{1P,0} = f_{\text{sf}} M_{\text{gmc}} + M_{\text{gmc}} (1 - F_{2P,0}) (R_s f_{\text{agb}} f_{\text{ej}} + f_g), \quad (25)$$

where f_{sf} is the fraction of new stars steadily formed before chemical pollution by AGB stars. It should be stressed here that a fraction of stars formed from pristine gas polluted by AGB stars can be classified as 1P due to their chemical abundances (e.g., lower [Na/Fe]). We show the results of the model with $f_{\text{sf}} = 0.02$ only, because the present results do

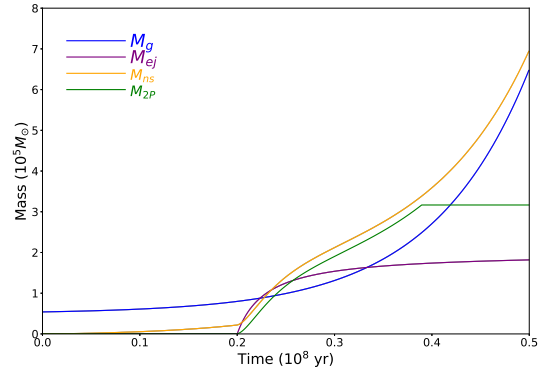


Figure 5. Time evolution of the total masses of pristine GMC gas (M_g , blue), AGB ejecta (M_{ej} , purple), all new stars (M_{ns} , orange), and 2P stars (M_{2P} , green) in the fiducial model.

not depend on f_{sf} . We can estimate M_{1P} from $M_{1P,0}$ as done for M_{2P} :

$$M_{1P} = (1 - f_{\text{lost}}) M_{1P,0}, \quad (26)$$

where f_{lost} is fixed at 0.75.

Our future simulations need to be run to find a reasonable range of f_{lost} for 1P and 2P stars, because f_{lost} could be significantly different due to possibly different initial distributions of these stars, as shown in previous and recent numerical simulations of GCs with MPs based on the classic AGB scenario (e.g., Vesperini et al. 2011). Having established the relative mass fractions between 1P and 2P stars, we now estimate the helium abundance of the 2P, which is a key observational diagnostic of the chemical enrichment by AGB stars. We estimate the helium abundances of 2P stars (Y_{2P}) as follows:

$$Y_{2P} = \frac{Y_{\text{gmc}} M_p + Y_{\text{agb}} M_{\text{ej}}}{M_p + M_{\text{ej}}}, \quad (27)$$

where Y_{gmc} and Y_{agb} are the helium abundances of GMC gas and AGB stars, respectively. We adopt the following definition of the helium abundance spread between 1P and 2P stars, where Y_{1P} is assumed to be equal to Y_{gmc} :

$$\delta Y = Y_{2P} - Y_{1P}, \quad (28)$$

We adopt $Y_{1P} = Y_{\text{gmc}} = 0.25$ and $Y_{\text{agb}} = 0.34$ (e.g., Ventura et al. 2013, V13) as fiducial values in order to estimate ΔY for GCs with different M_{gc} . We investigate 300 GCs for $5 \times 10^5 M_\odot \leq M_{\text{gmc}} \leq 5 \times 10^7 M_\odot$ (initial GMC mass) and $0.02 \leq f_g \leq 0.05$. Also, we consider that the $1 - \sigma$ dispersion of R_s for a given M_{gmc} is 0.2 to simulate the possible diverse 1P fractions among GCs with different M_{gmc} . We use a random number generator to determine M_{gmc} , f_g , and R_s for each GC.

3.2 One-zone models for chemical enrichment in growing GMCs

We investigate the time evolution of chemical abundances of new stars and gas within GMCs in order to discuss the

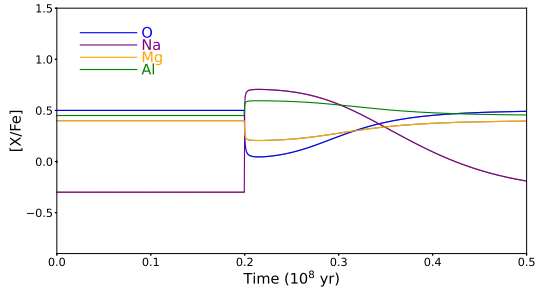


Figure 6. Time evolution of [O/Fe] (blue), [Na/Fe] (purple), [Mg/Fe] (orange), [Al/Fe] (green) for gas in the fiducial model.

observed abundance spread in various elements. We use the “one-zone” model in which gas and metals from AGB stars can be instantaneously mixed and converted into new stars. The mass and time units in the model is $10^6 M_{\odot}$ and 10^8 yr, respectively, and all model parameters are given in these units. The total masses of pristine GMC gas (M_g) and AGB ejecta (M_{ej}) are assumed to be time-dependent, and a GMC is assumed to grow exponentially within its lifetime (t_{life}):

$$M_g(t) = M_{g,0} + c_{g,1} \exp(c_{g,2}(t - t_{grow})/t_{grow}), \quad (29)$$

where $M_{g,0}$ is the initial mass for the GMC (“seed mass”), t_{grow} corresponds to the growth timescale, and $c_{g,1}$ and $c_{g,2}$ are parameters that control the details of the mass evolution. The ratio of the final mass of pristine gas (M_g) at $t = t_{life}$ to the total mass of AGB ejecta (M_{ej}) corresponds to F_{dil} , and is a key parameter that determines the abundance patterns of 2P stars. The value of $c_{g,1}$ is chosen such that $M_g(t)$ at $t = t_{life}$ can be M_g . We mainly show the results of the fiducial model with $M_g = 6 \times 10^5 M_{\odot}$ ($M_{gmc} = 6 \times 10^6 M_{\odot}$ for $f_g = 0.1$), $M_{ej} = 2 \times 10^5 M_{\odot}$, $t_{grow} = 10^7$ yr, $t_{life} = 5 \times 10^7$ yr, and $c_{g,2} = 1.0$ (in model unit).

The total mass of accumulated AGB ejecta can be time-dependent too, given that AGB stars with different initial masses eject gas at different times. We accordingly adopt the following simple analytic model to describe the time evolution:

$$M_{ej}(t) = c_{ej,1} \frac{(1 - c_{ej,2} t_{agb,min})}{(t - t_{agb,min} + c_{ej,2} t_{agb,max})}, \quad (30)$$

where $t_{agb,min}$ and $t_{agb,max}$ are the times at which AGB stars with $m = 10 M_{\odot}$ and $4 M_{\odot}$ start to eject gas, respectively, and $c_{ej,1}$ and $c_{ej,2}$ control the details of the mass evolution. The value of $c_{ej,1}$ is chosen such that $M_{ej}(t)$ at $t = t_{life}$ can be M_{ej} . We consider $t_{agb,min} = 2 \times 10^7$ yr and $t_{agb,max} = 3 \times 10^8$ yr in the present study. We adopt the above formula in order to mimic the time evolution of M_{ej} estimated in our previous calculations for the standard IMF (Bekki 2011). $c_{ej,2}$ is fixed at 0.01 (in model unit) in the fiducial model.

The star formation rate (SFR, $\phi(t)$) is assumed to be proportional to the total gas mass within a GMC:

$$\phi(t) = c_{sf}(M_g(t) + M_{ej}(t)), \quad (31)$$

where c_{sf} is the coefficient that controls the rapidity of star formation. We mainly show the results of the models with

$F_{dil} = 3$ in the present study, though the results depend on this parameter. Fig. 5 describes the time evolution of M_g , M_{ej} , M_{1P} , and M_{2P} in the fiducial model. The details of these mass evolution depend on the adopted model parameters in the present one-zone models.

The mass evolution of i -th element ($i=H, He, C$, etc) in a GMC is described by the following equation:

$$\frac{dM_i}{dt} = \frac{dA_{i,g}M_g}{dt} + \frac{d(A_{i,ej}M_{ej})}{dt}, \quad (32)$$

where $A_{i,g}$ and $A_{i,ej}$ are the mass fractions of i -th element in pristine gas and AGB ejecta, respectively. Since we use an idealized model for the mass evolution of AGB ejecta, we adopt an assumption that $A_{i,g}$ and $A_{i,ej}$ are fixed (i.e., time-independent). This assumption would be over-simplified, because AGB stars with different stellar masses have different chemical yields and pollute GC-forming GMCs at different times. Nevertheless, we adopt the above assumption, which enables us to more clearly elucidate the roles of AGB stars in the SCI scenario. We will discuss the relative contributions of AGB stars with different masses using a more fully self-consistent chemical evolution models in our future papers. Fig. 6 describes the time evolution of O, Na, Mg, and Al abundances of stars in the fiducial model over 5×10^7 yr, i.e., the lifetime of the GMC.

We adopt the chemical yields used by D10, V13, and Dell’Agli et al. (2018, D18) for AGB stars and by I16 and V12 for sAGB stars. It should be stressed here that AGB yields for elements investigated in this paper are different from those predicted from other groups including Karakas (2010, K10), Cristallo et al. (2011), and Straniero et al. (2014). Therefore, if we adopt AGB yields from other groups, then the results can be significantly changed. The yields from D18 are adopted in discussing how the observed anticorrelations between light elements depend on metallicities. The nucleosynthesis model in I16 is fine-tuned to reproduce the observed chemical abundance patterns of the low-metallicity GC NGC 2419 with $[Fe/H] \approx -2.1$. Understanding the metallicity dependence of sAGB yields, particularly for Mg and K, represents an important avenue for future stellar evolution calculations. Since K yields of sAGB stars with different masses and metallicities are not given in Doherty et al. (2015), we use only sAGB yields by I16 and V12. D’Antona et al. (2012, D12) proposed that Li production in massive AGB stars due to Cameron-Fowler effects is crucial in reproducing the Li abundances of GC stars. We here introduce a parameter (P_{Li}) for the fraction of massive AGB stars producing Li among all polluting AGB stars in order to discuss the correlations between Li abundances ($A(Li)$) and light element abundances (e.g., $[Na/Fe]$). We adopt $^{12}C/^{13}C$ ratios and F yields from K10 in order to briefly discuss the observed C-isotope ratios and $[Na/Fe]$ - $[F/Fe]$ anticorrelations in GCs.

We adopt the following initial elemental abundances for pristine gas: $[Fe/H] = -1.6$, $Y = 0.24$, $[O/Fe] = 0.5$, $[Mg/Fe] = 0.4$, $[Na/Fe] = -0.3$, $[Al/Fe] = 0$, $[K/Fe] = 0$, $^{25}Mg/Mg = 0.05$, $^{26}Mg/Mg = 0.02$, and $A(Li) = 2.3$. Using the standard Salpeter IMF with the slope of $\alpha = -2.35$, we estimate the IMF-averaged yields for O, Mg, Na, and Al abundances of AGB winds. For comparison, we also investigate the models with different α to understand how the IMF influences the chemical abundances of GCs. We

consider that the Mg isotope ratios of AGB ejecta, which are represented by $R(^{25}\text{Mg}/\text{Mg})$ and $R(^{26}\text{Mg}/\text{Mg})$, are free parameters, because the models with $R(^{25}\text{Mg}/\text{Mg}) \approx 0.2$ and $R(^{26}\text{Mg}/\text{Mg}) \approx 0.6$ predicted from Ventura et al. (2018) for $m = 5M_{\odot}$ AGB stars fail to reproduce the observed correlations between heavy Mg isotopes and $[\text{Al}/\text{Fe}]$. We thus consider that the observed relations between Mg isotope abundances can provide direct astrophysical constraints on the nuclear reaction rates governing the Mg-Al cycle in AGB and sAGB stars.

3.3 Observations to be compared with models

For this work, we adopt a set of elemental and isotopic abundance constraints to test the predictions of our GC formation model. The primary spectroscopic constraints are drawn from large, homogeneous abundance studies, including the optical GIRAFFE and UVES analysis of C09a and C09b, and the APOGEE-based analysis of ME20. Together, these studies provide broad coverage of the light-element abundance patterns that define MPs in GCs. C09a and C09b provide a large and homogeneous reference sample using optical wavelengths, with strong constraints on Na and O abundances. Additionally, ME20 derive Mg, Al, and Si abundances using infrared APOGEE spectra and a specialised abundance pipeline suitable for RGB GC stars.

We also include selected follow-up studies to constrain additional abundance patterns, including Li and K, which can be derived using optical wavelengths, and P and F abundances, which are primarily measured in the infrared. Isotopic abundances are more observationally challenging, often requiring very high signal-to-noise and high-resolution spectra. In this work, we compare to both carbon isotopic ratios from stars on the main sequence and Mg isotopic ratios from cool RGB stars. Although N enhancements are one of the most notable features of GC 2P populations, C and N abundances are often derived from molecular bands, making them more susceptible to degeneracies in the abundance determination. These elements and isotopes provide critical diagnostic constraints on the temperatures and nucleosynthetic pathways used by the cluster polluter. In addition to spectroscopy, we use photometric constraints on multiple stellar populations, primarily from Hubble Space Telescope-based studies. These include photometric estimates of the first-population fraction and He abundance spreads from Milone et al. (2017, 2018, M18).

We emphasise that the adopted literature constraints are not expected to lie on a single absolute abundance scale. Differences in wavelength coverage, line selection, spectral resolution, signal-to-noise, stellar parameter determination approaches, abundance pipelines, and the treatment of 3D and non-LTE effects can all introduce systematic offsets between studies. Additionally, estimates of spectroscopic errors and uncertainties are not uniformly defined across the literature. For this reason, we place an emphasis on the relative trends between abundances, rather than the absolute abundances themselves. Overall, this compilation represents one of the most extensive observational benchmarks assembled for testing a specific GC formation scenario, placing strong constraints on whether the model can simultaneously reproduce the diverse chemical, isotopic, and photometric signatures of MPs. Full observational references for each diagnos-

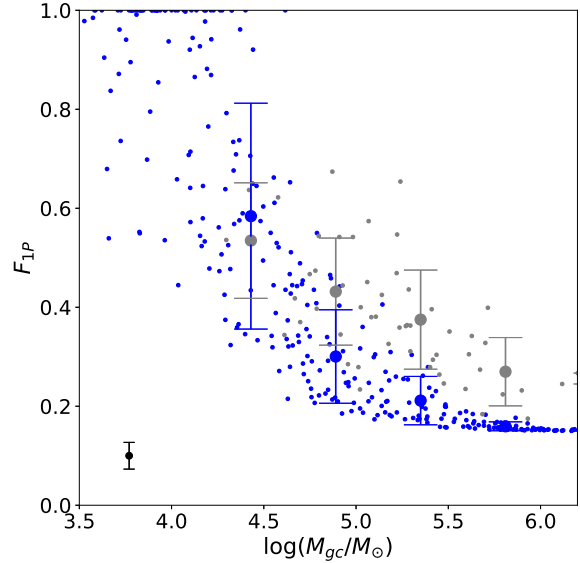


Figure 7. Mass fractions of 1P stars (F_{1P}) as a function of the present-day GC masses (M_{gc}) for simulated 300 GCs (blue) and observations (gray). Observational data from M18 is used here.

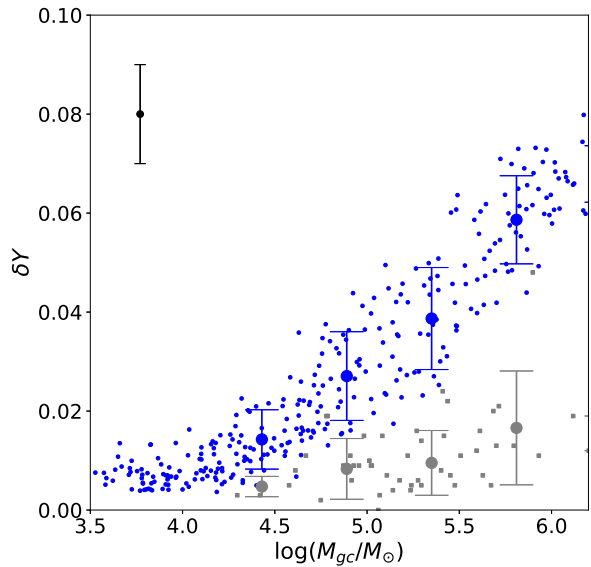


Figure 8. Differences in helium abundances (δY) between 1P and 2P stars as a function of M_{gc} . for simulated GCs (blue) and observations (gray). Observational data from M18 is used here.

tic are provided in the corresponding subsections of Section 4 and 5 where the model predictions are compared directly with the data.

4 RESULTS

4.1 F_{1P} and δY dependent on M_{gc}

Fig. 7 shows the distribution of the simulated 300 GCs on the M_{gc} - F_{1P} plane for the fiducial set of model parameters. Clearly, more massive GCs can have lower F_{1P} in this model, which is qualitatively consistent with the corresponding observations by MM22. The main reason for this M_{gc} -dependent F_{1P} is that more massive GMCs can have larger fractions of AGB stars within and around them to be chemically enriched to a greater extent. More massive GMCs with larger sizes can interact with larger numbers of AGB stars (per unit mass) and gravitationally trap stellar winds from these stars more efficiently. We note that unlike the classic AGB scenario, where the gravitational potential of the 1P plays a critical role in retaining AGB ejecta for 2P star formation, this is not required for the SCI scenario. The dispersions in F_{1P} for a given M_{gc} can be significant due to the adopted initial dispersion in R_s and F_{dil} . Since these results are for a model with a fixed standard IMF, the dispersions in F_{1P} could be even more pronounced if IMF variations across GMC masses are introduced. The present model does not include the effects of the dynamical evolution of GCs on F_{1P} , which is suggested to be important (e.g., Parmentier 2025). Therefore, if such effects are properly incorporated into the present model, scatters in the M_{gc} - F_{1P} relation could be even more pronounced.

The flat distribution of GCs for $M_{gc} > 5 \times 10^5 M_{\odot}$ is largely due to the adopted assumption that pre-existing stars are identified as 1P. Although the fractions of stars with low $[Na/Fe]$ are small, F_{1P} cannot become lower than a certain value due to the presence of pre-existing stars ($M_s = 0.01 M_{gmc}$ in this model). If these pre-existing stars are not counted as 1P, then a steeper anticorrelation between M_{gc} and F_{1P} can be obtained for $M_{gc} > 5 \times 10^5 M_{\odot}$. It is unclear how M_s depends on M_{gmc} without performing numerical simulations on the dynamical evolution of pre-existing stars within and around GC-forming GMCs. We also note that the observed F_{1P} values themselves carry a systematic uncertainty arising from the operational definition of 1P and 2P membership, which differs between photometric and spectroscopic studies. Chromosome maps, pseudo two colour diagrams constructed using Hubble space telescope photometry, tend to produce apparently discrete population grouping whereas spectroscopic surveys typically reveal a continuous distribution along the Na-O anticorrelation with no unambiguous gap between populations (e.g., C09a). The placement of the 1P/2P boundary therefore introduces a study dependent offset in the F_{1P} that likely contributes to some observed scatter.

It should be stressed here, however, that the GC distribution on the M_{gc} - F_{1P} plane depends strongly on the adopted M_{gmc} - R_s relation. If a flatter M_{gmc} - R_s relation is adopted, the simulated M_{gc} - F_{1P} relation can also become rather flat, which is inconsistent with the observed one (MM22). It would also be possible that low-mass GCs formed in galaxies with rather high R_s (≈ 1) can have low F_{1P} (< 0.4). Since global galactic properties such as sizes and gas mass fractions can determine the M_{gmc} - R_s relation, GC systems in galaxies with different galactic properties might have different M_{gc} - F_{1P} relations. While high resolution spectroscopy of individual stars sufficient to di-

rectly measure light element abundance variations remains limited to GCs within and immediately surrounding the Local Group, integrated light spectroscopic techniques have the potential to detect abundance variations characteristic of MPs in GCs at greater distances (e.g., Sakari et al. 2016; Larsen et al. 2018). Coupled with the advent of 30-meter class telescopes, there is a possibility of extending the M_{gc} - F_{1P} relation to more diverse extragalactic GC systems.

Fig. 8 describes how helium abundance differences between 1P and 2P stars (δY) depend on M_{gc} for the fiducial set of model parameters. More massive GCs can have larger δY in this model, which is at least qualitatively consistent with the corresponding observations (M18). The derived M_{gc} - δY relation results from larger R_s in higher M_{gmc} , as seen in Fig. 7. Helium-enriched stellar winds from massive AGB stars can mix well with the pristine gas of GC-forming GMCs so that 2P stars formed from the mixed gas can have higher Y . As a result of this, δY can be larger for GC-forming GMCs with larger R_s (i.e., larger numbers of more massive AGB stars interacting with GMCs).

The dispersion in δY is significant (≈ 0.01) for a given M_{gc} , which is due largely to the initial dispersion in R_s and F_{dil} . The simulated M_{gc} - δY correlation is steeper than the observed one, which could be a potentially serious problem in the new scenario. This inconsistency is due to the adopted large (0.34) Y yields of AGB ejecta in the present models.

Previous works have already claimed that the predicted large Y in 2P stars (thus large δY) in GC formation scenarios with polluters being AGB stars is a long standing tension (e.g., Bastian et al. 2015). Doherty et al. (2017) suggested that the primary processing sites of helium and Na in AGBs and sAGBs are physically distinct, with helium enrichment predominantly occurring through second dredge up during the early AGB, while Na and O are modified through hot bottom burning at the base of the convective envelope during the thermally pulsing AGB phase. Thus, helium and light element yields could in principle be decoupled. Clearly, if a smaller Y (≈ 0.28) can be adopted, the simulated M_{gc} - δY correlation can better match the observed one. GC distributions on the M_{gc} - δY plane also depend strongly on the adopted M_{gmc} - R_s relation, as seen in the M_{gc} - F_{1P} plane; these M_{gc} - F_{1P} and M_{gc} - δY relations have a common physical origin. Since it is beyond the scope of this paper to discuss why R_s and F_{dil} can be diverse in GC-forming GMCs with different M_{gmc} , we will investigate this point in our forthcoming study based on hydrodynamical simulations of GMC environments in galaxies. We note that helium abundances in RGB stars cannot be measured directly through optical spectroscopy as cool giants lack photospheric He lines in the optical wavelength range. The δY values must be derived indirectly from multiband photometric comparisons of population sequences using synthetic spectra and isochrone fitting (see M18).

4.2 O-Na anticorrelation

The O-Na anticorrelation is a direct signature of hydrogen burning at high temperatures. Oxygen depletion occurs through the ON cycle, while Na is simultaneously enhanced through proton capture on ^{22}Ne via the Ne-Na cycle (e.g., Langer et al. 1993). Both cycles are activated during hot bottom burning (HBB), the process by which the base of

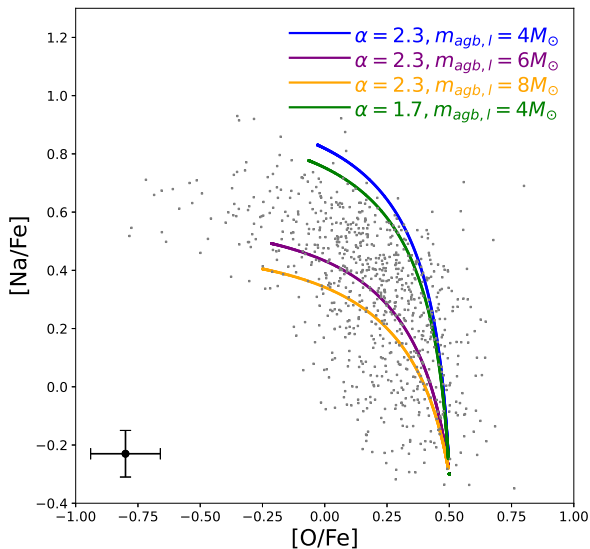


Figure 9. Anticorrelations between $[O/Fe]$ and $[Na/Fe]$ in three models with $\alpha = 2.3$ and $m_{\text{agb},1} = 4M_{\odot}$ (blue) $\alpha = 2.3$ and $m_{\text{agb},1} = 6M_{\odot}$ (purple) and $\alpha = 1.7$ and $m_{\text{agb},1} = 4M_{\odot}$ (orange) and observations from C09a and C09b (gray). $[O/Fe]$ and $[Na/Fe]$ at 1000 time steps are shown for each model in this figure. The AGB models from D10 are used to calculate the IMF-averaged AGB yields in these models.

the convective envelope in massive AGB stars reaches temperatures sufficient to activate proton-capture nucleosynthesis. Fig. 9 shows the time evolution of the present chemical evolution models on the $[O/Fe]$ - $[Na/Fe]$ plane for three different IMF-averaged AGB yields. The IMF slope (α) and the lower mass cutoff of AGB stars ($m_{\text{agb},1}$) are different between the three models so that the chemical abundances of star-forming GMCs can be quite different after mixing with AGB ejecta. Clearly, O-Na anticorrelations can be seen in the three models; however, the evolutionary locus and the final O and Na abundances are significantly different among the three. Although the IMF slope α does not significantly influence the time evolution of O and Na abundances, the evolutionary locus depends strongly on $m_{\text{agb},1}$, reflecting that AGB yields are different between different m_{agb} . The present models cannot simply explain the observed extreme (“E”) populations with rather low $[O/Na] < -0.9$ due to the adopted IMF-averaged AGB yields. The formation of E populations might be a result of star formation directly from the gaseous ejecta of very massive AGB stars.

C09a pointed out that a simple dilution model with the same AGB yields cannot reproduce the observed distributions of stars on the $[O/Fe]$ - $[Na/Fe]$ plane for NGC 2808 and M4 simultaneously. We suggest that the IMF-averaged yields can be quite different between NGC 2808 and M4, and this yield difference can account for the different evolutionary loci observed for these two GCs. Possibly, only high-mass AGB stars ($m_{\text{agb}} \geq 7M_{\odot}$) might have polluted a GMC forming NGC 2808 so that the 2P stars can have very low $[O/Fe]$ and $[Na/Fe]$. NGC2808 represents an extreme case in this context, hosting some of the most chemi-

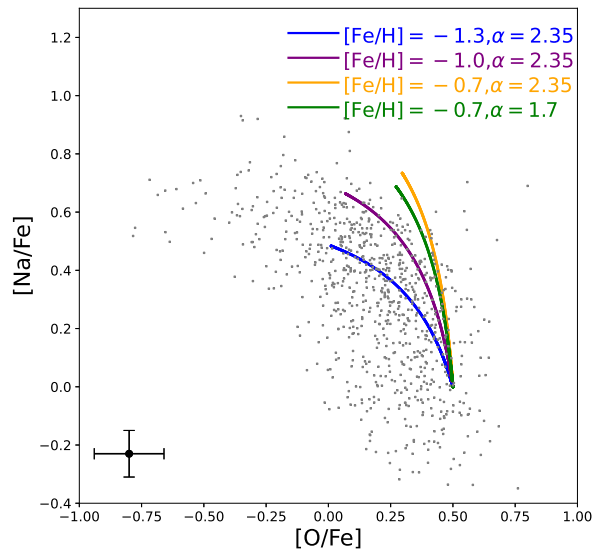


Figure 10. Same as Fig. 9 but for different $[Fe/H]$ and α .

cally anomalous populations of any Galactic GC, including a Mg-K anticorrelation (see Section 4.1.1), suggesting that its parent GMC was polluted by unusually massive sAGB stars operating at exceptionally high HBB temperatures, beyond what IMF-averaged yields for a standard mass range can reproduce. Although it is beyond the scope of this paper to discuss what determines the mass ranges of AGB stars that can pollute GMCs, t_{life} (GMC lifetime) could be one of the key factors for this.

Fig. 10 describes how the shapes of the simulated O-Na anticorrelations depend on $[Fe/H]$ and α in the models based on AGB yields from D18. Clearly, the slopes are steeper for higher $[Fe/H]$ in the three models with $[Fe/H] = -1.3, -1.0,$ and -0.7 for a given $\alpha (=2.35)$. The 1σ dispersions in $[Na/Fe]$ ($\sigma([Na/Fe])$) can therefore be smaller for lower $[Fe/H]$: 0.22, 0.19, and 0.14 for $[Fe/H] = -1.3, -1.0,$ and -0.7 , respectively. Therefore,

$$\Delta\sigma([Na/Fe])/\Delta[Fe/H] \approx -0.13 \quad (33)$$

in these models. Since the efficiency of the Ne-Na cycle during HBB is sensitive to the metallicity through its effects on the temperatures reached at the base of the convective envelope (e.g., V13), the present models predict a negative correlation between $\sigma([Na/Fe])$ and $[Fe/H]$ that represents a direct observational test of the temperature-dependent nucleosynthesis described above. The IMF slope α does not have a major effect on the shape of the O-Na anticorrelations in the high-metallicity models with $[Fe/H] = -0.7$.

4.3 Mg-Al anticorrelation

The Mg-Al anticorrelation requires more extreme HBB conditions than the O-Na anticorrelation, becoming active only when temperatures at the base of the convective envelope are sufficient to drive proton capture on ^{24}Mg through the Mg-Al chain to produce ^{27}Al (V13). The extent and variations in

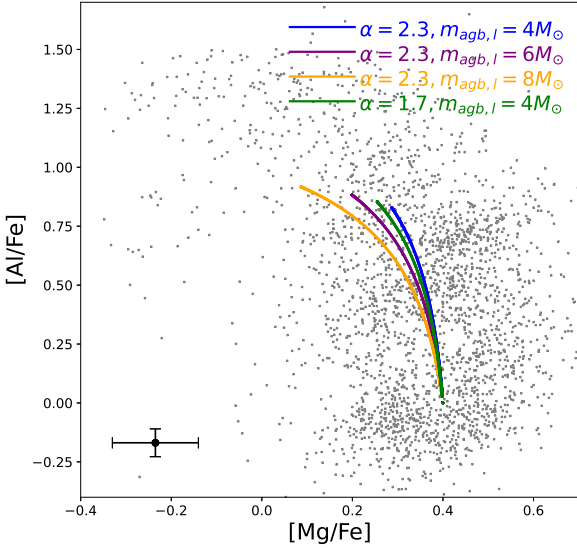


Figure 11. Same as Fig. 9 but for Mg-Al anticorrelations. Observational data from ME20 is used here.

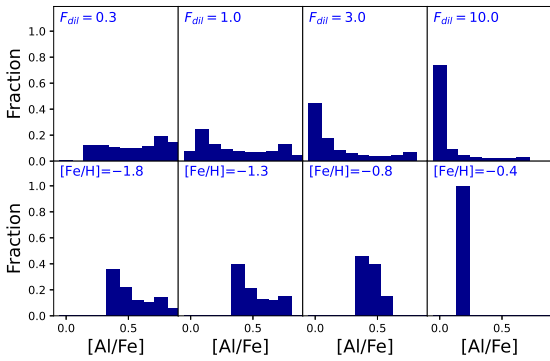


Figure 12. Upper and lower four panels shows how [Al/Fe] distributions of stars depend on F_{dil} and $[\text{Fe}/\text{H}]$ in GCs, respectively.

the strength of this anticorrelation relative to O-Na reflects this higher temperature threshold. Fig. 11 describes how the evolutionary loci of the three models on the $[\text{Mg}/\text{Fe}]$ - $[\text{Al}/\text{Fe}]$ plane are determined by α and $m_{\text{agb},l}$ for a fixed $m_{\text{agb},u}$ and a fixed star formation history. These models can reproduce the observed Mg-Al anticorrelation at least qualitatively, though they cannot reproduce the E populations with $[\text{Mg}/\text{Fe}] < 0$ observed in some GCs such as NGC 2808. ME20 reported a turn over in the Mg-Al anticorrelation among stars in the most metal poor GCs, specifically M15 and M92, where Al abundances decreased rather than continue to rise at low $[\text{Mg}/\text{Fe}]$. This behavior is interpreted as evidence that HBB temperatures in the polluters of these GCs were sufficiently extreme to activate proton capture on ^{27}Al to ^{28}Si . This reflects the temperature sensitivity of the Mg-Al chain. The $8 M_{\odot}$ model begins to reach these extreme $[\text{Mg}/\text{Fe}]$ abundances, but no model can replicate the $[\text{Al}/\text{Fe}]$ turnover that was reported for the most metal poor GCs.

The two models with different α yet the same $m_{\text{agb},l}$ have very similar evolutionary loci on the $[\text{Mg}/\text{Fe}]$ - $[\text{Al}/\text{Fe}]$ plane, which implies that the IMF is not crucial in the distributions of GC stars on this plane. The difference in $[\text{Mg}/\text{Fe}]$ between 1P and 2P stars is more remarkable in the models with different $m_{\text{agb},l}$, which confirms that $m_{\text{agb},l}$ is more important than α in determining chemical abundance patterns of GCs with MPs.

Fig. 12 shows the distributions of $[\text{Al}/\text{Fe}]$ (histograms) in 8 models with different F_{dil} and $[\text{Fe}/\text{H}]$. Two peaks in $[\text{Al}/\text{Fe}]$ distributions can be more clearly seen in the models with lower F_{dil} ($=0.3$ and 1.0) due to more efficient chemical enrichment by AGB stars. However, the predicted bimodality is less pronounced than observed in ME20, likely reflecting the simplified treatment of star formation history within GMCs in the present one-zone framework. It is found that 1σ dispersions in $[\text{Mg}/\text{Al}]$ ($\sigma([\text{Al}/\text{Mg}])$) are larger for smaller F_{dil} : $\sigma([\text{Al}/\text{Mg}])=0.27$ and 0.19 for $F_{\text{dil}} = 0.3$ and 10.0 , respectively. Pancino et al. (2017) investigated the Mg-Al anticorrelations of GCs using data from *Gaia*-ESO Survey and found a positive correlation between $\sigma([\text{Al}/\text{Mg}])$ and M_{gc} . This positive correlation is qualitatively consistent with the above predictions because F_{dil} is smaller for larger M_{gc} (due to larger M_{gmc}) in the present models,

Fig. 12 also demonstrates that (i) $[\text{Al}/\text{Fe}]$ distributions are more extended for lower $[\text{Fe}/\text{H}]$ and (ii) the $[\text{Fe}/\text{H}]=-0.4$ model does not clearly show a Mg-Al anticorrelation due to almost no $[\text{Al}/\text{Fe}]$ variation. This $[\text{Fe}/\text{H}]$ dependence of Mg-Al anticorrelations has been already discussed by Ventura et al. (2016). The metallicity dependence of $\sigma([\text{Al}/\text{Fe}])$ reflects the higher HBB temperatures reached in the AGB polluters at low $[\text{Fe}/\text{H}]$, enabling more complete Mg-Al processing. It is clear that 1σ dispersions in $[\text{Al}/\text{Mg}]$ are smaller for higher $[\text{Fe}/\text{H}]$ in these models: $\sigma([\text{Al}/\text{Mg}])=0.2$ and 0.06 for $[\text{Fe}/\text{H}]=-1.8$ and -0.4 , respectively. Accordingly, the slope in this anticorrelation is;

$$\Delta\sigma([\text{Al}/\text{Mg}])/\Delta[\text{Fe}/\text{H}] \approx -0.1 \quad (34)$$

in these models. Pancino et al. (2017) found that this slope is ≈ -0.2 , which is approximately twice as steep as the predicted slope in this study. Their results imply that although the present models can qualitatively reproduce the observed anticorrelation between $\sigma([\text{Al}/\text{Mg}])$ and $[\text{Fe}/\text{H}]$, quantitative reproduction of the anticorrelation would require inclusion of physical processes that are not implemented in the present models.

4.4 C-N anticorrelation

The C-N anticorrelation arises at the lowest temperatures of the proton-capture cycles relevant to GC chemical enrichment, with CN cycling converting ^{12}C to ^{14}N during HBB. Its near ubiquitous presence across GCs of different masses and metallicities reflects this comparatively low activation temperature, making it a less discriminating constraint on the precise masses of AGB polluters than the higher temperature cycles. Fig. 13 shows (i) the distribution of GC stars from ME20 on the $[\text{C}/\text{Fe}]$ - $[\text{N}/\text{Fe}]$ plane and (ii) the evolutionary loci of four models with different mass ranges of AGB stars contributing chemical enrichment within GMCs on the plane. Although C-N anticorrelations can be clearly

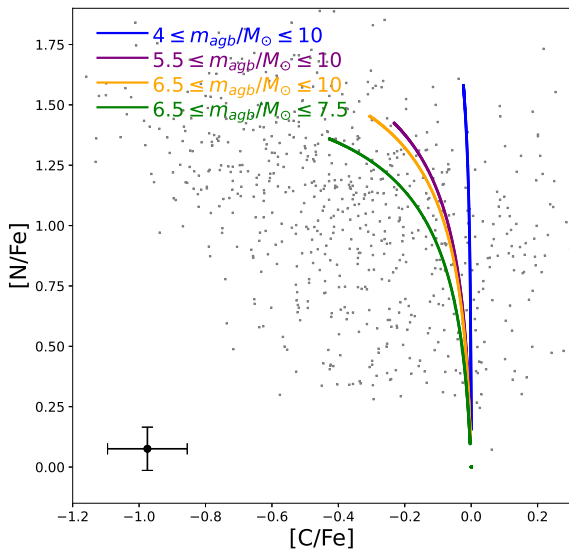


Figure 13. Same as Fig. 9 but for C-N anticorrelations. The AGB models by Ventura et al. (2013) are used to calculate the IMF-averaged AGB yields, because D10 does not provide C and N yields. Four models with $4 \leq m_{\text{agb}}/M_{\odot} \leq 10$ (blue), $5.5 \leq m_{\text{agb}}/M_{\odot} \leq 10$ (purple), $6.5 \leq m_{\text{agb}}/M_{\odot} \leq 10$ (orange), and $6.5 \leq m_{\text{agb}}/M_{\odot} \leq 7.5$ (green) are plotted for $\alpha = 2.3$. Observational data from ME20 is used here.

seen in individual GCs with MPs (ME20), such an anticorrelation is not so clearly apparent due to a large [C/Fe] dispersion at a given [N/Fe] in this plot including all stars from different GCs. This dispersion likely reflects a combination of genuine star-to-star abundance variations, measurement uncertainties arising from molecular CN and CO features, and evolutionary effects modifying initial C and N abundances. Clearly, the slopes of the simulated C-N anticorrelations depend on the mass ranges of AGB stars that can determine the IMF-averaged C and N yields. There is almost no C-N anticorrelation (i.e., an almost vertical line) seen in the model with $4 \leq m_{\text{agb}}/M_{\odot} \leq 10$, in which the IMF-averaged [C/Fe] of AGB winds is almost identical to initial [C/Fe] due to major contributions of lower mass AGB stars. C-N anticorrelations can be more pronounced in the models in which only high-mass stars with $m_{\text{agb}} \geq 5.5M_{\odot}$ contribute to chemical enrichment within GMCs. The model with $5.5 \leq m_{\text{agb}}/M_{\odot} \leq 7.5$ shows the shallowest slope in the C-N anticorrelation due to the lower IMF-average [C/Fe] and [N/Fe] of AGB winds.

The present models with AGB yields for $[\text{Fe}/\text{H}] = -1.6$ adopted from V13, has a difficulty in reproducing $[\text{C}/\text{Fe}] < -0.6$ observed in a fraction of GC stars (ME20), mainly because the minimum possible [C/Fe] of AGB winds in the lowest metallicity model by V13 is -0.59 . This problem may not be critical, given that higher C yields would be possible in the updated theoretical models for AGB stars. V13 predicts that [C/Fe] of AGB winds can be as low as -1 in their higher metallicity models ($Z = 8 \times 10^{-3}$), which implies that the observed stars with $[\text{C}/\text{Fe}] \approx -1$ and high [N/Fe] > 1 can be explained in the context of star formation from

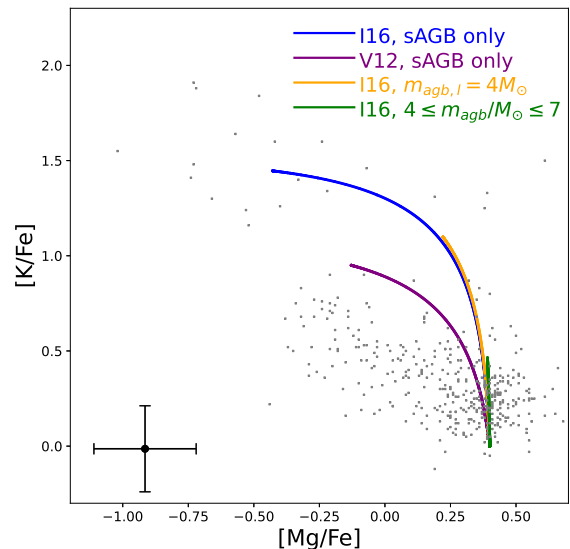


Figure 14. Same as Fig. 9 but for Mg-K anticorrelations. Different AGB yields are adopted in these four models. Only sAGB stars are assumed to contribute to chemical enrichment, and the yields of sAGB stars from I16 (blue) and from V13 (purple) are adopted in the first two models. The models with sAGB yields from I16 and IMF-averaged yields for $4 \leq m_{\text{agb},1}/M_{\odot} \leq 10$ (orange) and for $4 \leq m_{\text{agb},1}/M_{\odot} \leq 7$ (green) are also shown for comparison. Observational data sets for ω Cen (Alvarez-Garay et al. 2024) and for NGC 2419 (Mucciarelli et al. 2010) are used here.

AGB winds star with higher metallicity mixed with pristine GMC gas. Although the present models predict that the slopes of C-N anticorrelations could be diverse depending on the IMF and the mass ranges of polluting AGB stars, the observed slopes are consistent across clusters in ME20. Also, an almost vertical C-N anticorrelation cannot be seen in GC samples by ME20, which implies that AGB stars with $m_{\text{agb}} \approx 4M_{\odot}$ are unlikely to significantly contribute to the chemical enrichment in GMCs. This is consistent with their marginal HBB temperatures with the potential to produce carbon enhanced, rather than nitrogen enhanced ejecta.

4.5 Mg-K

The Mg-K anticorrelation represents the most extreme proton-capture signatures observed in GC stars, requiring HBB temperatures significantly higher than those needed to activate either the Ne-Na or Mg-Al cycles, through the Ar-K chain operating in the most massive sAGB polluters. Its detection in only a limited number of GCs is a direct consequence of this extreme temperature requirement. Recent theoretical studies of stellar nucleosynthesis have demonstrated that sAGB stars and nova are the best possible polluting stars responsible for the observed Mg-K anticorrelation of NGC 2419 (V12; I16; Fox et al. 2024). Clearly, if only sAGB stars with $6.5 \leq m_{\text{agb}}/M_{\odot} \leq 10$ contribute to chemical enrichment in GC formation, the observed Mg-K anticorrelation can be naturally reproduced for NGC 2419

(V12; I16). However, both AGB and sAGB would be able to enrich GMCs through their stellar winds in real GC formation. We therefore consider the following two cases: (i) only sAGB stars chemically enrich GMCs (“sAGB only” model) and (ii) both AGB and sAGB stars chemically enrich GMCs. Different evolutionary loci of the models on the Mg-K plane between the two cases can provide clues as to why the distributions of stars on the Mg-K plane appear to be different between different GCs. Since K yields are not available for AGB stars in D10 and V13, we adopt an assumption of $[K/Fe]=0$ for all AGB stars just for simplicity.

Fig. 14 demonstrates that the sAGB only model with I16 yields can show a Mg-K anticorrelation, though it does not produce 2P stars with very low Mg (≈ -1) due to too much dilution of sAGB ejecta with pristine GMC gas. 2P stars in the sAGB only model with V12 yields have systematically lower $[K/Fe]$ and higher $[Mg/Fe]$, as expected for the chemical yields by V12. A large fraction of stars have lower $[K/Fe]$ for a given $[Mg/Fe]$ compared with the predictions of these two models, in particular, for $-0.5 \leq [Mg/Fe] \leq 0.25$. This apparent inconsistency will need to be reassessed by our future theoretical models when sAGB yields for different m_{agb} and $[Fe/H]$ are available. It should be noted here that 2P stars with moderately high $[K/Fe]$ (≈ 0.5) and low $[Mg/Fe]$ (≈ -0.3) observed in NGC 1786 (Alvarez-Garay et al. 2025) cannot be well reproduced by any models in this study. We note that K abundance measurements in GCs carry additional systematic uncertainties. The primary K I diagnostic line at $\sim 7699 \text{ \AA}$ requires careful corrections for telluric contamination from the oxygen A band, while both KI resonance lines may be subject to significant departures from local thermodynamic equilibrium.

The model with $m_{\text{agb},1} = 4M_{\odot}$, in which both AGB and sAGB stars contribute to chemical enrichment within GMCs, shows a very steep Mg-K anticorrelation with a narrow range of $[Mg/Fe]$ in 1P and 2P stars. This result is due to mixing of gaseous ejecta with high IMF-averaged $[Mg/Fe]$ from AGB and sAGB stars with pristine GMC gas. The model with $4 \leq m_{\text{agb}}/M_{\odot} \leq 7$ has a narrow mass range of sAGB stars with $6.5 \leq m_{\text{agb}} \leq 7M_{\odot}$ so that the IMF-averaged $[Mg/Fe]$ and $[K/Fe]$ of AGB ejecta can be very similar to $[Mg/Fe]$ and $[K/Fe]$ of pristine GMC gas. Consequently, the 1P and 2P stars have similar $[Mg/Fe]$ and $[K/Fe]$ and no clear Mg-Al anticorrelation can be seen in this model. These results demonstrate that the mass range of AGB stars contributing to chemical enrichment in GC formation is a crucial factor to determine the distributions of 1P and 2P stars on the Mg-K plane. Mg-K plane, and by extension, the HBB temperatures reached by the more massive sAGB stars, driving more extreme nucleosynthesis.

Based on these results, we suggest that the GMC forming NGC 2419 was polluted only by sAGB stars, possibly because the lifetime of the GMC was not long enough so that AGB stars with $m_{\text{agb}} \leq 6.5M_{\odot}$, which can eject gas later than sAGB stars, can pollute the GMC. It would be possible that a large number electron-capture supernovae from massive stars with $8 \leq m/M_{\odot} \leq 10$ expelled the remaining pristine gas of the GMC immediately from chemical enrichment by sAGB stars. Such supernova explosions would be able to truncate further chemical enrichment by AGB stars with $m_{\text{agb}} \leq 6.5M_{\odot}$ completely. This explanation

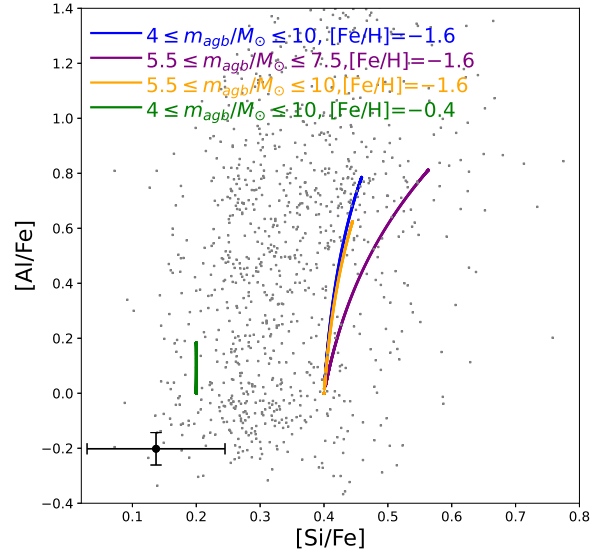


Figure 15. Same as Fig. 9 but for Si-Al correlations. The models with $[Fe/H]=-1.6$ and $4 \leq m_{\text{agb},1}/M_{\odot} \leq 10$ (blue), with $[Fe/H]=-1.6$ and $5.5 \leq m_{\text{agb},1}/M_{\odot} \leq 7.5$ (purple), with $[Fe/H]=-1.6$ and $5.5 \leq m_{\text{agb},1}/M_{\odot} \leq 10$ (orange), and with $[Fe/H]=-0.4$ and $4 \leq m_{\text{agb},1}/M_{\odot} \leq 10$ (green), are shown. For the high-metallicity model, initial $[Si/Fe]=0.2$ instead of 0.4 is used for consistency with model predictions by V13. Data from ME20 is used here.

is highly speculative, thus its validity needs to be assessed by numerical simulations of GC formation.

Alvarez Garay et al. (2026) has recently revealed no stars with $[Mg/Fe] < 0$ in M54, in which the majority of stars have $[Fe/H]$ ranging from -1.6 to -1.0 , though M54 shows a clear Mg-K anticorrelation. This observation cannot be simply explained by the present models with sAGB stars, which implies that metallicities play a role in shaping the anticorrelation. Dell’Agli et al. (2018) indeed demonstrated that $[Mg/Fe]$ of gaseous ejecta from AGB stars with $Z = 2.5 \times 10^{-3}$ and $4.5 \leq m_{\text{agb}}/M_{\odot} \leq 6.5$ cannot be lower than 0.2, though they did not show K yields of these stars. It is therefore possible that sAGB stars with higher $[Fe/H]$ (≈ -1) cannot produce gas with $[Mg/Fe] < 0$. Future models incorporating a broader grid of metallicity-dependent sAGB yields will enable a more complete exploration of how polluter metallicity shapes the Mg-K anticorrelation across the diversity of observed GCs.

Thus, both the mass ranges of polluting AGB stars and their metallicities can determine the shapes of Mg-K anticorrelations in the new scenario. The mass ranges of polluting AGB stars (i.e., $m_{\text{agb},1}$ and $m_{\text{agb},u}$) in GCs could be a complex function of star formation histories of their host galaxies, growth histories of their parent GMCs, and GMCs’ lifetimes (t_{life}). Our future hydrodynamical simulations of GC formation therefore need to clarify what determines the mass ranges of AGB stars polluting GMCs in various galaxy environments.

4.6 Si-Al correlation

The Si-Al correlation arises when HBB temperatures are sufficient to drive proton capture beyond the Mg-Al chain, with ^{27}Al serving as the seed nucleus for ^{28}Si production via the $^{27}\text{Al}(p,\gamma)^{28}\text{Si}$ reaction. The resulting positive correlation between Si and Al, rather than the anticorrelation seen in the Mg-Al plane, is therefore a signature of the most massive and metal-poor AGB polluters in which the full Mg-Al-Si nucleosynthetic pathway operates. Fig. 15 shows the evolutionary loci of four models with different AGB yields on the [Si/Fe]-[Al/Fe] plane and compares with the corresponding observations from ME20. Clearly, steep Si-Al correlations can be seen in the three low-metallicity models with [Fe/H]=-1.6, which is at least qualitatively consistent with observations by ME20. However, the adopted initial [Si/Fe] (=0.4), which is consistent with the V13 model, appears to be significantly higher than the observed mean [Si/Fe] of GC stars (ME20). Consequently, the simulated Si-Al correlation deviates from the observed one, which implies that lower initial [Si/Fe] (≈ 0.3) needs to be adopted in the three low-metallicity models to better reproduce the observed trend. The higher metallicity model with [Fe/H]=-0.4 shows an almost vertical evolutionary locus and a very narrow range of [Al/Fe], which simply reflects the small Al yields of the AGB models with [Fe/H]=-0.4 in V13. This result reflects the temperature requirements of Si production via HBB, that GCs with unlikely to possess a clear Si-Al correlation.

The slopes of Si-Al correlations in the models with [Fe/H]=-1.6 depend on the ranges of AGB stars that contribute to chemical enrichment in GCs, as seen in other elemental abundance patterns. The slope is the steepest in the model in which the IMF-averaged AGB yields for $4 \leq m_{\text{agb}}/M_{\odot} \leq 10$ are adopted, because the relative contributions of massive AGB stars, which have high Si yields in V13, are minor in the model. If only massive AGB stars with $5.5 \leq m_{\text{agb}}/M_{\odot} \leq 7.5$ contribute to chemical enrichment in GMCs, then the slope becomes flatter with a wider range of [Si/Fe]. The model with $5.5 \leq m_{\text{agb}}/M_{\odot} \leq 10$ shows narrower ranges of [Si/Fe] and [Al/Fe] due to the lower Si ([Si/Fe]=0.44) and Al yields ([Al/Fe]=0.6) of high-mass AGB stars with $m_{\text{agb}} \geq 7.5M_{\odot}$ in V13.

The IMF-averaged yields of Si and Al are used in the present models. Accordingly, even if AGB stars with a particular mass range (e.g., $5.5 \leq m_{\text{agb}}/M_{\odot} \leq 6$) eject winds with high [Al/Fe] (> 0.8) and high [Si/Fe] (> 0.6), new stars formed in the models do not show [Al/Fe] > 0.8 and [Si/Fe] > 0.6 due to mixing of ejecta from AGB stars with different masses. Reproducing stars with [Al/Fe] > 0.8 and [Si/Fe] > 0.6 simultaneously would require contributions from individual massive sAGBs operating at very high HBB temperatures where $^{27}\text{Al}(p,\gamma)^{28}\text{Si}$ reaction proceeds efficiently enough to produce both extreme Al enrichment and Si enhancement before the ejecta are diluted by pristine GMC gas. However, if gaseous ejecta from AGB star with $m_{\text{agb}} = 5.5M_{\odot}$ is mixed with pristine GMC gas to be converted into new stars, the observed high [Si/Fe] and [Al/Fe] can be achieved in the present models. A clear goal of our future study is to understand how stellar winds from individual AGB stars with different masses mix with pristine GMC gas and ejecta from other AGB stars.

4.7 Li-Na and Li-Al relations

Lithium represents a uniquely constraining diagnostic for GC formation scenarios because its surface abundance in giant stars is sensitive to both the original chemical enrichment by AGB polluters and the subsequent stellar evolution of the observed stars. In unevolved main sequence turn off stars, A(Li) reflects the original chemical composition of the gas from which they formed. However, as stars ascend the RGB, the first dredge up brings CN-cycle processed material to the surface, systemically depleting the original ^7Li through convective dilution with the interior layers where it has been destroyed (e.g., Karakas & Lattanzio 2014). For AGB polluters, ^7Li can be transiently produced through the Cameron-Fowler mechanism, where ^7Be synthesized at the base of the convective envelope during HBB is transported to cooler outer layers and converted to ^7Li via electron capture before it can be destroyed (Cameron & Fowler 1971; Sackmann & Boothroyd 1992). Measuring A(Li) in the context of MPs therefor ideally requires unevolved turnoff or subgiant stars to avoid the complications of RGB depletion, however spectra of high enough quality for this analysis are observationally expensive.

We here assume that there are two types of polluting stars, i.e., one ejecting Li-deficient gas with A(Li)=1.56 and the other ejecting Li-rich gas with A(Li)=2.8, in order to more clearly demonstrate whether Li-production in polluting stars is required to reproduce the observed (anti)correlations of A(Li) with [Na/Fe] and [Al/Fe]. P(Li) is defined as the mass fraction of polluters producing Li (A(Li)=2.8) among all stars with $4 \leq m/M_{\odot} \leq 10$ and considered to be a free parameter in the present study. Fig. 16 describes how the evolutionary loci of the present five models on the A(Li)-[Na/Fe] and A(Li)-[Al/Fe] planes depend on Li production rates (P(Li)). Steep A(Li)-[Na/Fe] and A(Li)-[Al/Fe] anticorrelations can be seen in the model without Li production (P(Li)=0), which is inconsistent with observational results (e.g., Lind et al. 2009; Monaco et al. 2010; D’Orazi et al. 2014). The models with larger P(Li) has flatter anticorrelations, which result from more A(Li) production in these models. A very flat A(Li)-[Na/Fe] relation can be seen only in the model with P(Li)=0.18, which suggests that a significant fraction of AGB stars need to produce Li-rich ejecta to reproduce the observed very flat A(Li)-[Na/Fe] and A(Li)-[Al/Fe] relations in GCs.

Since not all of AGB stars can produce Li with A(Li) > 2.3 (e.g., D12; V13), a crucial question here is whether P(Li) ≈ 0.2 is possible for a given IMF. Using the A(Li) table for AGB stars with different masses listed in D12, we find that the mass fraction of Li-producing AGB stars is 0.29, 0.29 and 0.25 for $\alpha = 1.7, 2.3,$ and $2.7,$ respectively. Therefore, the required P(Li) ≈ 0.2 for the flat A(Li)-[Na/Fe] and A(Li)-[Al/Fe] relations is possible in the present GC formation scenario. It is also found that the IMF-average A(Li) in AGB stars with $4 \leq m_{\text{agb}}/M_{\odot} \leq 10$ is 2.4 for the Li yields from D12. These results imply that the present SCI scenario is quite promising in terms of explaining the observed flat relations. Thus the observed lack of an A(Li)-[Na/Fe] and A(Li)-[Al/Fe] anticorrelations in GCs strongly suggests that GC formation scenarios incapable of Li production are disfavoured by the current observational evidence. The present scenario predicts that some GCs with

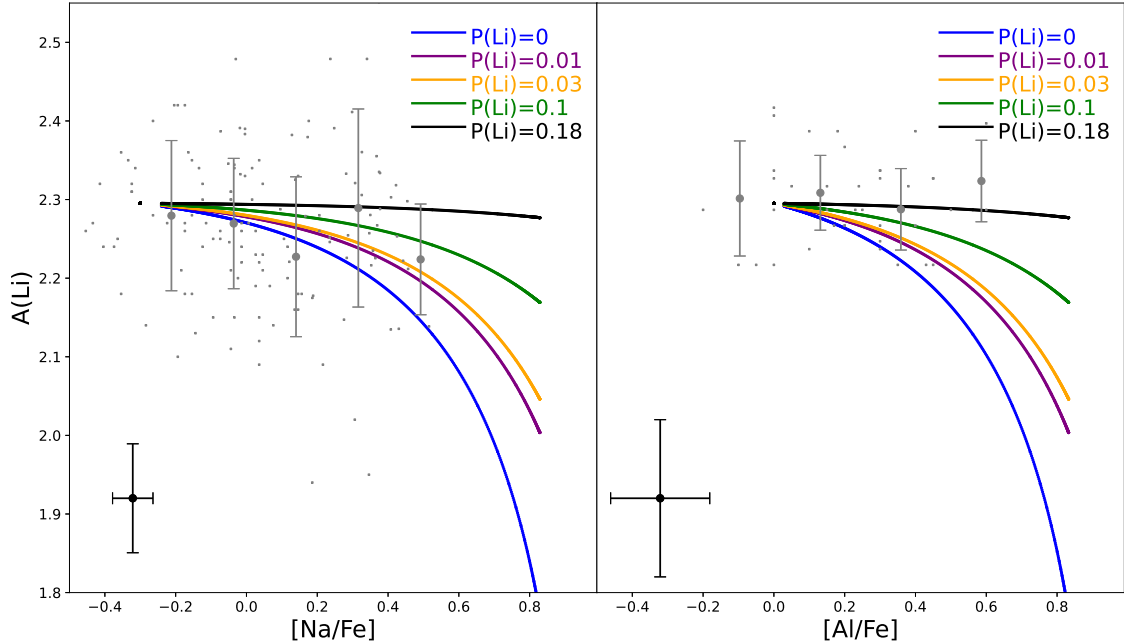


Figure 16. $A(\text{Li})$ as a function of $[\text{Na}/\text{Fe}]$ (left) and $[\text{Al}/\text{Fe}]$ (right) in the five models with different fractions of Li-producing AGB stars ($P(\text{Li})$): 0 (blue), 0.01 (purple), 0.03 (orange), 0.1 (green), and 0.18 (black). Observational results taken from Lind et al. (2009) and McKenzie et al. 2026 (MA26) are plotted in the left panel, and the mean and 1σ dispersion for five $[\text{Na}/\text{Fe}]$ bins are also plotted to reproduce the original $A(\text{Li})$ during unevolved phases in the right panel. We thus make a physically meaningful comparison between these observations and the model predictions for the (anti)correlation between $[\text{Al}/\text{Fe}]$ and $A(\text{Li})$.

lower $P(\text{Li})$ should show very mild $A(\text{Li})$ - $[\text{Na}/\text{Fe}]$ anticorrelations, which can explain the observed $A(\text{Li})$ - $[\text{Na}/\text{Fe}]$ in a few GCs (e.g., Pasquini et al. 2005).

The 1σ dispersions in $A(\text{Li})$ ($\sigma(A(\text{Li}))$) and differences in minimum and maximum $A(\text{Li})$ ($\delta_{\text{max}}A(\text{Li})$) in simulated GCs depend both on $P(\text{Li})$ and on F_{dil} , as summarized in Table 2. As expected, $\sigma(A(\text{Li}))$ and $\delta_{\text{max}}A(\text{Li})$ are larger in the models with smaller $P(\text{Li})$ due to more efficient formation of Li-deficient stars from cold gas polluted by AGB ejecta with lower $A(\text{Li})$. $\sigma(A(\text{Li}))$ and $\delta_{\text{max}}A(\text{Li})$ are larger in the models with smaller F_{dil} , which implies that more massive GCs are likely to have large $\sigma(A(\text{Li}))$ and $\delta_{\text{max}}A(\text{Li})$ due to smaller F_{dil} (caused by larger R_s) in the present scenario. It is currently unknown whether GCs have $\sigma(A(\text{Li}))$ and $\delta_{\text{max}}A(\text{Li})$ dependent on their total masses.

As pointed out by D12, 2P stars can have very high $A(\text{Li})$ (> 2.9), if they are formed from gaseous ejecta from sAGB stars with $m_{\text{agb}} = 8M_{\odot}$ without mixing so much with pristine gas. D12 also suggested that a few Li-rich stars observed in M4 and NGC 6397 could be intriguing examples of 2P stars formed almost directly from gaseous ejecta of sAGB stars. If 2P stars form only after the ejecta of multiple AGB stars with different masses have mixed within the GMC, the resulting $A(\text{Li})$ will reflect an IMF-averaged value that is significantly lower than that of the most Li-rich individual AGB ejecta because of the contributions of Li-poor lower mass AGB stars that dominate by number.

Table 2. Li abundance properties of GCs with MPs predicted from the new scenario.

$P(\text{Li})$	F_{dil}	$A_{\text{m}}(\text{Li})$	$\sigma(A(\text{Li}))$	$\delta_{\text{max}}A(\text{Li})$
0.0	3.0	2.22	0.13	0.52
0.01	3.0	2.25	0.07	0.29
0.03	3.0	2.25	0.06	0.25
0.10	3.0	2.27	0.03	0.13
0.18	3.0	2.25	0.00	0.02
0.01	0.3	2.13	0.11	0.34
0.01	1.0	2.20	0.10	0.33
0.01	10.0	2.28	0.04	0.21

It should be stressed here that the IMF-weighted Li yield ($A(\text{Li})$) depends on the mass range of AGB stars, $[m_{\text{agb},l}, m_{\text{agb},u}]M_{\odot}$, for a given IMF slope. It is 2.39 for $[3, 7.5]$, 2.20 for $[3, 7.5]$, 2.20 for $[4, 7.5]$, 2.25 for $[5, 7.5]$, 3.19 for $[3, 10.0]$, and 3.46 for $[5, 10.0]$ for the Salpeter IMF with $\alpha = 2.35$. Therefore, the average $A(\text{Li})$ depends strongly on how much sAGB stars with $m_{\text{agb}} \geq 7.5M_{\odot}$ can continue to chemical enrichment within GC-forming GMCs. The normal $A(\text{Li})$ observed in the Na-rich 2P stars in most GCs suggests that sAGB stars, despite their role in driving the Mg-K anticorrelation in extreme clusters such as NGC2419, do not dominate the bulk chemical enrichment responsible for the ubiquitous Na-O anticorrelation, consistent with their high predicted Li yields driving $A(\text{Li})$ far above observed values if they were the primary polluters.

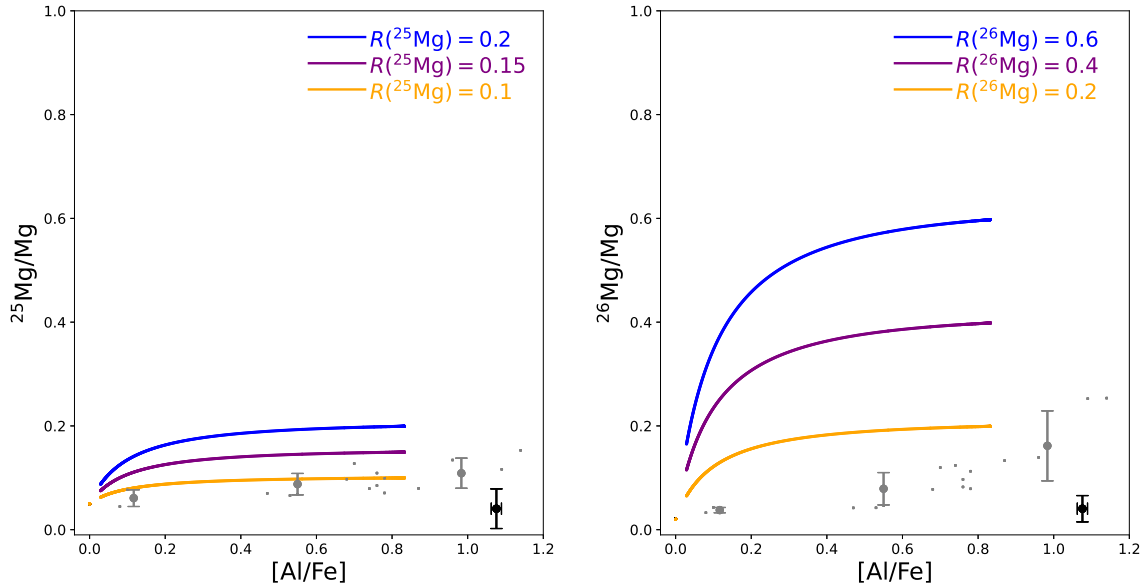


Figure 17. $^{25}\text{Mg}/\text{Mg}$ (left) and $^{26}\text{Mg}/\text{Mg}$ ratios (right) as a function of $[\text{Al}/\text{Fe}]$ for three models with different AGB ejecta compositions, denoted as $R(^{25}\text{Mg}/\text{Mg})$ and $R(^{26}\text{Mg}/\text{Mg})$, respectively. In the left panel, $R(^{25}\text{Mg}/\text{Mg})$ is set to 0.2 (blue), 0.15 (purple), and 0.1 (orange). In the right panel, $R(^{26}\text{Mg}/\text{Mg})$ is set to 0.6 (blue), 0.4 (purple), and 0.2 (orange). Reanalysis of archival data from Yong et al. (2003) for NGC 6752 (McKenzie et al. in prep) is also plotted: the mean observational errors are indicated by black error bars. The mean and 1σ dispersion for the $[\text{Al}/\text{Fe}]$ bins are indicated by gray points and error bars, respectively. For all models, the initial $^{25}\text{Mg}/\text{Mg}$ and $^{26}\text{Mg}/\text{Mg}$ ratios of the pristine gas are assumed to be 0.05 and 0.02, respectively.

4.8 Mg isotope ratios

Magnesium isotope ratios provide a uniquely sensitive probe of the temperatures and nuclear reaction conditions during HBB in AGB polluters, since ^{24}Mg is destroyed by the Mg-Al chain while ^{25}Mg and ^{26}Mg accumulate as intermediate products. The observed pattern of ^{26}Mg enhancement with increasing $[\text{Al}/\text{Fe}]$ was first established in Yong et al. (2003), and through a reanalysis of the spectra by McKenzie et al. (in prep), the first evidence of a correlation between ^{25}Mg and $[\text{Al}/\text{Fe}]$ has also been detected. Since the predicted abundances of Mg isotopes (^{25}Mg and ^{26}Mg) in stellar winds of AGB stars are given only for $m_{\text{agb}} = 5$ and $7M_{\odot}$ in V12, it is currently not possible with the available yields for the present study to derive the IMF-averaged yields of Mg isotopes. We accordingly adopt a wide range of Mg isotope yields and thereby investigate the time evolution of Mg isotope ratios in our GC formation models. We here focus particularly on the model behaviour on the $^{25}\text{Mg}/\text{Mg}$ - $[\text{Al}/\text{Fe}]$ and $^{26}\text{Mg}/\text{Mg}$ - $[\text{Al}/\text{Fe}]$ planes to find the best model that matches with observations. Fig. 17 describes how the evolutionary loci of different models on the $^{25}\text{Mg}/\text{Mg}$ - $[\text{Al}/\text{Fe}]$ and $^{26}\text{Mg}/\text{Mg}$ - $[\text{Al}/\text{Fe}]$ planes depend on the adopted the mass ratios of ^{25}Mg and ^{26}Mg to Mg.

MA26 have recently discovered a weak positive correlation between $[\text{Al}/\text{Fe}]$ and $^{25}\text{Mg}/\text{Mg}$ extending to $[\text{Al}/\text{Fe}] \approx 1.1$ in NGC 6752. However, this is the first cluster to see a trend in ^{25}Mg with light element abundances (see Da Costa et al. 2013, Thygesen et al 2016). Such a positive correlation can be reproduced well only by the model with $R(^{25}\text{Mg}) = 0.1$, though this $^{25}\text{Mg}/\text{Mg}$ yield is lower than

those predicted by Ventura et al. (2018) for $m = 5M_{\odot}$ stars. The apparent lack of stars between $[\text{Al}/\text{Fe}] = 0.1$ and 0.4 observed in NGC 6752 is not so well explained by the present models, which implies that the star formation histories of GCs in the models need to be revised. This could be also due to a selection effect. Future work will explore the impacts of mass and metallicity as more Mg isotopic measurements are made available for a larger range of clusters.

Although the two models with $R(^{26}\text{Mg})=0.4$ and 0.6 shows clear positive correlations between $[\text{Al}/\text{Fe}]$ and $^{26}\text{Mg}/\text{Mg}$, the predicted non-linear correlations (i.e., not straight lines) appear to be inconsistent with observations. Furthermore, the models predict high $^{26}\text{Mg}/\text{Mg}$ (> 0.2) already at $[\text{Al}/\text{Fe}] < 0.2$, which is not clearly seen in observations. This high $^{26}\text{Mg}/\text{Mg}$ is due largely to earlier chemical enrichment of GMCs by AGB stars in the models, which suggests that time evolution of chemical enrichment by AGB stars needs to be fine-tuned to explain the observations better in the present models. The model with $R(^{26}\text{Mg})=0.2$ can better reproduce the observed correlation, however, the model overpredicts $^{26}\text{Mg}/\text{Mg}$ for $[\text{Al}/\text{Fe}] < 0.8$. These results imply that the observed distribution of GC stars on the $[\text{Al}/\text{Fe}]$ and $^{26}\text{Mg}/\text{Mg}$ plane can contain both the Mg isotope yields and the earlier chemical enrichment of GMCs by AGB stars.

4.9 C isotope ratios

Carbon isotopic ratios provide a complementary diagnostic to lithium abundances in constraining GC formation,

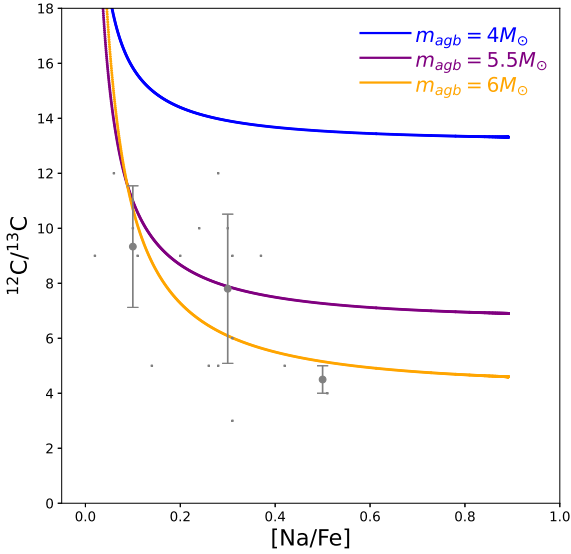


Figure 18. $^{12}\text{C}/^{13}\text{C}$ ratios as a function of $[\text{Na}/\text{Fe}]$ in the three models with $m_{\text{agb}} = 4M_{\odot}$ (blue), $m_{\text{agb}} = 5.5M_{\odot}$ (purple), and $m_{\text{agb}} = 6M_{\odot}$ (orange). The observed data points from Carretta et al. (2015) are plotted by small gray circles, and the mean and 1σ dispersion for $[\text{Na}/\text{Fe}]$ bins are indicated by large gray points and error bars, respectively. AGB yields from a selected mass (m_{agb}) are used in each model (i.e., no IMF-averaged yields are used).

but share the same fundamental observational limitations. Both $^{12}\text{C}/^{13}\text{C}$ and $A(\text{Li})$ are modified by stellar evolution as stars ascend the RGB. ^{12}C is progressively converted to ^{13}C through proton capture, producing lower ratios in the ejecta of more massive stars that reach higher temperatures. Therefore, meaningful comparisons between GC formation models and observations require measurements of unevolved main-sequence or subgiant stars. The distributions of stars on the $^{12}\text{C}/^{13}\text{C}$ - $[\text{Na}/\text{Fe}]$ plane predicted from the present models need to be compared with those observed for unevolved stars in GCs. Since Carretta et al. (2005, C05) is the main study in which C isotope ratios are investigated for dwarfs and subgiants in a few GCs, we here use their observational results. Since ^{12}C and ^{13}C yields are available for a limited mass range of AGB stars in K10, we are unable to calculate the IMF-averaged yields. We accordingly use the yields from a selected mass m_{agb} (4.0, 5.5, and $6.0M_{\odot}$) for $Z = 0.0001$ from K10. We here use the yields from K10 and adopt the same model parameters (e.g., F_{dil}) as those used in the fiducial model. Fig. 18 compares the predicted distributions of stars on the $[\text{Na}/\text{Fe}]$ - $^{12}\text{C}/^{13}\text{C}$ plane in three models with different m_{agb} with the corresponding observational results from C05. Clearly, the models with $m_{\text{agb}} = 5.5$ and $6M_{\odot}$ can reproduce the observed low $^{12}\text{C}/^{13}\text{C}$ ratios of GC stars from C05, which implies that the observed $^{12}\text{C}/^{13}\text{C}$ ratios can provide some constraints on the mass range of AGB stars polluting GMCs.

The observed anticorrelation between $^{12}\text{C}/^{13}\text{C}$ and $[\text{Na}/\text{Fe}]$ is at least qualitatively reproduced by the present models with higher m_{agb} . However, it is observationally un-

clear whether or not $[\text{Na}/\text{Fe}]$ - $^{12}\text{C}/^{13}\text{C}$ anticorrelations are as ubiquitous as O-Na anticorrelations in GCs with different masses and metallicities (i.e., not just observed in the three GCs by C05). Given the number of unevolved stars with estimated $^{12}\text{C}/^{13}\text{C}$ in C05 is only 18, it would be too early for this study to discuss whether the shape of the observed $[\text{Na}/\text{Fe}]$ - $^{12}\text{C}/^{13}\text{C}$ anticorrelation in C05 is consistent with the prediction. Although Smith et al. (1995) and Maas et al. (2019) also derived $^{12}\text{C}/^{13}\text{C}$ ratios in a few GCs, their sample stars are red giants (i.e., not unevolved stars) for which $^{12}\text{C}/^{13}\text{C}$ ratios have been much altered from their original values due to first dredge up, and mixing during the RGB bump. Since the observed $^{12}\text{C}/^{13}\text{C}$ ratios and $[\text{Na}/\text{Fe}]$ - $^{12}\text{C}/^{13}\text{C}$ can give strong constraints on the theory of GC formation with MPs, as discussed later in this paper, it is crucial for future observational studies to derive $[\text{Na}/\text{Fe}]$ and $^{12}\text{C}/^{13}\text{C}$ for a much larger number of unevolved stars in GCs.

5 DISCUSSION

Based on these results, we here provide theoretical interpretations and implications for the various observed properties of GCs with MPs: Table 3 summarizes which observational properties can (and cannot) be reproduced well by the new GC formation scenario. We do not discuss several key properties of GCs, such as the binary star fractions in 1P and 2P (e.g., Lucatello et al. 2015; Dalessandro et al. 2018) and the central concentrations of 2P populations (e.g., Leitinger et al. 2023), because this study does not utilize numerical simulations of GC formation.

5.1 Surface densities of massive AGB stars (Σ_{agb}) as a key to MP phenomena

5.1.1 $\Sigma_{\text{SFR}}-F_{2\text{P}}$ correlation

The interaction of GMCs with AGB stars is a physical process indispensable for the formation of GCs with MPs in the SCI scenario. If GCs all form within the gas disks of galaxies, then the surface number densities of AGB stars with ages of 0.02–0.1 Gyr (Σ_{agb}) within and around growing GMCs represent the key parameter controlling the GMC–AGB interaction process. Σ_{agb} could vary radially within a galaxy, and the mean Σ_{agb} could differ dramatically between galaxies of different masses and morphological types. Since Σ_{agb} is not a directly observable property of a galaxy, we have proposed that the star formation rate surface density (Σ_{SFR}) can serve as an observable indicator to assess whether massive SCs in star-forming galaxies can develop MPs. Furthermore, the scenario predicts a positive correlation between Σ_{SFR} and $F_{2\text{P}}$, suggesting that the observed diversity in $F_{2\text{P}}$ can be discussed in the context of the baseline Σ_{SFR} in GC-forming galaxies.

For example, a rather high Σ_{SFR} (≈ 3 – $10 M_{\odot} \text{ yr}^{-1} \text{ kpc}^{-2}$) is observed in the gravitationally lensed Sunburst galaxy at $z = 2.37$ (Vanzella et al. 2022). Mowla et al. (2024) discovered 10 massive young SCs within a $1 \text{ kpc} \times 1 \text{ kpc}$ region of a star-forming, low-mass galaxy with a possible current SFR of $\approx 1 M_{\odot} \text{ yr}^{-1}$ at $z = 8.3$, implying that Σ_{SFR} in such systems is high enough to generate MPs within their constituent clusters.

Table 3. Comprehensive diagnosis of the SCI scenario. If the predicted property for each diagnostic item is consistent (inconsistent) with observations (1st column) at least qualitatively, ✓ (✗) is given in the second column. It should be stressed here that ✓ does not necessarily mean "quantitatively consistent" with observations. If the listed observation is yet to be explained by the scenario, "?" is given. The physical processes/conditions involved in reproducing observations are briefly given in the 3rd column

Observation	Consistency	Required physics/conditions
(A) Correlation with GC mass		
Anticorrelation between F_{1P} and M_{gc}	✓	Higher R_s for larger M_{gmc}
Correlation between δY and M_{gc}	✓	Higher R_s for larger M_{gmc}
(B) Abundance patterns		
Ubiquitous Na-O anticorrelations in the Galactic GCs	✓	Enrichment by AGB stars (IMF-averaged yields)
Diversity in O-Na anticorrelations	✓	Diversity in IMF-averaged AGB yields
Steep or no O-Na anticorrelation in the bulge GCs	✓	Metallicity-dependent AGB yields
Metallicity-dependent Mg-Al anticorrelations	✓	Metallicity-dependent AGB yields
C-N anticorrelations	✓	Diversity in IMF-averaged AGB yields
Mg-K anticorrelations	✓	Major contributions of sAGB stars
Flat Na-Li and Al-Li relations	✓	Significant contributions of AGB stars producing Li
Li variations	✓	Diversity in AGB fractions producing Li
Positive $^{26}\text{Mg}/\text{Mg}$ -Mg correlation	✓	Contributions of massive AGB stars
Helium spreads between 1P and 2P	✗	Helium yields need to be reduced ?
(C) MPs in young clusters		
No MPs phenomena in young clusters	✓	Too low mass densities of AGB stars
MPs phenomena in intermediate-age LMC clusters	✓	Higher mass densities of AGB stars due to starburst
(D) Type I-II GCs		
Type I and II GC dichotomy	✓	Merging of GCs formed in gas-rich dwarf galaxies
Two distinct O-Na anticorrelations in Type II	✓	Chemical enrichment in two different GMCs
High fraction of s-rich stars in Type II	✓	Chemical enrichment by field AGB stars
Diverse fractions of s-rich populations in Type II	✓	Diversity in the mass-ratios of GC merging
Chemical abundances of s-rich populations in Type II	✓	Chemical enrichment by low-mass AGB stars
Type II GC fraction in the Galaxy	?	Diverse GC merging probability in dwarfs ?
(E) 1P-2P difference		
Structural differences between 1P and 2P	?	Efficient enrichment in inner GMCs ?
Kinematic differences between 1P and 2P	?	Radially dependent gas kinematics of GMCs ?
Binary star fractions in 1P and 2P	?	Efficient binary formation in inner GMCs ?
Larger metallicity spreads in 1P	✓	Pre-existing 1P stars around GMCs
(F) Miscellaneous		
Possible dependence of F_{2P} on GC ages and $[\text{Fe}/\text{H}]$	✓	Higher R_s for GC-host galaxies with lower $[\text{Fe}/\text{H}]$ and higher z
F_{1P} - $\delta_{\text{max}}Y$ anticorrelation	✓	Dilution factor dependent on GMC mass
Discrete MPs	?	Different levels of enrichment in smaller gas clouds ?
Smaller abundance spread in light s-process elements	✓	Pollution by massive AGB stars
P-rich stars in a few GCs	✓	GMCs polluted by AGB stars and ONE nova
Stellar halos around GCs	✓	Pre-existing field stars around GMCs
Apparent lack of cold gas in young SCs	✓	All stars formed before GMC dispersal

Conversely, young SCs observed in present-day galaxies with low $\Sigma_{\text{SFR}} \leq 1 \text{ M}_{\odot} \text{ yr}^{-1} \text{ kpc}^{-2}$ (e.g., Adamo et al. 2020) are highly unlikely to develop MPs. Main-sequence galaxies with baseline values of $\Sigma_{\text{SFR}} \leq 0.1 \text{ M}_{\odot} \text{ yr}^{-1} \text{ kpc}^{-2}$ are similarly highly unlikely to host young SCs with MPs, though they can still successfully form SCs without chemical anomalies. While the formation of young massive SCs is observed in interacting ultra-diffuse galaxies (UDGs) with low Σ_{SFR} (e.g., Buzzo et al. 2025), and recent numerical simulations have confirmed that massive SCs can form in interacting and merging gas-rich UDGs (Truman et al. 2026), we suggest that these SCs in UDGs are highly unlikely to host MPs due to their rather low ambient Σ_{SFR} .

5.1.2 Two types of young massive clusters with and without MPs

The present study predicts that neither ages nor metallicities are fundamentally important parameters for the formation of GCs with MPs. It furthermore predicts that massive young clusters formed in gas-rich galaxies cannot

possess MPs if the baseline Σ_{SFR} in their hosts is low. For example, the Σ_{SFR} of the present-day LMC is around $2 \times 10^{-3} \text{ M}_{\odot} \text{ yr}^{-1} \text{ kpc}^{-2}$ (for an SFR of $0.15 \text{ M}_{\odot} \text{ yr}^{-1}$ and $R = 5 \text{ kpc}$), which is extremely low compared with the required threshold value of $\Sigma_{\text{SFR}} \approx 1 \text{ M}_{\odot} \text{ yr}^{-1} \text{ kpc}^{-2}$. Accordingly, the present-day LMC is highly unlikely to form GCs with MPs, even if it can still form massive young star clusters via dynamical interactions with the SMC. Recent observations have shown that clusters with ages younger than $\approx 2 \text{ Gyr}$ do not display MPs, leading to the suggestion of an explicit "age threshold" for GC formation with MPs. However, the present study suggests that this observed apparent age threshold is caused not by a physical age constraint, but rather by the very low Σ_{SFR} characterizing the LMC over the last 2 Gyr.

The LMC is observed to have experienced a significant enhancement in its global SFR a few billion years ago, likely because it interacted strongly with both the MW and the SMC (e.g., Harris & Zaritsky 2009). Such galaxy-scale interactions could dramatically increase the local Σ_{SFR} around star-forming GMCs, ultimately triggering the forma-

tion of GCs with MPs. Therefore, the observed existence of intermediate-age GCs hosting MPs (e.g., Martocchia et al. 2018; Li et al. 2021) could be due to a strong starburst event a few Gyr ago in the LMC rather than an intrinsic age effect. Similarly, the formation of intermediate-age GCs with MPs in the SMC (e.g., Niederhofer et al. 2017; Hollyhead et al. 2018) could be attributed to a strong starburst about 6 Gyr ago associated with the assembly of its spheroidal component through the major merger of two gas-rich dwarfs.

The present scenario furthermore predicts that young massive SCs formed in luminous galaxy mergers (e.g., the Antennae) cannot possess MPs if the local Σ_{SFR} within their birthplace environments is too low. A prime example of such a young massive cluster is Cluster 1 in NGC 34, which features $M_{\text{gc}} = 10^7 M_{\odot}$ at an age of ≈ 100 Myr (Cabrera-Ziri et al. 2014) yet lacks light-element variations. Thus, present-day galaxies with low global Σ_{SFR} , such as the MW and the LMC, are unlikely to host newly forming massive SCs with MPs.

Blue compact dwarf galaxies (BCDs) with highly compact sizes ($R \approx 1$ kpc) and high star formation rates ($> 1 M_{\odot} \text{ yr}^{-1}$) represent the most promising environments for hosting forming GCs with MPs in the present-day universe. However, it is currently impossible for spectroscopic studies of young clusters in BCDs to directly resolve star-to-star variations of chemical abundances. If the mean $[\text{N}/\text{Fe}]$ ratios of these unresolved SCs in BCDs are observed to be quite high (≥ 0.5), then these systems can be inferred to host a significant fraction of 2P stars with enhanced nitrogen. We predict a strong positive correlation between the mean $[\text{N}/\text{Fe}]$ of these SCs derived from integrated-light spectroscopy and the global Σ_{SFR} of their host star-forming dwarf galaxies.

5.1.3 Can $F_{2\text{P}}$ depend on GC ages and metallicities?

ME20 investigated how the 2P mass fraction ($F_{2\text{P}}$) of GCs correlates with cluster mass (M_{gc}), age (T_{age}), and metallicity ($[\text{Fe}/\text{H}]$) in Galactic GCs observed by APOGEE. Although they did not confirm the positive correlation between $F_{2\text{P}}$ and M_{gc} previously discovered by other studies (e.g., C09a; Milone & Marino 2022), they revealed a positive correlation between T_{age} and $F_{2\text{P}}$ alongside an anticorrelation between $[\text{Fe}/\text{H}]$ and $F_{2\text{P}}$. At first glance, the new scenario appears unable to explain the origin of these relationships because the formation epochs and gaseous metallicities of GMCs are not the parameters that directly determine $F_{2\text{P}}$. However, if galaxies during their earlier assembly phases systematically experience higher Σ_{SFR} , then the massive SCs formed during those epochs will evolve into the present-day GCs characterized by older T_{age} and higher $F_{2\text{P}}$. Since these early-phase host galaxies also feature less enriched interstellar media, their constituent SCs will naturally evolve into modern GCs with lower $[\text{Fe}/\text{H}]$ and higher $F_{2\text{P}}$.

To quantitatively verify whether $F_{2\text{P}}$ can depend on T_{age} and $[\text{Fe}/\text{H}]$, we have run several one-zone chemical evolution models of galaxies using the numerical code developed by Bekki & Tsujimoto (2012); Appendix C briefly describes these models and their results. We find that Σ_{SFR} is systematically higher during the early epochs of galactic chemical evolution, which directly implies that GCs formed earlier (and thus possessing older T_{age}) will exhibit higher

$F_{2\text{P}}$ values. We also find that Σ_{SFR} is systematically higher at lower $[\text{Fe}/\text{H}]$, down to a threshold metallicity floor that depends on the gas infall timescale (τ_{inf}). This result similarly implies that GCs with lower $[\text{Fe}/\text{H}]$ are more likely to host larger 2P fractions. While the above arguments remain somewhat qualitative within these idealized one-zone models—given that the actual co-evolution of $[\text{Fe}/\text{H}]$ and Σ_{SFR} is determined by complex structural processes of galaxy formation—we will discuss the physical origins of these trends in a more quantitative manner in a forthcoming paper based on hydrodynamical simulations of GC assembly within evolving dark matter halos.

5.1.4 Is $F_{2\text{P}}$ different between in situ and accreted GCs?

Monty et al. (2024) recently demonstrated that the abundance ratios of europium to α elements ($[\text{Eu}/\alpha]$) in Galactic GCs can be utilized to distinguish between in situ and accreted (ex situ) populations. One plausible reason for the elevated $[\text{Eu}/\alpha]$ ratios in ex situ GCs is that their host dwarf galaxies possessed a top-light IMF characterized by either a steeper high-mass slope or a reduced upper-mass cutoff (e.g., Tsujimoto 2024). A top-light IMF has also been invoked to explain the detailed chemical abundance patterns of massive dwarf galaxies in the Local Group, such as the Fornax dwarf spheroidal (e.g., McWilliam et al. 2013). Such a top-light IMF is expected in star-forming galaxies with lower overall star formation rates according to the integrated galaxy-wide IMF theory (e.g., Weidner & Kroupa 2005), implying that a top-light IMF is a natural consequence of lower Σ_{SFR} .

If the defunct dwarf galaxies hosting ex situ GCs possessed lower baseline values of Σ_{SFR} (and thus a top-light IMF), then the SCI scenario suggests that ex situ GCs with elevated $[\text{Eu}/\alpha]$ should systematically display lower $F_{2\text{P}}$ values for a given global cluster mass M_{gc} . Because it is observationally established that $F_{2\text{P}}$ depends strongly on M_{gc} (e.g., C09a), discovering a clear, isolated signature in $F_{2\text{P}}$ between in situ and ex situ GCs may prove observationally challenging. Furthermore, this hypothesis assumes that a top-light IMF is the primary driver of elevated $[\text{Eu}/\alpha]$ ratios in accreted clusters; if other environmental factors play a dominant role in determining $[\text{Eu}/\alpha]$ in ex situ GCs, then the predicted difference in $F_{2\text{P}}$ between the two populations becomes less definitive. Notably, Lardo et al. (2026) have recently revealed a wide diversity of $F_{2\text{P}}$ values among different accreted GC streams (such as the Sequoia stream showing $F_{2\text{P}} \approx 0.45$). Within the framework of the new scenario, this behavior can be naturally explained by variations in the baseline Σ_{SFR} environments among the different defunct dwarf galaxies that originally hosted these clusters.

5.2 Type II GC formation from GC merging

The origin of metal-complex Type II GCs is yet to be fully understood. The observed significant $[\text{Fe}/\text{H}]$ spreads can result either from (i) secondary star formation and the subsequent iron enrichment in existing GCs (e.g., D’Antona et al. 2016) or (ii) the merging of GCs with different $[\text{Fe}/\text{H}]$ (BY12, BT16). The self-enrichment scenario of star-forming GMCs by multiple CCSNe (e.g., Bailin 2018; Wirth et al. 2021) might also be responsible for the formation of Type

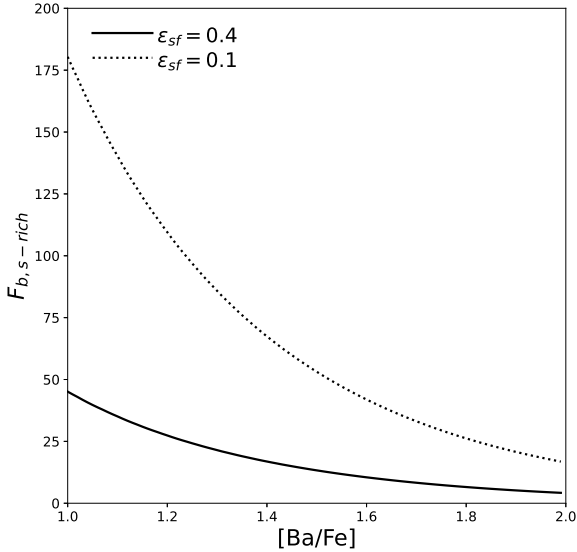


Figure 19. Mass budget factors for s -rich stars ($F_{b,s-rich}$) as a function of $[Ba/Fe]$ of polluting AGB stars for $\epsilon_{sf} = 0.4$ (solid) and 0.1 (dotted). The observed total stellar masses and $[Ba/Fe]$ in s -poor and s -rich stars in M22 are used to plot these. $F_{b,s-rich} > 1$ means that the total mass required to explain the observed $[Ba/Fe]$ of s -rich stars is larger than the total mass of s -poor stars. The required large $F_{b,s-rich}$ in this figure thus clearly demonstrates the mass budget problem for s -rich stars in M22.

II GCs, although these studies did not discuss the origin of the s -poor and s -rich populations within the clusters. We first point out a severe mass-budget problem regarding s -rich populations in Type II GCs based on the observed properties of M22, and then discuss how GC merging can better explain the physical properties of Type II GCs.

5.2.1 The severe mass-budget problem of s -rich populations

We here divide the stars of a Type II GC into two categories: an s -poor population with lower $[Fe/H]$ and $[Ba/Fe]$, and an s -rich one with higher $[Fe/H]$ and $[Ba/Fe]$. The total GC mass is accordingly the sum of the total mass of the s -poor ($M_{gc,s-poor}$) and s -rich populations ($M_{gc,s-rich}$):

$$M_{gc} = M_{gc,s-poor} + M_{gc,s-rich}. \quad (35)$$

Using the observed properties of M22 (e.g., an s -rich fraction of ≈ 0.5), we can estimate (i) the total mass of the initial gas (M_o) a fraction of which can evolve into low-mass AGB stars and (ii) the mass-budget factor for the s -rich population:

$$F_{b,s-rich} = \frac{M_o}{M_{gc,s-poor}}. \quad (36)$$

If this factor is quite large (> 10 , i.e., $M_o \gg M_{gc,s-poor}$), then it suggests that the s -poor population is unlikely to be responsible for the formation of the s -rich population in M22. As discussed in §2.3, the present-day mass of the s -rich population should be smaller than its original mass because

it can lose a fraction of its original mass through stellar evolution and internal/external dynamical processes:

$$M_{gc,s-rich} = (1 - f_{lost})\epsilon_{sf}M_o, \quad (37)$$

where $\epsilon_{sf}M_o$ corresponds to the original mass of the s -rich population, and f_{lost} and ϵ_{sf} represent the mass loss fraction and the star formation efficiency, respectively. We here adopt $f_{lost} = 0.4$, and $\epsilon_{sf} = 0.1$ and 0.4.

We here assume that the s -rich population is formed from pristine gas mixed with stellar winds from the s -poor, low-mass AGB stars. The observed difference in $[Ba/Fe]$ between the two distinct populations is defined as follows:

$$\Delta[Ba/Fe] = [Ba/Fe]_{s-rich} - [Ba/Fe]_{s-poor}. \quad (38)$$

Likewise, we use $\Delta[Fe/H]$ and Δt_{age} for the $[Fe/H]$ and age differences between the two populations, respectively. The Ba abundance of the s -rich population ($A_{Ba,s-rich}$) can be calculated using the total mass of pristine gas (M_g), the AGB ejecta mass (M_{ej}), and the Ba yield of low-mass AGB stars ($f_{Ba,ej}$):

$$A_{Ba,s-rich} = \frac{f_{Ba,g}M_g + f_{Ba,ej}M_{ej}}{M_g + M_{ej}}, \quad (39)$$

where $f_{Ba,g} = f_{Ba,s-poor}$ and $M_o = M_g + M_{ej}$. Since $[Ba/Fe]_{s-rich} (= 0.55)$, $[Ba/Fe]_{s-poor} (= 0)$, and the fraction of Ba-rich stars ($= 0.5$) are observed, we can estimate M_g (and thus M_o and $F_{b,s-rich}$) for a given M_{ej} . Since a narrow mass range of AGB stars polluting the intracluster gas ($3 \leq m_{agb}/M_\odot \leq 4$) is required to produce Ba-rich ejecta and explain the observed possible age difference between the s -poor and s -rich populations (e.g., Marino et al. 2015; McKenzie et al. 2022), we adopt $f_{agb} = 0.03$ as a fiducial value. We investigate $F_{b,s-rich}$ for $[Ba/Fe]$ yields ranging from 1 to 2 for low-mass stars.

As shown in Fig. 19, $F_{b,s-rich}$ is quite high, ranging from 20 to 180 for $\epsilon_{sf} = 0.1$, which means that M_o should be as large as $8.8 \times 10^6 M_\odot$ for $\epsilon_{sf} = 0.1$. Given that the total mass of s -poor stars in M22 is only $\approx 2 \times 10^5 M_\odot$, the required large M_o is clearly the manifestation of a “mass-budget problem” that is more severe than the mass-budget problem for GCs with high 2P fractions. $F_{b,s-rich}$ ranges from 5 to 45 for $\epsilon_{sf} = 0.4$, which means that the required M_o is still much larger than the mass of s -poor stars. Thus, chemical enrichment by AGB stars from s -poor stellar populations cannot explain the observed total mass of s -rich stars in M22.

Chemical evolution models of dwarf galaxies predict that $[Fe/H]$ and $[Ba/Fe]$ can increase by ≈ 0.2 dex and ≈ 0.5 dex, respectively, within 300 Myr, depending on the adopted star formation histories and IMFs (BT16). Therefore, if two GCs form from separate GMCs at different epochs within their host dwarf galaxy separated by ≈ 300 Myr and then merge together to form a new single GC, the new GC can have both s -poor (formed earlier) and s -rich (formed later) populations. Since each of the merger progenitor GCs contains MPs, the new GC should have MPs in both its s -poor and s -rich populations. Accordingly, this GC merger scenario can naturally and self-consistently explain both (i) the observed high fraction of s -rich populations and (ii) the presence of MPs in both the s -poor and s -rich populations of M22. We thus suggest that GC merging is not limited to M22, but is an essential ingredient in the formation of Type II GCs.

5.2.2 Diversity in Type II GC properties?

GC merging is more likely to occur among more massive GCs with higher internal stellar velocity dispersions (σ_{gc}) within their host dwarf galaxies, because σ_{gc} should be comparable to the stellar velocity dispersion of the hosts. The mass ratio of two merging GCs can vary, which explains the observed diversity in the fractions of metal-rich populations. Using N -body simulations of GC merging, Gavagnin et al. (2016) demonstrated that the radial profiles of 1P-to-2P ratios and the rotational kinematics of the merger remnants (e.g., solid-body or differential rotation) depend on the mass and density ratios of the two progenitor clusters. Their results imply that there can be diversity in the radial profiles of F_{1P} and rotational kinematics among Type II GCs.

Our recent hydrodynamical simulations of GC formation in gas-rich mergers have shown that multiple mergers among a number of massive young star clusters (SCs) lead to the formation of nuclear SCs with large [Fe/H] and age spreads (Matsui et al. 2025; Truman et al. 2026). The origin of MPs in Type II GCs like ω Cen and M54, which might have originated from the nuclei of defunct dwarf galaxies, can therefore be understood in the context of GC merging. Since age differences between stars in Type II GCs can be quite diverse due to the different formation epochs of the two merging GCs in this scenario, there could exist Type II GCs with large age spreads (e.g., 3 Gyr). However, such large age spreads have not been observationally confirmed in Type II GCs with two distinct populations. Possibly, two GCs forming at similar epochs can share similar 3D positions within their host galaxy (i.e., clustered GC formation), allowing them to merge together to form a new single Type II GC.

The observed fraction of Type II GCs ($\approx 20\%$) among Galactic GCs suggests that only 20% of the initial GC populations formed in their host galaxies merged to form Type II GCs. It is not entirely clear why only $\approx 20\%$ of GCs experienced merger events within their host galaxies in the GC merging scenario. Our future studies need to clarify the origins of these observed diverse Type II GC properties based on more sophisticated simulations of GC formation in galaxies.

Terzan 5 is observed to host two distinct populations with [Fe/H] = -0.8 and 0.3 at least (e.g., Ferraro et al. 2009; Zullo et al. 2026), featuring a very large age spread of ≈ 7 Gyr between them (e.g., Zullo et al. 2026). Although the origin of this GC or “bulge fossil” (Ferraro et al. 2009) can also be discussed in the context of GC merging within the Galactic bulge, it remains unclear how a GC merger could occur 7 Gyr after the formation of the progenitor GC with [Fe/H] = -0.8 . Furthermore, all delayed CCSNe and most SNe Ia would have already exploded 7 Gyr after the formation of the initial [Fe/H] = -0.8 population. Therefore, for this particular cluster, secondary star formation fueled by gas accretion onto the GC and a subsequent starburst (e.g., McKenzie & Bekki 2018; Romano et al. 2023) provides a compelling alternative scenario for the formation of Terzan 5.

5.3 Larger metallicity spreads in 1P stars?

Our recent hydrodynamical simulations of GC formation in gas-rich dwarf galaxies have predicted that GC-forming GMCs can have large [Fe/H] spreads (typically 0.1 dex) due to (i) the merging of smaller clouds with different [Fe/H] formed at different locations within their host galaxies and (ii) self-enrichment by stellar feedback effects (McKenzie & Bekki 2021b). Furthermore, they have also predicted that (i) GC-forming GMCs can gravitationally trap the surrounding field stars of their host dwarf galaxies and (ii) these trapped stars can eventually become a more metal-poor precursor population (“0P”). Since the 1P consists of stars formed earlier in GMCs and field stars trapped by GMCs in this new scenario, these simulation results imply that the 1P can have larger metallicity spreads. It is possible that GCs formed in galaxies with steeper metallicity gradients have larger metallicity spreads among their 1P stars in the new scenario.

The 2P stars can form from GMC gas mixed with AGB ejecta later than 1P stars in this scenario. Accordingly, they are highly likely to form from gas that has already experienced metal homogenization due to turbulent mixing within the GMCs. 2P stars can therefore have smaller metallicity spreads than 1P stars in this scenario. Since this explanation is speculative and not very quantitative, we will need to investigate whether and how metal diffusion processes within GC-forming massive GMCs can reduce the initial metallicity spreads of the GMCs using new hydrodynamical simulations of GC formation in galaxies.

Recent HST observations have shown that 1P stars display larger degrees of metallicity spreads compared with their 2P counterparts (e.g., Legnardi et al. 2022). However, Carretta & Bragaglia (2025) were not able to confirm such large metallicity spreads in 1P stars. Lardo et al. (2022), on the other hand, confirmed large metallicity spreads among red giant branch stars from the 1P in M92, NGC 2808, and NGC 6362. Although ME20 found that the typical intrinsic [Fe/H] scatter in GCs observed by APOGEE is about 0.1 dex and does not depend on GC masses and ages, they did not discuss whether 1P stars have larger [Fe/H] spreads. The question of whether 1P stars have larger [Fe/H] spreads remains actively debated, and disentangling intrinsic metallicity variations from systematic photometric and spectroscopic effects will require coordinated approaches to large homogeneous GC samples. The next generation of high resolution spectroscopic facilities will help to resolve these tensions.

5.4 Li abundances as a crucial diagnosis for different GC formation scenarios

Recent spectroscopic studies of Li abundances ($A(\text{Li})$) and their correlations with light-element abundances in GCs with MPs have revealed that Li is not very depleted in 2P stars with rather high [Na/Fe] (e.g., McKenzie et al. in prep). These results disfavour GC formation scenarios in which polluters destroy Li but cannot produce it at all. As shown in this paper, these observations are consistent with the SCI scenario, and they can be used as a new constraint on the fraction of AGB stars that can produce Li due to the Cameron-Fowler effect. G19 have already shown that

the simple dilution of gaseous ejecta from polluters by pristine gas cannot explain the observed levels of Li depletion in GCs; we have shown for the first time that the observed levels can be naturally explained by our models, with $\approx 20\%$ of AGB stars producing Li.

The observed Li depletion ($A(\text{Li}) \approx 0.2$ dex) in the extreme “E” populations of some GCs indicates that these stars were formed from pristine gas chemically enriched by polluters in which Li was destroyed (G19). This observation and the observed lack of an Li-Al anticorrelation combine to suggest that there should be polluters producing and destroying Li during GC formation: a single type of polluter cannot explain the observations self-consistently. D12 showed that (i) $A(\text{Li})$ depends strongly on the masses of AGB stars (m_{agb} in units of M_{\odot}), (ii) $A(\text{Li})$ can be rather large, reaching $A(\text{Li})=2.75$ and 4.39 for $m_{\text{agb}} = 7.5$ and 8.0 , respectively, and (iii) $A(\text{Li})$ values are less than 2.3 for $4 \leq m_{\text{agb}} \leq 6.3$. If GMCs are polluted by larger fractions of AGB stars with $4 \leq m_{\text{agb}} \leq 6.3$, GCs can have larger fractions of E populations. Given that IMF slopes determine the fractions of these intermediate-mass AGB stars, the observed diverse fractions of E populations might imply that IMF slopes vary across different GCs.

The observed anticorrelation between $A(\text{Li})$ and $[\text{Na}/\text{Fe}]$ in NGC 6752 and NGC 6397 is suggested to be consistent with the pollution of pristine gas by intermediate-mass AGB stars (e.g., Pasquini et al. 2005; Lind et al. 2009). Shen et al. (2010) pointed out that the observed extended Li-O correlation in unevolved stars can be explained not by Li-poor ejecta mixed with (i.e., diluted by) pristine gas alone, but by Li-poor ejecta mixed with both pristine gas and Li-enriched gas. Although Bonifacio et al. (2007) found an Li-Na anticorrelation among 4 turn-off stars in 47 Tuc, Dobrovolskas et al. (2014) did not find convincing evidence for it among 110 turn-off stars. D’Orazi & Marino (2010) discovered that both the 1P and 2P in M4 share the same Li abundance and thus suggested that Li production is required to reproduce the observed flat $[\text{Na}/\text{Fe}]$ - $A(\text{Li})$ relation. Mucciarelli et al. (2011) found an almost flat $[\text{O}/\text{Fe}]$ - $A(\text{Li})$ relation among stars with a wide range of $[\text{O}/\text{Fe}]$ (i.e., both 1P and 2P) in M4, and Villanova & Geisler (2011) also showed almost identical mean $A(\text{Li})$ values between N-poor (1P) and N-rich (2P) stars in M4.

D’Orazi et al. (2014) revealed that Li production is required to reproduce the observed $[\text{Al}/\text{Fe}]$ - $A(\text{Li})$ relations in M5 and M12 and suggested that GC masses can possibly determine the extent to which Li production occurs. These existing observations, as well as observations from the Galactic Archaeology with HERMES (GALAH) survey (Buder et al. 2025), are difficult to reconcile with scenarios where the ejecta of the primary polluter is devoid of Li. If MP progenitors such as very massive stars, supermassive stars and massive interacting binary stars can not either retain, or regenerate Li, it may be challenging for them to reproduce these observations. The SCI scenario predicts that (i) the fraction of AGB stars producing Li (i.e., $P(\text{Li})$) can determine the $[\text{Al}/\text{Fe}]$ - $A(\text{Li})$ relations in GCs and (ii) $P(\text{Li})$ is a function of the IMF (e.g., α). If less massive GCs have larger $P(\text{Li})$, this new scenario can explain the observed smaller scatter of $A(\text{Li})$ in less massive GCs (D’Orazi et al. 2014). If less massive GCs have less top-heavy IMFs, they could have larger $P(\text{Li})$ due to a smaller fraction of massive AGB stars

with low $A(\text{Li})$ in their winds. It is theoretically unclear, however, how the IMF might depend on GC masses at their birth. It is thus the focus of our future study to investigate how the IMFs of GCs determine $P(\text{Li})$ and eventually cause the observed $A(\text{Li})$ dispersions that possibly depend on GC masses.

5.5 $^{12}\text{C}/^{13}\text{C}$ ratios in unevolved stars as a constraint on GC formation

C05 first derived $^{12}\text{C}/^{13}\text{C}$ ratios for 21 dwarfs and subgiants in NGC 6752 and NGC 104 using the CH molecular band. One intriguing result is that the $^{12}\text{C}/^{13}\text{C}$ ratios are quite low, ranging from 3 to 12 (see their Table 1), which led them to conclude that evolved intermediate-mass AGB stars are the most likely polluters for these GCs. If $^{12}\text{C}/^{13}\text{C}$ ratios are investigated for *unevolved stars* unaffected by stellar evolution in GCs with MPs, the observed ratios can provide crucial constraints on GC formation because the ratios are predicted to be significantly different between stellar winds from AGB stars and massive stars (e.g., Figs. 4 and 5 in Rizzuti et al. 2025).

The $^{12}\text{C}/^{13}\text{C}$ ratio in stellar winds from AGB stars with $m = 3M_{\odot}$ and $Z = 0.0001$ is ≈ 50 (K10), which suggests that chemical enrichment by low-mass AGB stars cannot explain the observed low $^{12}\text{C}/^{13}\text{C}$ ratios (< 12). These predictions will be tested against observational results when $^{12}\text{C}/^{13}\text{C}$ ratios are estimated for many unevolved 1P and 2P stars in GCs. Rotating and non-rotating massive stars with $13 \leq m/M_{\odot} \leq 120$ at $[\text{Fe}/\text{H}] = -2$ and -1 can eject stellar winds with rather large $^{12}\text{C}/^{13}\text{C}$ ratios ranging from ≈ 10 to 10^5 (Rizzuti et al. 2025); the IMF-averaged $^{12}\text{C}/^{13}\text{C}$ ratio is expected to be rather large (> 100) for a Salpeter IMF. Accordingly, it is possible that the $^{12}\text{C}/^{13}\text{C}$ ratio of 2P stars formed from these ejecta can be quite large too (> 100). This means that the future observational derivation of $^{12}\text{C}/^{13}\text{C}$ ratios in unevolved stars can provide a new constraint on GC formation scenarios. It is not clear whether the $^{12}\text{C}/^{13}\text{C}$ ratios of stellar winds from very massive stars, supermassive stars, and massive interacting binaries are as large as those of the massive stars mentioned above. It is thus safe to say that the low $^{12}\text{C}/^{13}\text{C}$ ratios observed in C05 are consistent with the predictions from the new scenario with $4 \leq m_{\text{agb}}/M_{\odot} \leq 10$.

5.6 $[\text{Na}/\text{Fe}]$ - $[\text{F}/\text{Fe}]$ anticorrelations ?

Fluorine occupies a unique nucleosynthetic position in the context of GC chemical enrichment, being produced and destroyed at the interface between the CNO and Ne-Na proton capture cycles. $[\text{F}/\text{Fe}]$ is sensitive to both the depth of the third dredge up, and the efficiency of HBB, making the Na-F anticorrelation a probe of the balance between these two competing processes in AGBs (Forestini et al. 1992, Lugaro et al. 2004, Karakas & Lattanzio 2014). Previous observations revealed (anti)correlations of $[\text{F}/\text{Fe}]$ with $[\text{O}/\text{Fe}]$ and $[\text{Na}/\text{Fe}]$ in several Galactic GCs, which provided a constraint on the nucleosynthesis site of polluting stars in GC formation (e.g., Cunha et al. 2003; Smith et al. 2005; Yong et al. 2008 Alves-Brito et al. 2012; D’Orazi et al. 2013). It is, however, observationally unclear whether these correlations and

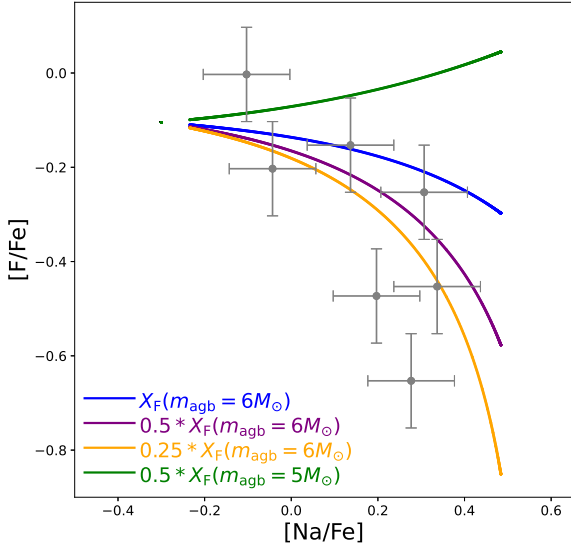


Figure 20. Evolution of the four models with $X_F = X_F(m_{\text{agb}} = 6M_{\odot})$ (blue), $0.5 \times X_F(m_{\text{agb}} = 6M_{\odot})$ (purple), $0.25 \times X_F(m_{\text{agb}} = 6M_{\odot})$ (orange), and $0.5 \times X_F(m_{\text{agb}} = 5M_{\odot})$ (green) on the $[\text{Na}/\text{Fe}]$ - $[\text{F}/\text{Fe}]$ plane. The observed abundances taken from Smith et al. (2005) for M4 are shown by gray circles with observational error bars. The observed Na-F anticorrelation can be better reproduced by the models with reduced F yields.

anticorrelations are ubiquitous in the vast majority of GCs (e.g., de Laverny & Recio-Blanco 2013). Nevertheless it is worthwhile for this study to investigate whether or not these observations can be well reproduced by the present scenario. We here particularly investigate the $[\text{Na}/\text{Fe}]$ - $[\text{F}/\text{Fe}]$ anticorrelation observed in M4 (Smith et al. 2005) by adopting the F yields from K10 for different m_{agb} at $Z = 10^{-4}$ in the fiducial model. Since the mass fraction of F (X_F) is available only for AGB stars with $m_{\text{agb}} \leq 6M_{\odot}$ (i.e., unable to derive an IMF-averaged F yield), we here demonstrate what X_F (thus what particular m_{agb}) can better reproduce the observed Na-F anticorrelation. We adopt the initial $[\text{Na}/\text{Fe}]$ of -0.3 and $[\text{Na}/\text{Fe}] = 0.6$ in AGB ejecta in all four models.

Fig. 20 shows the evolutionary loci of the four models with different X_F on the $[\text{Na}/\text{Fe}]$ - $[\text{F}/\text{Fe}]$ plane. For example, the model with $0.5 X_F(m_{\text{agb}} = 6M_{\odot})$ means that the F yield is the half of X_F for $m_{\text{agb}} = 6M_{\odot}$ adopted from K10. The model with $X_F(m_{\text{agb}} = 6M_{\odot})$ shows a $[\text{Na}/\text{Fe}]$ - $[\text{F}/\text{Fe}]$ anticorrelation that is significantly flatter than the observed one. As shown in the models with $X_F = 0.25 X_F(m_{\text{agb}} = 6M_{\odot})$ and $0.5 X_F(m_{\text{agb}} = 6M_{\odot})$, the F yields for $m_{\text{agb}} = 6M_{\odot}$ need to be reduced to match well with the observed Na-F anticorrelation. These results suggest that (i) $m_{\text{agb}} = 6M_{\odot}$ AGB models by K10 appear to overproduce F and (ii) other models with smaller X_F for massive AGB stars (e.g., Siess 2010) can possibly explain the Na-F anticorrelation better. The model with $X_F = 0.5 X_F(m_{\text{agb}} = 5M_{\odot})$ shows a Na-F correlation, which implies that AGB stars with $m_{\text{agb}} \leq 5M_{\odot}$ cannot contribute greatly to chemical enrichment in forming GCs.

Doherty et al. (2017) and Siess (2010) predicted

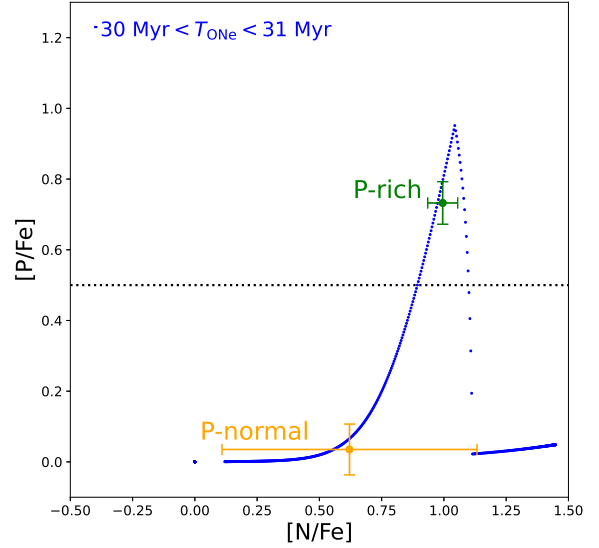


Figure 21. Evolution of the fiducial model with P-enrichment by ONe novae during GC formation within a GMC (blue dots). It is assumed in this model that ONe nova explosions can enrich cold gas of the GMC at time steps (T_{ONe}) between 30 and 31 Myr. The mean (filled circles) and 1σ dispersion of $[\text{P}/\text{Fe}]$ (error bars) are shown separately for “P-normal” ($[\text{P}/\text{Fe}] < 0.5$; orange) and “P-rich” stars ($[\text{P}/\text{Fe}] \geq 0.5$; green).

$[\text{F}/\text{Fe}] \approx 0$ and -2.4 , respectively for sAGB stars with $m_{\text{agb}} = 7.5M_{\odot}$ at $Z = 10^{-4}$. These vastly different F yields from the two groups make it difficult to assess the possible role of sAGB stars in the formation of the Na-F anticorrelation. If the F yields of sAGB stars are indeed very low ($[\text{F}/\text{Fe}] < -1$), mixing of pristine GMC gas with sAGB stars can end up with the formation of stars with $[\text{F}/\text{Fe}] < -0.6$. So far, other theoretical models based on other polluters (e.g., supermassive stars etc) are yet to comprehensively explore the constraints placed on the relationship between Na and F. It would be thus too early to make a robust conclusion on whether the Na-F anticorrelation is due to chemical enrichment by AGB and sAGB stars in forming GCs.

5.7 P-rich stars as a new clue to MPs phenomena

Recent observations have discovered “P-rich stars” in some Galactic GCs, such as M4 and NGC 6316 (e.g., Brauner et al. 2024; Barbuy et al. 2025). Although the nucleosynthesis sites for P production are yet to be fully understood (e.g., Masseron et al. 2020), one of the sites can be ONe novae formed from binary stellar systems with massive stars with $m > 7M_{\odot}$ (e.g., Bekki & Tsujimoto 2024). If multiple ONe nova explosions occur within and around star-forming GMCs, then the new stars formed from the gas mixed with ONe nova ejecta should be able to have high $[\text{P}/\text{Fe}]$ depending on the dilution levels. Given that ONe nova explosions start to occur $\sim 10^8$ yr after star formation events (e.g., Kemp et al. 2022), chemical enrichment of GMCs by ONe novae (from pre-existing 0P populations) can be discussed in the context of the SCI scenario. The SCI scenario ac-

cordingly needs to explain why star-forming GMCs can be chemically enriched by ONe novae so efficiently and why only some GCs have such P-rich stars.

In order to discuss P-enrichment in forming GCs in a more quantitative manner, we here investigate the fiducial model with $t_{\text{life}} = 5 \times 10^7$ yr and $F_{\text{dil}} = 1$, in which the ONe nova model adopted in Bekki & Tsujimoto (2023) is implemented. Fig. 21 shows the evolutionary locus of the model on the [N/Fe]-[P/Fe] plane in the model in which the mass of P per unit star-forming mass, initial [P/Fe], and [N/Fe] of AGB ejecta are assumed to be 1.69×10^{-7} , 0, and 1.5, respectively. Although the epoch of ONe nova explosions (T_{ONe}) determines the locus of a model on the [N/Fe]-[P/Fe] plane, ONe novae are assumed to occur at $30 \text{ Myr} \leq T_{\text{ONe}} \leq 31 \text{ Myr}$ in this model: It should be stressed here that this is only a possible locus on the [N/Fe]-[P/Fe] plane among many possible loci. Clearly, P-rich stars with $[\text{P}/\text{Fe}] > 0.5$ can be formed only after ONe nova explosions in this model, which demonstrates that ONe novae can be a possible candidate for polluting stars responsible for the origin of P-rich stars.

The predicted fraction of P-rich ($[\text{P}/\text{Fe}]$) stars is 0.05 in this particular model with a short timescale of P-enrichment by ONe novae, which will be able to be compared with future observational studies on the fraction of P-rich stars in GCs. Obviously, the P-rich star fractions in GCs strongly depend on the P yields and the epoch and the duration of ONe novae. If ONe novae occur later in GC formation (i.e., later in GMC evolution), as in this model, P-rich stars can also be N-rich (> 0.5) and have a smaller dispersion in [N/Fe] compared with P-normal stars with a larger [N/Fe] dispersion. Indeed, Barbuy et al. (2025) have found P-rich stars with high [N/Fe] in the Galactic bulge GCs, which is consistent with the model with $30 \text{ Myr} \leq T_{\text{ONe}} \leq 31 \text{ Myr}$. On the other hand, if ONe novae can occur only in the early GC formation phases, P-rich stars can have lower [N/Fe], because field AGB stars have not yet chemically enriched the pristine GMC gas. Therefore, whether P-rich stars are also N-rich is determined by when ONe novae explode.

It is also likely that ONe novae cannot always occur within and around GC-forming GMCs, because binary fractions of massive stars could be quite small in some GMCs, which means that only some GCs can have P-rich stars. Since the total number of ONe novae can be small due to the short lifetime of GMCs, the level of P-enrichment is likely to show a large cluster-to-cluster variation. This stochastic ONe nova enrichment scenario can explain why Barbuy et al. (2025) found P-rich stars with $[\text{P}/\text{Fe}] > 0.5$ only in a few GCs. This observed presence and absence of P-rich stars in GCs can be nicely explained by the P-enrichment of GMCs by sporadic ONe nova events.

CCSNe originating from massive stars with pre-supernova carbon-oxygen (C-O) shell merging are demonstrated to produce a large amount of P and are thus a major driver for the chemical evolution of P in the Galaxy (e.g., Ritter et al. 2018). However, such CCSNe with O-C shell merging cannot be responsible for the formation of P-rich stars in GCs with small [Fe/H] spreads, because CCSNe can introduce large [Fe/H] spreads in GCs with MPs. Therefore, ONe novae originating from binary stars appear to be the only polluter that is responsible for the formation of P-rich stars in GCs. If this is the case, then it would be reason-

able to propose that P-rich stars discovered in the Galactic field (e.g., Masseron et al. 2020) can also be formed from gas enriched by ONe novae. It is, however, unclear whether these P-rich field stars were formed in GC-forming GMCs or in the ISM enriched by ONe novae. It is likely that the high-density cold gas of GMCs can dramatically decelerate the high-speed ($1600 - 6000 \text{ km s}^{-1}$) ONe nova ejecta to finally trap it for further star formation. The present study accordingly suggests that the chemical properties of P-rich stars in GCs with small [Fe/H] spreads can also provide a clue to the origin of the Galactic P-rich field stars.

5.8 Abundance spreads in light *s*-process elements ?

Internal abundance spreads in *s*-process elements have been so far revealed in a number of the Galactic GCs with MPs such as NGC 1851, and M22 (Yong & Grundahl 2008, Yong et al. 2009, 2014; Marino et al. 2015; McKenzie et al. 2022). The detailed abundance patterns of GC stars with abundance enhancement in *s*-process elements can not only determine the nucleosynthesis site (e.g., AGB stars or massive stars) but also constrain the mass range of the polluters (e.g., Shingles et al. 2014; McKenzie et al. 2022). For example, Yong et al. (2014) suggested that AGB stars with $3-5M_{\odot}$ are the major polluters responsible for the formation of MPs in M2 based on the observed ratios of light (*ls*) and heavy (*hs*) *s*-process abundances ($[ls/hs]$) as well as [Pb/La]. Yong et al. (2012) also found a possible correlation of [Y/Fe] and [Zr/Fe] (light *s*-process elements) with [Na/Fe] in M2, which would support chemical pollution by AGB stars in forming GCs.

The present study did not investigate the time evolution of light *s*-process elements in forming GCs, though recent AGB and sAGB models have provided theoretical predictions on these chemical yields. For example, Doherty et al. (2017) predicted [X/Fe] for light *s*-process elements can be as high as 0.5 for sAGB stars with $m = 7M_{\odot}$ and $Z = 10^{-3}$ (see Lugaro et al. 2012 for the yields of AGB stars with $[\text{Fe}/\text{H}] = -2.3$). This result implies that even 2P stars in Type I GCs can have significant abundance spreads (> 0.05) in light *s*-process elements depending on F_{dil} in the SCI scenario. Doherty et al. (2017) also predicted that [X/Fe] of heavy *s*-process elements (e.g., Ba) can be significantly smaller than those of light *s*-process elements in low-metallicity sAGB stars.

Schiappacasse-Ulloa et al. (2025) have derived [Y/Fe] and [Zr/Fe] of stars in 14 GCs and thereby investigated the spreads of these abundances separately for 1P and 2P stars. 2P stars in some GCs appear to show $\Delta[\text{Y}/\text{Fe}]$ and $\Delta[\text{Zr}/\text{Fe}]$ larger than the typical uncertainty in the abundance measurements (0.15 dex), which implies that massive AGB and sAGB stars polluted GC-forming GMCs. However, it is not so clear why only some GCs show such larger abundance spreads in the SCI scenario: Possibly, only GCs with small F_{dil} can have observable spreads in these elements. There appears to be no evidence supporting that $\Delta[\text{Y}/\text{Fe}]$ and $\Delta[\text{Zr}/\text{Fe}]$ are systematically larger than $\Delta[\text{Ba}/\text{Fe}]$ and $\Delta[\text{La}/\text{Fe}]$ in Schiappacasse-Ulloa et al. (2025). Future spectroscopic observations with more accurate abundance measurements (errors of < 0.05 dex) will be able to reveal abundances spreads of light and heavy *s*-process elements in 2P

stars caused by chemical enrichment by massive AGB and sAGB stars in the new scenario.

5.9 R-process enrichment

Internal abundances spreads for r -process elements have been so far confirmed only in a small number of Galactic GCs such as M15 and M92 (e.g., Sneden et al. 1997; Roederer 2011; Worley et al. 2013; Kirby et al. 2023). Recent theoretical models and numerical simulations of GCs (e.g., M5) with abundance spreads in r -process elements (e.g., [Eu/Fe]) have shown that the origin of the spreads can result from chemical enrichment by neutron star (NS) merging in the early formation histories of GCs (e.g., Bekki & Tsujimoto 2017; Tarumi et al. 2021). NSs originating from 1P stars explode during 2G formation so that gaseous ejecta from NS merging can enrich intracluster gas in the classic AGB scenario (Bekki & Tsujimoto 2017). As a result of this, 2P stars can have higher abundances of r -process elements and a larger abundance spread in r -process elements (e.g., [Eu/Fe]) compared with 1P stars. Recent observations have shown that the abundance spread in r -process elements is larger in 1P than in 2P for M15 (Henderson et al. 2025). If this trend is observationally confirmed in other GCs for a large number of stars, chemical enrichment by merging of NSs from 1P can be ruled out.

In the SCI scenario, AGB stars polluting star-forming GMCs in a host galaxy can initially have a large abundance spread in their r -process element due to the possible large abundance spreads in field stars of the host. If metal diffusion processes in high-density environments of GMCs can significantly reduce the initial abundance spreads in r -process elements within a few 10^7 yr, then 2P stars are likely to have the smaller abundance spread compared with 1P stars. The present study is unable to provide predictions on how much initial abundance spreads in GMCs can be reduced during GMC growth due to metal diffusion. It is thus our future study to understand the origin of the observed possible large abundance spreads of r -process elements in 1P stars of GCs using numerical simulations of GC formation based on the SCI scenario.

5.10 Discrete MPs of GCs from GMC growth merging

Although the distributions of stars along the anticorrelations were assumed to be continuous in previous observational and theoretical studies of GCs, Recent precise spectroscopic measurements of [Mg/Fe] and [Al/Fe] for GC stars in NGC 2808 have revealed that at least three distinct groups of stars exist in the Mg-Al diagram (Carretta 2014). Such discrete stellar populations have been found in other GCs like NGC 6752 and M22 (Marino et al. 2011; Carretta et al. 2012; Milone et al. 2013), which implies that the distributions of stars along the anticorrelations of light elements could not be continuous. The origin of this discreteness is yet to be fully understood, though our previous theoretical models of GC formation suggested that the observed discrete distributions are due to sudden truncation of star formation by supernova feedback effects (Bekki et al. 2017).

If a GMC grows through merging of smaller molecular clouds (e.g., Kobayashi et al. 2017) and if the smaller

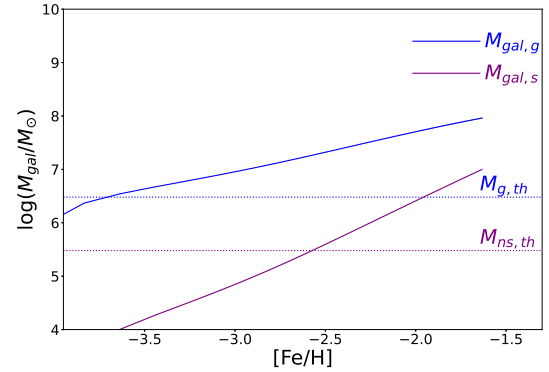


Figure 22. Total gaseous (blue) and stellar masses (purple) of a gas-rich dwarf galaxy as a function of [Fe/H] in the one-zone chemical evolution model of the galaxy for the first 1 Gyr evolution. The blue and purple dotted lines indicate the threshold gaseous ($M_{g,th}$) and stellar masses ($M_{ns,th}$) for GC formation with MPs, respectively. The crosspoint between the solid and dotted lines can mark the threshold [Fe/H] ($[Fe/H]_{th}$; “metallicity floor”) above which GC formation with MPs is possible in the SCI scenario. Since the threshold [Fe/H] is higher for new stars (i.e., the crosspoint between the two purple lines), the metallicity floor in this particular model is around -2.5 .

clouds are enriched by AGB stars to different degrees, a group of stars formed from a cloud should be able to have chemical abundance pattern that are distinct from those of any other groups of stars formed in other clouds. Accordingly, the young massive SC formed from this growing GMC through molecular cloud merging should be able to have discrete MPs. The establishment of discrete MPs within the building blocks of GC-hosting GMCs has been already suggested by Elmegreen (2017), though the chemical enrichment processes are quite different between his model and the present SCI scenario. It is our future study to demonstrate that the formation of discrete MPs is indeed possible in GC formation from growing GMCs based on our new hydrodynamical simulations of GC formation.

5.11 A possible minimum [Fe/H] for MPs formation in the Galactic and extragalactic GC systems (GCSs)

The present new scenario predicts that only massive GMCs can become GCs with MPs if they are chemically polluted by a sufficient number of AGB stars. This means that there is a threshold total gas mass of GMCs ($M_{g,th}$) over which GCs with MPs can be formed from GMCs. The required larger ratio of new stars interacting with a GMC to the GMC mass ($R_s = M_{ns}/M_{gmc} > 0.1$) also means that there is a threshold total mass of new stars ($M_{ns,th}$) over which the GMC can be converted into a GC with MPs. In order for a galaxy to form a GC with MPs, its total gaseous and stellar masses ($M_{gal,s}$ and $M_{gal,g}$, respectively) should meet the following conditions at least:

$$M_{gal,g} \geq M_{g,th} \quad (40)$$

and

$$M_{\text{gal},s} \geq M_{\text{ns,th}}. \quad (41)$$

Not all GMCs can form GCs in galaxies, and not all stars are new stars with ages of 0.02 – 0.1 Gyr. Therefore, the above required $M_{\text{gal,g}}$ and $M_{\text{gal,s}}$ are regarded as lower limits. Since $M_{\text{gal,g}}$ and $M_{\text{gal,s}}$ can be related to $[\text{Fe}/\text{H}]$ through galactic chemical evolution, we can derive the minimum $[\text{Fe}/\text{H}]$ required for the formation of GCs with MPs ($[\text{Fe}/\text{H}]_{\text{min}}$) using our chemical evolution models (Bekki & Tsujimoto 2012, BT12). Here we investigate the time evolution of $[\text{Fe}/\text{H}]$, $M_{\text{gal,g}}$, and $M_{\text{gal,s}}$ for the first 1 Gyr based on our chemical evolution models of dwarf galaxies with the final total masses of $M_{\text{gal}} = 10^8 M_{\odot}$ at $T = 1$ Gyr. The model parameters such as gas the IMF and chemical yields in these models are exactly the same as those adopted in BT12. We particularly discuss the results of the model with the Salpeter IMF ($\alpha = 2.35$) in which the gas infall timescale (τ_{inf}) and the star formation efficiency (C_{SF}) are assumed to be 3 Gyr and 0.02, respectively. Based on these results, we derive $[\text{Fe}/\text{H}]_{\text{min}}$ for $M_{\text{gc}} = 3 \times 10^5 M_{\odot}$, $F_{\text{b}} = 10$, and $R_{\text{s}} = 0.1$.

Fig. 22 shows that the blue solid line for $M_{\text{gal,g}}$ evolution crosses with the dotted line for $M_{\text{th,g}}$ at $[\text{Fe}/\text{H}] \approx -3.7$, which means that $[\text{Fe}/\text{H}]$ should be higher than -3 for the formation of massive GMCs: The gas might not be in the form of molecular hydrogen due to such low dust abundances though. On the other hand, the cross point is around $[\text{Fe}/\text{H}] \sim -2.6$ for $M_{\text{gal,s}}$, which is higher than $[\text{Fe}/\text{H}]_{\text{min}}$ estimated from $M_{\text{gal,g}}$ and $M_{\text{g,th}}$. This means that when a dwarf galaxy becomes as metal-rich as $[\text{Fe}/\text{H}] \sim -2.6$, then it can start to form a GC with MPs in this particular model.

It should be noted here that $[\text{Fe}/\text{H}]_{\text{min}}$ can become lower or higher depending on the model parameters of chemical evolution models. For example, $[\text{Fe}/\text{H}]_{\text{min}}$ can be higher in dwarf galaxies with lower M_{gal} for a given set of model parameters for star formation and gas infall. It is beyond the scope of this paper to describe how $[\text{Fe}/\text{H}]_{\text{min}}$ depends on galaxy masses, star formation histories, and gas infall rates etc in detail. However, the present study indicates that there should be $[\text{Fe}/\text{H}]_{\text{min}}$ for the formation of GCs with MPs in each of galactic building blocks. The minimum of $[\text{Fe}/\text{H}]_{\text{min}}$ among all building blocks of the Galaxy corresponds to the observed “metallicity floor” (e.g., Beasley et al. 2019).

We note that the metallicity floor predicted by the SCI scenario arises from a distinct physical mechanism compared to that proposed by Kruijssen (2019), who argued that the observed paucity of GCs with $[\text{Fe}/\text{H}] \leq -2.5$ reflects the galaxy mass-metallicity relation at high redshift. In the SCI scenario, an additional floor specific to MP formation arises from the requirement for sufficient AGB star density around GC forming GMCs, which is only met above a threshold galactic gaseous and stellar mass that corresponds to $[\text{Fe}/\text{H}]_{\text{min}} \approx -2.5$ in the models. Both mechanisms may operate simultaneously, with the Kruijssen (2019) floor setting an absolute lower limit on GC survival and the SCI floor setting an additional constraint on which surviving GCs can develop MPs.

The metallicity floors of extragalactic GCSs could be quite different from that of the Galactic GCS due to different formation histories of galactic building blocks. For example, if the building blocks of a galaxy have systematically longer

star-formation timescales (i.e., slower chemical enrichment), then $[\text{Fe}/\text{H}]_{\text{min}}$ of the GCS can be higher. It is currently very difficult to observationally investigate the presence or absence of MPs in all GCs of a galaxy outside the Local Group and thereby infer $[\text{Fe}/\text{H}]_{\text{min}}$ of the GCS, because it is exceptionally challenging to find observational evidence of MPs in integrated spectrum of such extragalactic GCs. Nevertheless it is an intriguing observational question whether GCSs have different $[\text{Fe}/\text{H}]_{\text{min}}$ and how their $[\text{Fe}/\text{H}]_{\text{min}}$ depend on the global properties of their host galaxies.

The chemical evolution models described above can also predict the total mass of intermediate-mass stars ($4 \leq m/M_{\odot} \leq 10$), denoted as M_{TO} , that have just left the main sequence at any given time step (every Myr) in a galaxy. This quantity, $M_{\text{TO}} (4 \leq m_{\text{TO}}/M_{\odot} \leq 10)$, serves as a useful gauge for determining when (or at what $[\text{Fe}/\text{H}]$) a galaxy contains a sufficient amount of gas ejected from AGB stars to form a GC with MPs within the SCI scenario. Fig. 23 illustrates how the time evolution of M_{TO} depends on the star formation efficiency or rapidity (C_{SF}) and the IMF slope (α) across six different models. Here, M_{TO} is normalized by the total mass of gas (M_{gas}) that infalls onto the galaxy over its entire evolution. For example, if $M_{\text{TO}} (4 \leq m_{\text{TO}}/M_{\odot} \leq 10) = 10^{-5}$, the total mass of stars that have entered the AGB phase over the last 10^6 yr is $10^4 M_{\odot}$ for a galaxy with $M_{\text{gas}} = 10^9 M_{\odot}$. This implies that the total gas mass ejected from massive AGB stars over the last 10^8 yr is $\approx 9 \times 10^5 M_{\odot}$, assuming an ejection fraction of $f_{\text{ej}} = 0.9$.

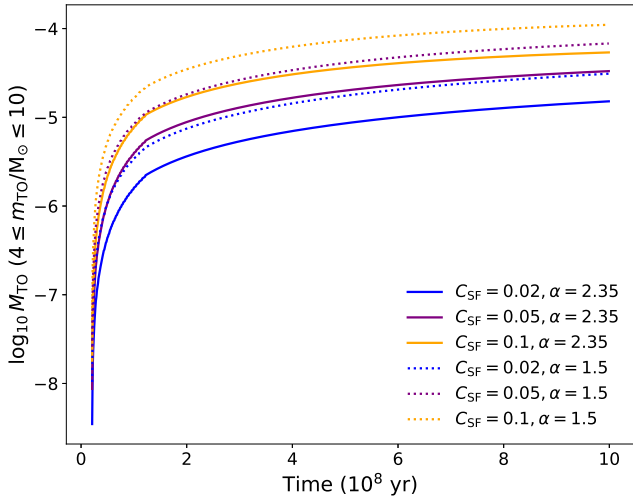
Fig. 23 clearly demonstrates that at a given time T , M_{TO} for massive AGB stars is larger in models with a higher C_{SF} for a fixed α , which is driven by more rapid star formation. Regardless of the chosen C_{SF} and α , M_{TO} remains very low during the initial epoch ($T = 0$ –30 Myr). This implies that the formation of GCs with MPs is less likely during the very early phases of galaxy evolution. Given that stars formed earlier typically possess lower $[\text{Fe}/\text{H}]$, this result supports the existence of a metallicity floor for the formation of GCs with MPs. Furthermore, models featuring a top-heavy IMF ($\alpha = 1.5$) systematically exhibit larger M_{TO} values across all three C_{SF} , suggesting that the IMF is also a key determinant of the 2P fraction ($F_{2\text{P}}$) in GCs. It should be emphasized that within the SCI scenario, both the total mass of the AGB ejecta and the mass function of the AGB stars polluting GMCs are crucially important. Appendix D describes how M_{TO} evolves as a function of the turn-off mass (m_{TO}) over time (T), thereby demonstrating when GMCs can be exclusively polluted by massive AGB stars.

5.12 Formation of N-rich stars from disintegration of low-mass clusters

The inner regions of the Galaxy are observed to have field stars with $[\text{N}/\text{Fe}] > 0.5$, the origin of which is yet to be fully understood (e.g., Fernández-Trincado et al. 2019; Spite et al. 2022; Kane et al. 2026). Although these N-rich stars might have originated from disintegration of GCs with MPs (e.g., Martell et al. 2010; Fernández-Trincado et al. 2019) or from disruption of the Galactic building blocks containing N-rich stars (e.g., Bekki 2019c), we here suggest an alternative idea about their origins. Although low-mass clusters in the present-day Galaxy do not have MPs with anticor-

Table 4. Predicted properties of GCs with MPs from the new scenario to be compared with future observations.

Properties	Predictions	Comments
$F_{2P} - \Sigma_{\text{SFR}}$ relation	Higher F_{2P} in GCs forming with higher Σ_{SFR}	Higher F_{2P} is likely for GCs formed at higher z .
$F_{2P} - [\text{Eu}/\text{Mg}]$ relation	Lower F_{2P} in GCs with higher $[\text{Eu}/\text{Fe}]$	This can be clearly seen for a given M_{gc} .
Li-Al (Li-Na) anticorrelations	Diverse slopes (from flat to shallow)	The polluter's mass range determines the slopes.
$\delta A(\text{Li}) - M_{\text{gc}}$ relation	Larger $A(\text{Li})$ spreads in larger M_{gc}	This is due to F_{dil} dependent on M_{gc} .
Nitrogen of P-rich stars	High $[\text{N}/\text{Fe}]$ (> 0.5)	P-rich stars can be preferentially found in 2P.
$^{12}\text{C}/^{13}\text{C}$ ratios in unevolved stars	Very low ratios (≈ 5) in 2P depending on F_{dil}	1P-2P difference in this ratio can be quite large.
$^{12}\text{C}/^{13}\text{C} - [\text{Na}/\text{Fe}]$ anticorrelation	Lower $^{12}\text{C}/^{13}\text{C}$ ratios for higher $[\text{Na}/\text{Fe}]$	This is expected for other light elements.
Precursor (0P) stars in GCs' halos	Peculiar chemical abundance patterns	They originate from field stars of GC-hosts.


Figure 23. M_{TO} of intermediate-mass stars as a function of time (T) in six models with $C_{\text{SF}} = 0.02$ (blue), 0.05 (purple), and 0.1 (orange) for the IMF slope $\alpha = 2.35$ (solid lines) and 1.5 (dotted lines). The total mass of intermediate-mass stars ($M_{\text{TO}}(4 \leq m_{\text{TO}}/M_{\odot} \leq 10)$) that have just left the main-sequence at a given time step is calculated in these models. M_{TO} normalized by the total mass of in falling gas is plotted every Myr in this figure. Larger C_{SF} means that gas is more rapidly consumed by star formation.

relations between light elements (e.g., Pancino et al. 2011), the present model predicts that even low-mass SCs can possess MPs if their progenitor GMCs are chemically enriched by AGB stars to a large extent due to rather high Σ_{SFR} of their host galaxies. NGC 6535 with $M_{\text{gc}} \approx 10^{3.53} M_{\odot}$ and a O-Na anticorrelation (e.g., Bragaglia et al. 2017) is an example of such low-mass SCs with MPs. These low-mass SCs can be quickly disintegrated by their host galaxies' tidal fields and two-body dynamical relaxation effects to finally become field stars. These field stars can have high $[\text{N}/\text{Fe}]$ and thus be observed as N-rich stars in the inner region of the Galaxy. The total number and mass of these low-mass SCs with N-rich stars are much larger than those of the Galactic GCs, which implies that the observed large fraction (~ 0.15) of N-rich stars can be naturally explained. Therefore the present study suggests that the stripping of 2P stars from the Galactic GCs with MPs is not the only process for the formation of the observed N-rich stars in the Galaxy: the vast majority of N-rich stars in the Galaxy might originate from disintegrated young low-mass SCs with N-rich stars.

Low-mass SCs with N-rich stars could be the fundamental building blocks of a galaxy, if the building blocks

(i.e., dwarf galaxies) of the galaxy have rather high Σ_{SFR} . There are a number of spectroscopic observations that support the presence of N-rich stellar populations in giant elliptical galaxies (e.g., Schiavon 2007) and ultra-compact dwarf galaxies (e.g., Strader et al. 2013). It is our future work to discuss whether the building blocks of these galaxies could have rather high Σ_{SFR} for longer timescales based on our new hydrodynamical simulations of these galaxies. The disintegration of such low-mass SCs with N-rich stars could be related to the long-standing problem of the UV upturn phenomenon in giant elliptical galaxies (Bekki 2012; Goudfrooij 2018; Goudfrooij et al. 2026), because N-rich stars are also He-rich in the SCI scenario.

5.13 Observational evidence of AGB-GMC interaction in our backyards

The chemical abundance patterns of presolar grains have long been considered to contain fossil records of interactions between the parent GMC of our solar system ("Sun-hosting MC") and various types of stars (e.g., CCSNe, AGB stars, novae) encountering with the GMC (e.g., Lugaro 2005). For example, the elevated ^{26}Al abundances of presolar grains were suggested to result from mixing of gaseous ejecta from massive AGB stars with original gas of the Sun-hosting GMC (e.g., Kastner & Myer 1994; Wasserburg et al. 2006; Trigo-Rodríguez et al. 2009; Parker & Schoettler 2003).

Trigo-Rodríguez et al. (2009) showed that if a massive AGB star with $m = 6.5 M_{\odot}$ polluted the Sun-hosting MC with a dilution factor ($M_{\text{g}}/M_{\text{ej}}$) of ≈ 300 , then the observed abundances of ^{26}Al , ^{41}Ca , ^{60}Fe , and ^{107}Pd in presolar grains can be self-consistently reproduced. The large dilution factor implies that the initial mass of the GMC (M_{gmc}) is at least $\approx 2000 M_{\odot}$ (for $f_{\text{ej}} = 0.9$). If the entire GMC was polluted by multiple AGB stars, and if the initial mass of the SC (M_{sc}) hosting the Sun is $10^3 M_{\odot}$ (Adams 2010), then the total number of AGB stars (N_{agb}) polluting the MC is ≈ 6 for $\epsilon_{\text{sf}} = 0.1$. Therefore, it is likely that the Sun-hosting MC might have been chemically enriched by multiple massive AGB stars.

If the Sun-hosting GMC was polluted by AGB stars with low N_{agb} due to low Σ_{SFR} of the Galaxy about 4.6 Gyr ago, it would be quite reasonable that GMCs within compact dwarf galaxies with rather high Σ_{sf} at high- z are polluted by a large number of AGB stars. The present study predicts that low-mass SCs can have star-to-star abundance inhomogeneities to much smaller degrees due to small numbers of AGB stars interacting with their parent GMCs. However, it is very difficult for observational studies of low-mass SCs to reveal subtle differences in chemical abundances be-

tween their member stars. The observed extremely accurate chemical abundance patterns of presolar grains are the only fossil records that can be used to discuss whether GMC-AGB interactions occurred in the early stages of low-mass SC formation from GMCs. Thus, AGB-GMC interactions are relevant to not only GC formation with MPs but also to the origin of presolar grains in our own solar system - representing an independent but cohesive line of evidence for the physical processes central to the SCI scenario.

5.14 Comments on other scenarios

Recent hydrodynamical simulations of star formation within GMCs have demonstrated that pre-SN feedback effects of massive stars, such as radiation pressure and photoevaporation, can dramatically decrease the SFEs (e.g., 2–10%; Kim et al. 2021). Given that stellar feedback effects of massive stars with $m = [10 - 100]M_{\odot}$ are incorporated in these simulations, the feedback effects of very massive and supermassive stars with $m > 1000M_{\odot}$ could be by several orders of magnitude stronger than those predicted in these simulations (owing to $L \propto M^{3.5}$, where L and M are stellar luminosity and mass, respectively). Accordingly, although such very massive stars may form in young SCs (e.g., Lahań et al. 2025), such stars are highly likely to quench star formation rather than promote it. This enormously strong feedback effect of very massive and supermassive stars on star formation needs to be quantitatively investigated in GC formation scenarios with these stars being major polluters.

As previously discussed in preceding sections of this paper, the observed slopes in the anticorrelations (correlations) of A(Li) with [Al/Fe] ([O/Fe]) rule out GC formation scenarios in which intracluster gas is chemically enriched *only by a polluter* that cannot produce Li. Accordingly, the observed slopes imply that stellar sources ejecting Li-free or extremely Li-depleted gas, such as very massive and supermassive stars, fast-rotating massive stars, and massive interacting binaries, cannot be a major polluter responsible for the formation of MPs in GCs. However, if such Li-free gas is mixed with both pristine gas and Li-enhanced ejecta from other stellar sources (e.g., AGB stars) to form 2P stars, the observed slopes in Li-Al anticorrelations can be well explained. Therefore, a hybrid scenario in which both AGB stars and massive stars chemically enrich pristine GMC gas to form 2P stars can be explored for a better formation scenario of GCs with MPs.

Cluster environments soon after the removal of all remaining pristine gas of GMCs by the feedback effects of CCSNe might not be as hospitable for secondary star formation as the classic AGB scenario envisaged. If 15% of all CCSNe are delayed ones that can explode 50–200 Myr after cluster formation (Zapartas et al. 2017), then the time interval (δt_{dCCSN}) between two consecutive explosions of delayed CCSNe can be as short as $\approx 3 \times 10^4$ yr for a total CCSN number of $\approx 10^4$, which is reasonable for GCs with $M_{\text{gc},0} = 10^6 M_{\odot}$ with the Salpeter IMF. If this δt_{dCCSN} is shorter than the typical timescale of star formation (t_{sf}), the classic AGB scenario has a serious problem. Likewise, if the timescale of disruptive interactions between proto-stellar cores and already existing (1P) stars ($t_{\text{int}} = 10^3 - 10^4$ yr; Bobrick et al. 2025) is shorter than t_{sf} , the scenario also has a serious problem. Thus, GC formation models based on the

classic AGB scenario will need to investigate whether and how t_{sf} can be shorter than δt_{dCCSN} and t_{int} in order to assess the validity of the scenario.

Almost all models for GC formation with MPs assume that star formation from gaseous ejecta of polluters mixed with pristine gas is possible even after the formation of clusters of massive stars ($m > 10M_{\odot}$). These models have not yet assessed the validity of the assumption using hydrodynamical simulations of GC formation with various stellar feedback effects; the assumption could be unrealistic and unreasonable. The present study has shown that chemical enrichment of GMCs by existing AGB stars before the formation of clusters of massive stars ($m > 10M_{\odot}$) is closely associated with the formation of GCs with MPs in galaxies with high Σ_{SFR} . Given that AGB stars are not the only stellar objects that can influence the chemical and dynamical evolution of GMCs, other sources such as CO and ONe novae, CCSNe, delayed CCSNe, and SNe Ia surrounding GMCs can also play some roles in GMC evolution within galaxies with high Σ_{SFR} . We will need to investigate the roles of these various star-cloud interactions in GMC evolution, because such interactions might be imprinted on the chemical abundance patterns of GCs.

6 CONCLUSIONS

We have presented a scenario in which globular clusters (GCs) with multiple stellar populations (MPs) can be formed from massive star-forming gas clouds being chemically polluted by pre-existing Asymptotic Giant Branch (AGB) stars in gas-rich dwarf galaxies. In this star-cloud-interaction (“SCP”) scenario, it is assumed that the GC-forming gas clouds have physical properties similar to present-day giant molecular clouds (GMCs), though the mass fractions of molecular hydrogen gas could be lower than those of typical GMCs due to low metallicities. This new scenario differs from the classic AGB scenario in that AGB stars formed before GMC formation can enrich star-forming GMCs through their stellar winds. Accordingly, the new scenario does not suffer from the potentially serious problems inherent to the classic one, such as the mass-budget and the dilution timing problems.

Using idealized analytic models for GC formation with MPs based on the new scenario, we have investigated various physical properties of GCs—such as correlations between first-population (1P) fractions and global GC masses, as well as chemical abundance patterns—and thereby compared the results with corresponding observations. We have found that most of the observed GC properties, such as chemical abundances, can be well reproduced by the new scenario with a particular set of model parameters, though a number of properties are yet to be fully reproduced (see Table 3). We have also provided key theoretical predictions of the scenario to be compared with future observational studies of GCs; Table 4 summarizes these predictions. The principal results are as follows:

(1) The surface number densities of intermediate-mass stars with ages ranging from 0.02 to 0.1 Gyr (Σ_{agb}) around and within star-forming GMCs can determine whether GCs formed within the GMCs can develop MPs. GCs can host

MPs if they are formed from GMCs that are chemically polluted by AGB stars due to a high Σ_{agb} . It is proposed that the observable surface densities of star formation rates (Σ_{SFR}) can be used as a proxy for Σ_{agb} in discussing whether GCs with MPs can be formed in galaxies. A value of $\Sigma_{\text{SFR,th}} \approx 1 \text{ M}_{\odot} \text{ kpc}^{-2} \text{ yr}^{-1}$ is suggested as a threshold SFR density above which GCs with MPs can form within galaxies.

(2) More massive GCs can have smaller 1P fractions ($F_{1\text{P}}$), mainly because more massive GC-forming GMCs can interact with larger numbers of AGB stars (per unit mass) within and around the GMCs to be chemically enriched by their stellar winds to a greater extent (i.e., larger R_s for larger M_{gmc}). The predicted $M_{\text{gc}}-F_{1\text{P}}$ relation is consistent with the observed one, though the simulated dispersions of $F_{1\text{P}}$ for a given M_{gc} are smaller than observed. The present model predicts that low-mass SCs ($< 10^4 \text{ M}_{\odot}$) can initially host a small fraction of second-population (2P) stars in galaxies with high Σ_{SFR} , though they can be completely disintegrated over 13 Gyr.

(3) More massive GCs can also have larger spreads in helium abundance (δY) between 1P and 2P stars, alongside larger differences between the minimum and maximum Y ($\delta_{\text{max}} Y$). Therefore, $F_{1\text{P}}$ is anticorrelated with δY and $\delta_{\text{max}} Y$ in simulated GCs. The simulated 1σ dispersion of δY for each M_{gc} bin is significant (≈ 0.01), resulting primarily from the initial R_s dispersion for a given GMC mass. Notably, this simulated 1σ dispersion is consistent with the corresponding observational data.

(4) The predicted $M_{\text{gc}}-\delta Y$ relation is significantly steeper than the observed one, which means either that the Y yields adopted in the present study are too large or that the SCI scenario has a potentially serious problem in explaining these helium observations. It should be noted here that the δY values must be derived indirectly from multi-band photometric comparisons of population sequences using synthetic spectra and isochrone fitting (M18).

(5) The SCI scenario can successfully reproduce the observed O–Na and C–N anticorrelations of GCs, consistent with the established results of the classic AGB scenario. The evolutionary loci of the present models on the [O/Fe]–[Na/Fe] plane depend on the adopted model parameters, such as the stellar initial mass function (IMF), mass ranges of polluting AGB stars, and metallicities. This result implies that the observed diverse O–Na anticorrelations can be caused by variations of these parameters during GC formation. The high-metallicity models ([Fe/H] = -0.4) show significantly steeper O–Na anticorrelations compared with the low-metallicity ones ([Fe/H] = -1.8), which appears to be consistent with the latest observations.

(6) Both the Mg–Al anticorrelation and the Si–Al correlation observed in low-metallicity GCs can be qualitatively reproduced by the new scenario. There is expected to be no such correlation or anticorrelation in high-metallicity GCs under the new scenario, because gaseous ejecta from massive AGB stars at high metallicities does not exhibit Mg-depletion and Si-enhancement. The observed Si–Al relation shows a larger spread in [Si/Fe] compared with the model predictions, which suggests that further improvement of the models and AGB yields is required to better match the observations.

(7) The Mg–K anticorrelation observed in NGC 2419

can be reproduced well by the models in which: (i) super-AGB (sAGB) stars are the major sources polluting star-forming GMCs, and (ii) sAGB yields from Iliadis et al. (2016) are adopted. However, these models do not reproduce the Mg–K anticorrelations observed in ω Centauri and NGC1786 with the same fidelity. This inconsistency has the following two implications. One is that the Mg and K yields of sAGB stars contributing to the chemical enrichment of forming GCs could differ due to metallicity or mass differences among the sAGB stars. If the (IMF-averaged) Mg and K yields of sAGB stars are indeed different, diverse Mg–K anticorrelations observed in different GCs could be explained within the SCI scenario. The other implication is that sAGB stars are not responsible for the formation of Mg–K anticorrelations, meaning the SCI scenario has a serious problem. Since Mg and K yields dependent on the physical parameters of sAGB stars are currently lacking, we are unable to definitively conclude whether the SCI scenario has a serious problem in reproducing the observed Mg–K anticorrelations in GCs.

(8) The models with lithium production by massive AGB stars can much better reproduce the observed, remarkably flat relation between $A(\text{Li})$ and [Al/Fe] compared with those without Li production. In particular, the observed 2P stars with [Al/Fe] ≈ 0.5 and $A(\text{Li}) \approx 2.3$ can be best explained by the models in which the fraction of Li-producing AGB stars among all AGB stars ($P(\text{Li})$) is as high as 20%. These results suggest that GC formation models with polluters incapable of producing Li are disfavoured as a viable framework for the origin of MPs in GCs. The models with lower $P(\text{Li})$ show weak anticorrelations of $A(\text{Li})$ with [Na/Fe] and [Al/Fe], which can explain the origin of the trends observed in NGC 6752. Detailed comparison with the observed $A(\text{Li})$ –[Al/Fe] relation allows us to tightly constrain the fraction of AGB stars that need to produce Li in the new scenario.

(9) The observed relations between [Al/Fe] and magnesium isotopes ($^{25}\text{Mg}/\text{Mg}$ and $^{26}\text{Mg}/\text{Mg}$ ratios) can be well reproduced by the new scenario, but only if we adopt abundance ratios of $^{25}\text{Mg}/\text{Mg}$ and $^{26}\text{Mg}/\text{Mg}$ in the AGB ejecta that are a factor of 2–3 lower than the values predicted in the literature. This discrepancy suggests that current stellar models of AGB stars over-predict the abundances of ^{25}Mg and ^{26}Mg isotopes in their stellar winds. It remains possible that the required smaller abundances of these Mg isotopes could represent a potential problem for the SCI scenario.

(10) The new scenario predicts that the metallicity spreads in the 1P stars of GCs are inherited from those in their parent GMCs and from the field stars trapped by the GMCs (“0P”). It also predicts that the metallicity spreads in the 2P population can be smaller than those in the 1P population, because 2P stars form later from gas that has experienced substantial metal homogenization due to turbulent diffusion within the forming GMCs.

(11) The origin of the observed Type-I versus Type-II GC dichotomy can be well understood in the context of the SCI scenario. First, two distinct GCs form from separate GMCs polluted by AGB stars within their host dwarf galaxy at different epochs. The later-formed GC can have a higher [Fe/H] and higher abundances of s -process elements (e.g., [Ba/Fe]) due to background chemical enrichment by core-collapse supernovae (CCSNe) and lower-mass AGB stars

($m < 4 M_{\odot}$) within the host galaxy, provided it forms more than ≈ 100 Myr after the earlier cluster. The two clusters then merge together to form a single, complex GC that displays two distinct populations with different [Fe/H] (hence “iron-complex”) and [Ba/Fe] profiles (s -poor and s -rich), while each population internally maintains the characteristic light-element anticorrelations. This GC merging mechanism can naturally solve the severe mass-budget problem for s -rich stars in Type-II GCs (e.g., M22) and firmly links internal [Fe/H] and [Ba/Fe] spreads to galaxy-scale chemical evolution in the early universe.

(12) The observed fraction of Type-II GCs among Galactic clusters ($\sim 20\%$) can be understood in the context of GC merging probabilities within the Galactic building blocks (i.e., now-defunct dwarf galaxies). The differences in the mass fractions of s -rich stars among different Type-II GCs can be attributed to variations in the mass ratios of the two merging clusters in their host dwarf galaxies. Furthermore, the chemical abundance patterns of s -process elements in Type-II GCs are better explained by chemical pollution from low-mass AGB stars rather than the weak s -process in massive stars.

(13) The chemical abundances of phosphorus-rich stars with [P/Fe] > 0.5 recently discovered in a few Galactic GCs with MPs (e.g., M4) provide unique new constraints on the theory of GC formation. The chemical abundance patterns of such P-rich stars can be explained if they formed from P-rich gaseous ejecta from oxygen-neon (ONe) novae that mixed thoroughly with N-rich AGB ejecta within the cluster-forming GMCs. High-speed ($\approx 1000 \text{ km s}^{-1}$) ejecta from ONe novae can be efficiently trapped by GMCs through hydrodynamical interactions between the fast ejecta and the cold, dense cloud gas, enabling it to mix with the ambient GMC material and AGB stellar winds for star formation. Thus, the SCI scenario offers a plausible explanation for the origin of P-rich stars, although the fine details of P-rich star formation must be investigated in depth by our future hydrodynamical simulations of GC formation with ONe novae.

(14) There should be a strict “metallicity floor” that defines the minimum metallicity ($[\text{Fe}/\text{H}]_{\text{min}}$) required for GC formation with MPs. The new scenario predicts that GCs with MPs can form: (i) if the gas mass M_{g} is larger than a threshold cloud mass ($M_{\text{g,th}}$), and (ii) if the pre-existing stellar mass M_{ns} is larger than a threshold mass of intermediate-mass stars with ages of 0.02–0.1 Gyr. Therefore, GC-host dwarf galaxies are required to have global gaseous and stellar masses ($M_{\text{gal,g}}$ and $M_{\text{gal,s}}$) that are larger than $M_{\text{g,th}}$ and $M_{\text{ns,th}}$, respectively. This lower limit on $M_{\text{gal,g}}$ and $M_{\text{gal,s}}$ directly implies the presence of a metallicity floor ($[\text{Fe}/\text{H}]_{\text{min}}$), because [Fe/H] strongly correlates with galactic gas and stellar masses through global star formation and chemical evolution in dwarf galaxies. The present scenario predicts that $[\text{Fe}/\text{H}]_{\text{min}}$ can vary between different galactic GC systems because the masses and star formation histories of their primordial building blocks were likely quite diverse.

(15) Since Σ_{SFR} must be exceptionally high for the formation of GCs with MPs in the new scenario, it is highly unlikely that the present-day LMC can form GCs with MPs due to its low global Σ_{SFR} . The LMC may last have formed GCs with MPs about a few billion years ago, when it experienced a massive starburst triggered by tidal interactions with the MW and the Small Magellanic Cloud (SMC).

Therefore, the observed apparent age threshold above which LMC clusters exhibit MPs results not from a physical age constraint, but from the lack of intense starburst activity over the last few Gyr (leading to a lower Σ_{SFR} and thus an insufficient Σ_{agb}). Under the new scenario, starbursting blue compact dwarf galaxies (BCDs) with compact sizes can successfully produce GCs with MPs, whereas star-forming, gas-rich ultra-diffuse galaxies (UDGs) are highly unlikely to form them.

(16) The present scenario predicts that the mass fraction of 2P stars ($F_{2\text{P}}$) in GCs with MPs formed in galaxies with higher Σ_{SFR} will be systematically larger due to more efficient chemical enrichment of the parent GMCs by AGB stars. The scenario also predicts that GCs with older ages and lower metallicities tend to have higher $F_{2\text{P}}$ values, because their primordial host galaxies were likely to feature much higher baseline values of Σ_{SFR} . Therefore, the observed relationship between redshift evolution (z), Σ_{SFR} , and metallicity in high-redshift star-forming galaxies can provide crucial hints regarding the origin of the observed dependence of $F_{2\text{P}}$ on cluster ages and metallicities.

(17) A top-light IMF is expected for lower Σ_{SFR} environments within the framework of the integrated galaxy-wide IMF theory (Weidner & Kroupa 2005), and it represents a key ingredient in chemical evolution models that reproduce the lower $[\alpha/\text{Fe}]$ and elevated $[\text{Eu}/\alpha]$ ratios observed in massive satellite galaxies in the Local Group (e.g., Tsujimoto 2024). It is thus possible that accreted (ex-situ) GCs with elevated $[\text{Eu}/\alpha]$ ratios that formed in defunct dwarf galaxies characterized by top-light IMFs and lower Σ_{SFR} will exhibit lower $F_{2\text{P}}$ values for a given global GC mass.

(18) Future observational studies of $^{12}\text{C}/^{13}\text{C}$ ratios in unevolved main-sequence stars and their correlations with light-element abundances (e.g., [Na/Fe]) and M_{gc} are crucial, because these observations can provide completely independent constraints on GC formation scenarios. The new scenario explicitly predicts low $^{12}\text{C}/^{13}\text{C}$ ratios (≈ 5) for the enriched population and large differences in this ratio between 1P and 2P stars (≈ 90). It is thus important for alternative GC formation frameworks to predict their own expected $^{12}\text{C}/^{13}\text{C}$ ratios for 2P stars to allow for clean observational tests.

(19) The classic AGB scenario would still be promising if both the feedback effects of delayed CCSNe and the disruptive encounters of existing (1P) stars with protostellar cores are shown to be unable to severely suppress secondary star (2P) formation within dense stellar environments. Conversely, GC formation scenarios invoking polluters unable to produce lithium (e.g., massive stars and massive interacting binaries) face a serious problem in reproducing the observed, remarkably flat correlation of $A(\text{Li})$ with [Al/Fe]. Other scenarios based on gas accretion onto existing 1P stars, stellar collisions, or stellar mergers have not yet been demonstrated to reproduce the full range of chemical abundance patterns characteristic of GCs, though further development of these frameworks may yet provide viable alternatives. Now that recent observational studies of GCs with MPs have revealed a diverse array of physical properties and clear correlations with global cluster parameters, predictions from all these candidate formation scenarios must be tested against these rich empirical datasets in a comprehensive manner.

(20) Since the present study is based on idealized analytic models, our future studies will need to demonstrate that GC formation proceeds along the pathways outlined here using more sophisticated hydrodynamical simulations of GC formation from GMCs polluted by AGB stars. We will also need to compare the observed structural and kinematic differences between 1P and 2P stars within GCs hosting MPs against the corresponding multi-dimensional predictions from our forthcoming numerical simulations. Ultimately, future observational searches for young massive star clusters with MPs across a wide range of host galaxy environments will validate or disprove this new scenario.

7 DATA AVAILABILITY

The data used in this paper (outputs from computer simulations) will be shared on reasonable request to the corresponding author.

8 ACKNOWLEDGMENT

The hydrodynamical simulations of gas-rich disks galaxies were performed on the OzSTAR national facility at Swinburne University of Technology. The OzSTAR program receives funding in part from the Astronomy National Collaborative Research Infrastructure Strategy (NCRIS) allocation provided by the Australian Government, and from the Victorian Higher Education State Investment Fund (VHESIF) provided by the Victorian Government. Support for this work was provided by NASA through the NASA Hubble Fellowship grant #HST-HF2-51560 awarded by the Space Telescope Science Institute, which is operated by the Association of Universities for Research in Astronomy, Inc., for NASA, under contract NAS5-26555.

REFERENCES

Adamo, A., et al., 2020, *MNRAS*, 499, 3267
 Adams, F. C., 2010, *ARA&A*, 48, 47
 Alvarez Garay, D. A., et al., 2022, *ApJ*, 928 L11
 Alvarez Garay, D. A., et al., 2025, *A&A*, 704, 114
 Alvarez Garay, D. A., et al., 2026, *A&A*, 707, 280
 Bailin, J., 2018, *ApJ*, 863, 99
 Barbuy, B., et al., 2025, *AJ*, 170, 245
 Bastian, N., Cabrera-Ziri, I., Davies, B., Larsen, S. S., 2013, *MNRAS*, 436, 2852
 Bastian, N., Lamers, H. J. G. L. M., de Mink, S. E., et al. 2013, *MNRAS*, 436, 2398
 Bastian, N., Cabrera-Ziri, I., & Salaris, M. 2015, *MNRAS*, 449, 3333
 Bastian, N., Lardo, C., 2018, *ARA&A*, 56, 83
 Baumgardt, H., & Kroupa, P., 2007, *MNRAS*, 380, 1589
 Beasley, M. A., et al., 2019, *MNRAS*, 487, 1986
 Bedin, L. R., Piotto, G., Anderson, J., et al., 2004, *ApJ*, 605, L125
 Bekki, K., 2010, *ApJ*, 724, L99
 Bekki, K., 2011, *MNRAS*, 412, 2241
 Bekki, K., 2012, *ApJ*, 747, 78
 Bekki, K., 2015, *MNRAS*, 449, 1625
 Bekki, K., 2019, *A&A*, 622, 53 (2019a)

Bekki, K., 2019, *MNRAS*, 486, 2570 (2019b)
 Bekki, K., 2019, *MNRAS*, 490, 4007 (2019c)
 Bekki, K., 2023, *MNRAS*, 518, 3274
 Bekki, K., Norris, J. E., 2006, *ApJ*, 637, L109
 Bekki, K., et al., 2007, *MNRAS*, 377, 335
 Bekki, K., Mackey, A. D., 2009, *MNRAS*, 394, 124
 Bekki, K., Tsujimoto, T., 2012, *ApJ*, 761, 180 (BT12)
 Bekki, K., Yong, D., 2012, *MNRAS*, 419, 2063 (BY12)
 Bekki, K., Tsujimoto, T., 2016, *ApJ*, 831, 70 (BT16)
 Bekki, K., Tsujimoto, T., 2017, *ApJ*, 844, 34
 Bekki, K., Tsujimoto, T., 2024, *ApJ*, 937, L1
 Bekki, K., Furuya, K., Shimonishi, T., 2025, *MNRAS*, 543, 2997
 Bianchini, P., et al., 2026, preprint (arXiv:2603.26195)
 Bobrick, A., Davies, M. B., Perets, H. B., 2025, *MNRAS*, 544 3601
 Bonifacio, P. et al., 2007 *A&A*, 470, 153
 Brauner, M., et al., 2023, *A&A*, 637, 123
 Bragaglia, A., et al., 2017, *A&A*, 607, 44
 Buder, S., et al., 2025, *PASA*, 42, 51
 Buzzo, M. L., et al., 2025, *A&A*, 695, 124
 Cabrera-Ziri, I., Bastian, N., Davies, B., Magris, G., Bruzual, G., Schweizer, F., 2014, *MNRAS*, 441, 2754
 Cameron, A. G. W., Fowler, W. A., 1971, *ApJ*, 164, 111
 Carretta, E., 2014, *ApJ*, 795, L28
 Carretta, E., et al., 2005, *A&A*, 433, 597
 Carretta, E., et al., 2009, *A&A*, 505, 117 (C09a)
 Carretta, E., Bragaglia, A., Gratton, R. G., Lucatello, S., 2009, *A&A*, 505, 117 (C09b)
 Carretta, E., et al., 2010, *ApJ*, 722, L1
 Carretta, E., Bragaglia, A., Gratton, R. G., Lucatello, S., D’Orazi, V., 2012, *ApJ*, 750, L14
 Carretta, E., Bragaglia, A., 2025, *A&A*, 696, 120
 Chevance, M., et al., 2020, *Space Science Reviews*, 216, 50
 Cohen, M., Kuhi, L. V., 1979, *ApJS*, 41, 743
 Conroy, C. & Spergel, D. N. 2011, *ApJ*, 726, 36
 Cottrell, P. L.; Da Costa, G. S., 1981, *ApJL*, 245, 79
 Cristallo, S., et al., 2011, *ApJS*, 197, 17
 Cunha, K., et al., 2003, *AJ*, 126, 1305
 Da Costa, G. S., Norris, J. E., Yong, D., 2003, *ApJ*, 769, 8
 Dalessandro, E., Mucciarelli, A., Bellazzini, M., et al. 2018, *ApJ*, 864, 33
 D’Antona, F., & Caloi, V. 2004, *ApJ*, 611, 871
 D’Antona, F., et al. 2012, 426, 1710
 D’Antona, F., Vesperini, E., D’Ercole, A., Ventura, P., Milone, A. P., Marino, A. F., & Tailo, M. 2016, *MNRAS*, 458, 2122
 Decressin, T., Meynet, G., Charbonnel, C., Prantzos, N. & Ekström, S. 2007, *A&A*, 464, 1029
 Dell’Aglì, F., et al., 2018, 475, 3098 (D18)
 de Mink, S. E., Pols, O. R., Langer, N., 2009, *A&A*, 507, L1
 Denissenkov, P. A., Hartwick, F. D. A., 2014, *MNRAS*, 437, L21
 D’Ercole, A., Vesperini, E., D’Antona, F., McMillan, S. L. W., & Recchi, S. 2008, *MNRAS*, 391, 825 (D08)
 D’Ercole, A., D’Antona, F., Ventura, P., Vesperini, E., McMillan, S. L. W., 2010, *MNRAS*, 407, 854 (D10)
 D’Orazi, V., Marino, A. F., 2010, *ApJ*, 716, L166
 D’Orazi, V., et al., 2014, *ApJ*, 791, 39
 Dobrovolskas, V., et al., 2014, *A&A*, 565, 121
 Doherty, C. L., et al., 2015, 446, 2599

- Doherty, C. L., et al., 2017, *PASA*, 34, 56
 Elmegreen B. G., & Efremov, Y. N., 1997, *ApJ*, 480, 235
 Elmegreen B. G., 2017, *ApJ*, 836, 80
 Fenner, Y., Campbell, S., Karakas, A. I., Lattanzio, J. C., Gibson, B. K., 2004, *MNRAS*, 353, 789
 Fernández-Trincado, J. G., et al., 2019, *A&A*, 631, 97
 Ferraro, F. R., 2009, *Nat*, 462, 483
 Forestini, M., Goriely, S., Jorissen, A., Arnould, M., 1992, *A&A*, 261, 157
 Fox, W., et al. 2024, *PhRvL*, 132, 2701
 Grasha, K., et al., 2019, *MNRAS*, 483, 4707
 Gavagnin, E., Mapelli, E., Lake, G., 2016, *MNRAS*, 461, 1276
 Geyer, M. P., Burkert, A., 2001, *MNRAS*, 323, 988
 Gieles, M., et al., 2025, *MNRAS*, 544, 483
 Gratton, R. G., Carretta, E., Bragaglia, A., 2012, *A&ARv*, 20, 50
 Gratton, R. G., et al., 2019, *ARA&A*, 27, 8
 Goudfrooij, P., 2018, *ApJ*, 857, 16
 Goudfrooij, P., et al., 2026, accepted by *MNRAS* (arXiv:2606.07751)
 Harris, J., Zaritsky, D., 2009, *AJ*, 138, 1243
 Harris, W. E., Pudritz, R. E., 1994, *ApJ*, 429, 177
 Henderson, L. E., Gerasimov, R., Kirby, E. N., 2025, *ApJ*, 992, L14
 Hills, J. G., 1980, 235, 986
 K. Hollyhead, K., et al., 2018, *MNRAS*, 476, 114
 Iliadis, C., et al. 2016, *ApJ*, 818, 98
 Kane, S. G., et al., 2026, *MNRAS*, 546, 2272
 Karakas, A. I., 2010, *MNRAS*, 403, 1413
 Karakas, A. I., Lattanzio, J. C., 2014, *PASA*, 31, 30
 Kawamura, A., et al., 2009, *ApJS*, 181, 1
 Kemp, A., et al., 2022, *MNRAS*, 509, 1175
 Kirby, E. N., Ji, A. P., Kovalev, M., 2023, *ApJ*, 958, 45
 Kobayashi, M. I. N., et al., 2017, *ApJ*, 836, 175
 Kastner, J. H., Myers, P. C., 1994, *ApJ*, 421, 605
 Kroupa, 2002, *Sci*, 295, 82
 Kruijssen, J. M. D., 2019, *MNRAS*, 486, L20
 Kruijssen, J. M. D., et al., 2019, *Nat*, 569, 519
 Lacchin, E., et al., 2022, *MNRAS*, 517, 1171
 Lacchin, E., et al., 2026, *A&A*, 708, 25
 Lahen, N., et al. 2025, *MNRAS*, 543, 1023
 Langer, G. E., Hoffman, R., Sneden, C., 1993, *PASP*, 105, 301
 Lardo, C., Pancino, E., Mucciarelli, A., Milone, A. P., 2012, *A&A* 548, 107
 Lardo, C., et al., 2022, *A&A*, 662, 117
 Lardo, C., Valcin, D., Jimenez, R., 2026, submitted to *A&A* (arXiv:2603.11814)
 Larsen, S. S., et al., 2016, *A&A*, 613, 56
 Lee, J.-W., 2015, *ApJS*, 219, 7
 Legnardi, M. V., et al. 2022, *MNRAS*, 413, 735
 Leitinger, E., et al. 2023, *MNRAS*, 520, 1456
 Li, C., et al. 2021, *ApJ*, 906, 133
 Lucatello, S., Sollima, A., Gratton, R., et al. 2015, *A&A*, 584, A52
 Lugaro, M., 2005, *Stardust from meteorites, Scientific Series in Astronomy and Astrophysics, Vol 9*, New Jersey, London, Singapore
 Lugaro, M., et al., 2004, *ApJ*, 615, 934
 Lugaro, M., et al., 2012, *ApJ*, 747, 2
 Lund, K., et al., 2009, *A&A*, 503, 545
 Maas, Z. G., Cescutti, G., Pilachowski, C. A., 2019, *AJ*, 878, 43
 Martell, S. L., Grebel, E. K., 2010, *A&A*, 519, 14
 Martocchia, S., et al., 2018, *MNRAS*, 473, 2688
 Masseron, T., 2020, *NatCO*, 11, 3759
 Matsui, H., et al., 2025, *PASJ*, 77, 370
 Marino, A. F. et al. 2011, *A&A*, 532, 8
 Marino, A. F. et al. 2015, *MNRAS*, 450, 815
 Mastrobuono-Battisti, A., Perets, H. B., 2021, *MNRAS*, 505, 2548
 Mastrobuono-Battisti, A., Perets, H. B., 2016, *ApJ*, 823, 61
 McKenzie, M., Bekki, K. 2018, *MNRAS*, 479, 3126
 McKenzie, M., Bekki, K. 2021, *MNRAS*, 500, 4578 (MB21a)
 McKenzie, M., Bekki, K. 2021, *MNRAS*, 507, 834 (MB21b)
 McKenzie, M., et al., 2022, *MNRAS*, 516, 3515
 McKenzie, M., et al., 2024, *MNRAS*, 527, 7940
 McKenzie, M., et al., 2026, submitted to *MNRAS* (MA26)
 McWilliam, A., Wallerstein, G., Mottini, M., 2013, *ApJ*, 778, 149
 Mészáros, S., et al. 2020, *MNRAS*, 492, 1641 (ME20)
 Milone, A. P., et al. 2013, *A&A*, 555, 143
 Milone, A. P., et al. 2017, *MNRAS*, 464, 3636
 Milone, A. P., et al., 2018, *MNRAS*, 481, 5098 (M18)
 Milone, A. P., Marino, A. F., 2022, *Univ*, 8, 359 (MM22)
 Monaco, L., Bonifacio, P., Sbordone, L., Villanova, S., & Pancino, E. 2010, *A&A*, 519, L3
 Monty, S., et al., 2024, 533, 2420
 Mucciarelli, A., Origlia, L., Ferraro, F. R., Pancino, E., 2009, *ApJ*, 695, L134
 Mucciarelli, A., et al., 2011, *MNRAS*, 412, 81
 Mowla, L., et al., 2024, *Nat*, 636, 332
 Nataf, D. M., et al. 2019, *AJ*, 158, 14
 Navarro, J. F., Frenk, C. S., White, S. D. M., 1996, *ApJ*, 462, 563 (NFW)
 Nguyen, M., Sills, A., 2024, *ApJ*, 969, 18
 Niederhofer, F., et al., 2017, *MNRAS*, 465, 4159
 Norris, J., Cottrell, P. L. 1979, *ApJ*, 229, L69
 Pancino, E., et al. 2010, *A&A*, 511, 19
 Pancino, E., et al. 2017, *A&A*, 601, 112
 Parker, R. J., Schoettler, C., 2023, *ApJ*, 952, L16
 Pasquini, L., et al., 2005, *A&A*, 441, 549
 Piotto G. et al. 2005, *ApJ*, 621, 777
 Parmentier, G., 2025, *ApJ*, 986, 14
 Pfeffer, J. et al., 2024, *MNRAS*, 529, 4914
 Prantzos, N., Charbonnel, C., 2006, *A&A*, 458, 135
 Ramirez, S. V., Cohen, J. G., 2002, *AJ*, 123, 3277
 Renzini, A., et al., 2015, *MNRAS*, 454, 4197
 Rizzuti, F., et al., 2025, *A&A*, 698, 118
 Roederer, I. U., 2011, *ApJ*, 732, L17
 Sackmann, I.-J., Boothroyd, Arnold I., 1992, *ApJL*, 392, 71
 Sakari, C. M., et al. 2016, *ApJ*, 829, 116
 Salpeter, E. E. 1955, *ApJ*, 121, 161
 Schiappacasse-Ulloa, J., et al. 2025, *A&A*, 699, 41
 Schiavon, R. P., 2007, *ApJS*, 171, 146
 Shen, Z.-X., Bonifacio, P., Pasquini, L., Zaggia, S., 2010, *A&A*, 524, L2
 Shingles, L. J., et al., 2014, *ApJ*, 795, 34
 Smith, V. V., et al., 2005, *ApJ*, 633, 392
 Sneden, C., Kraft, R. P., Shetrone, M. D., Smith, G. H.,

Langer, G. E., & Prosser, C. F. 1997, *AJ*, 114, 1964
 Sobek et al. 2011, *AJ*, 141, 175
 Spite, M., et al., 2022, *A&A*, 667, 139
 Schiavon, R. P., 2007, *ApJS*, 171, 146
 Strader, J., et al., 2013, *ApJ*, 775, L6
 Straniero, O., et al., 2014, *ApJ*, 785, 77
 Suntzeff, N. B., 1981, *ApJS*, 47, 1
 Tarumi, Y., Yoshida, N., Inoue, S., 2021, *ApJ*, 921, L11,
 Thygesen, A. O., et al., 2016, *A&A*, 588, 66
 Trigo-Rodriguez, J. M., et al. 2009, *M&PS*, 44, 627
 Truman, T., et al, 2026, submitted to *MNRAS*
 Vanbeveren, D., et al., 2012, *A&A*, 543, 4
 Vanzella, E., et al., 2022, *A&A*, 659, 2
 Ventura, P., D'Antona, F., 2009, *A&A*, 499, 835
 Ventura, P., Carini, R., D'Antona, F., 2011, *MNRAS*, 415, 3865
 Ventura, P., et al., 2012, *ApJ*, 76, L30 (V12)
 Ventura, P., et al., 2013, *A&A*, 431, 3642 (V13)
 Ventura, P., et al. 2016, 831, L17
 Ventura, P., et al. 2018, *MNRAS*, 477, 438
 Vesperini, E., et al., 2011, *MNRAS*, 416, 355
 Vesperini, E., et al., 2013, *MNRAS*, 429, 1913
 Vesperini, E., et al., 2021, *MNRAS*, 502, 4290
 Villanova, S., Geisler, D., 2011, *A&A*, 535, 31
 Wasserburg, G. J., et al. 2006, *NuPhA*, 777, 5
 Webb, J. J., Leigh, N. W. C., 2015, *MNRAS*, 453, 327
 Weidemann, V., 2000, *A&A*, 363, 647
 Weidner, C., Kroupa, P., 2005, *ApJ*, 625, 754
 Wirth, H., et al., 2021, *MNRAS*, 506, 4131
 Worley, C. C., Hill, V., Sobek, J., & Carretta, E. 2013, *A&A*, 553, 47
 Yaghoobi, A., et al., 2022, *MNRAS*, 510, 4330
 Yong, D., et al., 2003, *A&A*, 402, 985
 Yong, D., et al., 2008, *ApJ*, 689, 1020
 Yong, D., Grundahl, F., D'Antona, F., Karakas, A. I., Lattanzio, J. C., Norris, J. E., 2009, *ApJ*, 695, L62
 Yong, D., et al., 2014, *MNRAS*, 441, 3396
 Yong, D., Grundahl, F., 2018, *ApJ*, 672, L29
 Zapartas, E., et al., 2017 *A&A*, 601, 29
 Zullo, G., et al. 2026, *A&A*, 709, 212

APPENDIX A: FRACTIONS OF AGB STARS WITHIN AND AROUND GMCs

The mass ratios of AGB stars within and around GMCs to total GMC masses (R_s) is a crucial parameter for GC formation with MPs in the SCI scenario. Although simple analytical models can be used to estimate R_s , as done in this study, numerical simulations of galaxy evolution with H_2 formation on dust grains and new star formation within GMCs enable us to more accurately estimate R_s in galaxies of different masses and various types. Using our original hydrodynamical simulations with H_2 formation on dust grains, dust and metal enrichment, and star formation (Bekki 2015, 2025), we here investigate how R_s depends on M_{gmc} in simulated galaxies. To do so, we first identify GMCs in each simulated galaxy at each time step, and then investigate M_{gmc} and the total mass of intermediate-mass stars (M_{ns}) with $4 \leq m/M_\odot \leq 10$ and ages ranging from 0.02 to 0.1 Gyr within $2R_{\text{gmc}}$ from the center of each GMC, where R_{gmc} is the size of the GMC. Since the total mass of young

intermediate-mass stars can be a good proxy for M_{agb} , we investigate R_s for each GMC in simulated galaxies.

The total masses of dark matter, stars, and gas in an initial gas-rich dwarf disk galaxy are denoted as $M_{\text{gal,dm}}$, $M_{\text{gal,s}}$, and $M_{\text{gal,g}}$, respectively. The density profile of the dark matter halo is represented by the NFW model with a central concentration of 12.0. The stellar and gaseous disks are assumed to have exponential profiles, with the size being $R_{\text{gal,d}}$ for both components. The disk galaxy is assumed to have an initial gaseous metallicity of $[\text{Fe}/\text{H}]=-1.6$ and no radial gradient of $[\text{Fe}/\text{H}]$. The standard (fixed) Kroupa IMF with the three IMF slopes, α_1 , α_2 , and α_3 being 1.3, 2.3, and 2.3, respectively, is adopted in estimating the total mass of intermediate-mass stars from the mass of each new stellar particle. The size-mass relation of GMCs ($R_{\text{gmc}} \propto M_{\text{gmc}}^{0.5}$) adopted by Bekki & Mackey (2009) is also used in selecting intermediate-mass stars around each GMC. It should be stressed here that M_{ns} is a value estimated at a given time step (i.e., an instantaneous value), whereas M_{agb} is the total mass of AGB stars that have interacted with a GMC over the GMC's lifetime (i.e., an integrated value). Therefore, M_{agb} is not exactly the same as M_{ns} .

We mainly describe the results of the model in which $M_{\text{gal,dm}} = 10^{10}M_\odot$, $M_{\text{gal,s}} = 1 \times 10^8M_\odot$, $M_{\text{gal,g}} = 9 \times 10^8M_\odot$, $c = 12$, and $R_{\text{gal,d}} = 1$ kpc, and where the gas mass and size resolutions are $100M_\odot$ and 3 pc, respectively. M_{gmc} and M_{ns} are estimated for each GMC at 6 selected time steps. Fig. A1 shows the time evolution of the projected gas density in this gas-rich dwarf disk model for 0.1 Gyr. Clearly, multiple high-density gaseous clumps are formed within the gas disk, where massive star clusters can form from the clumps.

Fig. A2 describes how $R_s = M_{\text{ns}}/M_{\text{gmc}}$ depends on M_{gmc} in this model, in which many GMCs are identified at the selected time steps. Here, R_s can be used to estimate the total mass of AGB stars that can contribute to the chemical enrichment of GMCs (see the main text for details). Clearly, R_s is systematically higher in GMCs with larger M_{gmc} , though the dispersion in R_s at a given M_{gmc} is not small. This result can thus justify the adopted positive $M_{\text{gmc}}-R_s$ correlation in the SCI scenario (see Eqn. (22) in the main text). It should be stressed here, however, that the slope of the $M_{\text{gmc}}-R_s$ correlation depends on the model parameters of the simulations. For example, the slope becomes flatter in models with lower initial mean gas densities (e.g., due to lower gas mass fractions). This means that the coefficients a_s and b_s in Eqn. (22) could be different in different galaxies. Also, R_s becomes rather small (< 0.01) in models with larger gas disk sizes due to lower gas densities, which means GCs cannot have MPs. We will extensively discuss how R_s depends on model parameters for gaseous disks in dwarf galaxies in our forthcoming works based on numerical simulations of dwarf galaxies.

APPENDIX B: RELATIONS BETWEEN F_{DIL} , F_{1P} , AND $\delta_{\text{MAX}Y}$

Using an idealized dilution model for AGB ejecta, we can investigate how the dilution factors (F_{dil}) determine the fractions of 1P stars (F_{1P}), the differences between minimum and maximum Y ($\delta_{\text{max}Y}$), and those between minimum and

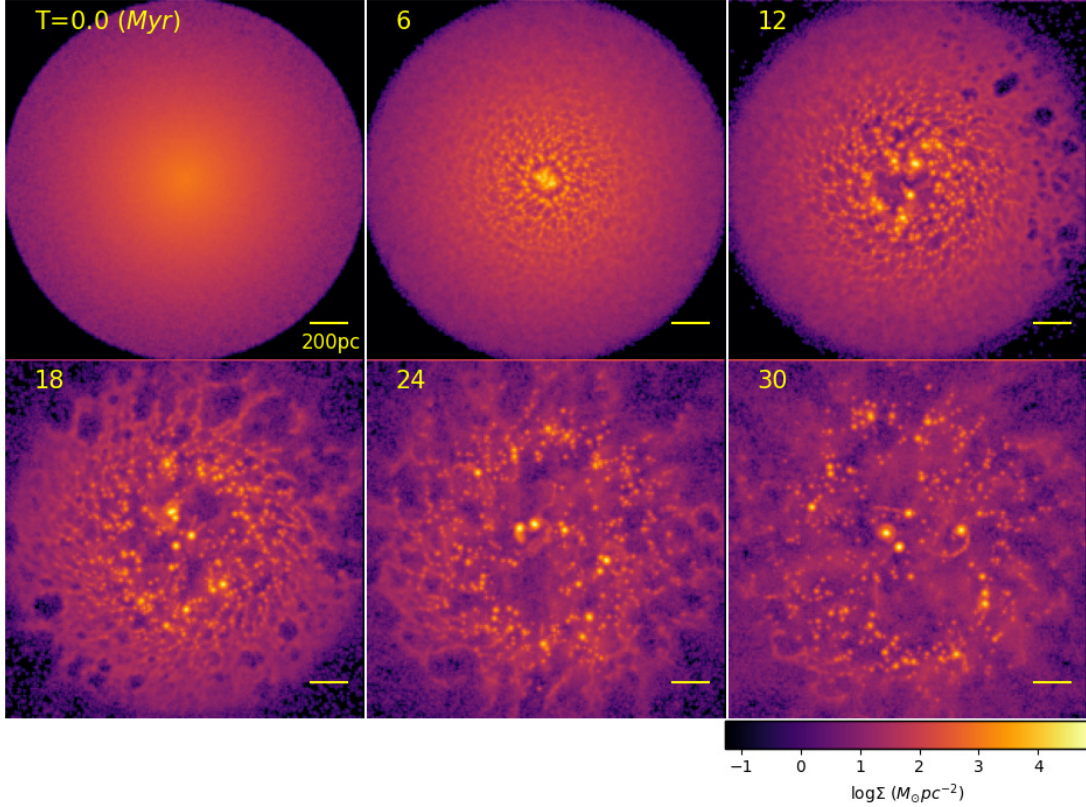


Figure A1. Time evolution of the surface gas densities (Σ_g) projected onto the x - y plane for a gas-rich compact dwarf galaxy model in which massive GMCs can be formed during the evolution of the gas disk. The time T that has elapsed since the start of this simulation is shown in the upper left corner at each panel, and the bar in the lower right corner measures 200 pc.

maximum $[\text{Na}/\text{Fe}]$ ($\delta_{\text{max}}[\text{Na}/\text{Fe}] = [\text{Na}/\text{Fe}]_{\text{max}} - [\text{Na}/\text{Fe}]_{\text{min}}$) in GCs. Here we assume that (i) the initial total mass of pristine GMC gas to be mixed with AGB ejecta is M_g , (ii) the total mass of AGB ejecta within a GC-forming GMC ($M_{\text{ej}}(t)$) increases steadily with time, and (iii) the mixed gas is converted into new stars with the star formation efficiency of ϵ_{sf} . We consider that the increase rate of $M_{\text{ej}}(t)$ is simply fixed at $M_{\text{ej},t}/T_{\text{sf}}$, where $M_{\text{ej},t}$ is the total mass of AGB ejecta and T_{sf} is the duration of star formation in GMCs: $M_{\text{ej}}(t) = M_{\text{ej},t}/T_{\text{sf}}$. Therefore, the total mass of new stars formed from the mixed gas (M_{ns}) at each time step is as follows:

$$M_{\text{ns}}(t) = \epsilon_{\text{sf}}(M_g + M_{\text{ej}}(t)). \quad (\text{B1})$$

At each time step in each model, we calculate the total mass, Y , and $[\text{Na}/\text{Fe}]$ of new stars. We run the models with $0 < F_{\text{dil}} < 1$ in order to find the correlations of $F_{1\text{P}}$, $\delta_{\text{max}}Y$, and $\delta_{\text{max}}[\text{Na}/\text{Fe}]$ with F_{dil} . Following C09, we consider that stars with $[\text{Na}/\text{Fe}]$ less than $[\text{Na}/\text{Fe}]_{\text{min}} + 0.3$ are classified as 1P.

Fig. B1 clearly demonstrates that F_{dil} is a crucial parameter that determines $F_{1\text{P}}$ for $\epsilon_{\text{sf}} = 0.03$. As expected, $F_{1\text{P}}$ is larger for larger F_{dil} , because most of new stars formed from AGB ejecta mixed with pristine GMC gas have lower $[\text{Na}/\text{Fe}]$ to be classified as 1P. It is also found that both $\delta_{\text{max}}Y$ and $\delta_{\text{max}}[\text{Na}/\text{Fe}]$ are larger for smaller F_{dil} . Fig. A2

shows that $\delta_{\text{max}}Y$ is larger for smaller F_{dil} , because the later formed 2P stars can have larger Y in the models with smaller F_{dil} . These clear correlations and anticorrelations of $F_{1\text{P}}$ and $\delta_{\text{max}}Y$ with F_{dil} can be used to discuss how the total masses of GMCs, which determine F_{dil} , can influence $F_{1\text{P}}$ and $\delta_{\text{max}}Y$ in the SCI scenario. These results also justify the adopted relation between F_{dil} and $F_{1\text{P}}$ in the preset models (see §2).

APPENDIX C: POSSIBLE CORRELATIONS OF $F_{2\text{P}}$ WITH AGES AND METALLICITIES OF GCS

The SCI scenario predicts that $F_{2\text{P}}$ can be larger in GCs forming in galaxies with larger ρ_{agb} (and thus larger Σ_{SFR}). Therefore, if Σ_{SFR} is larger for galaxies with older ages and lower metallicities, then the observed relations of $F_{2\text{P}}$ with ages and metallicities (ME20) can be qualitatively explained by the scenario. In order to briefly discuss whether $F_{2\text{P}}$ can depend on the ages and metallicities of GCs, we here investigate how Σ_{SFR} depends on the ages and metallicities of GC-forming galaxies by using our one-zone chemical evolution models of galaxies (BT12). We adopt the ‘‘wind model’’ of BT12, in which gas can be ejected from galaxies by supernova feedback effects through galactic winds, and about

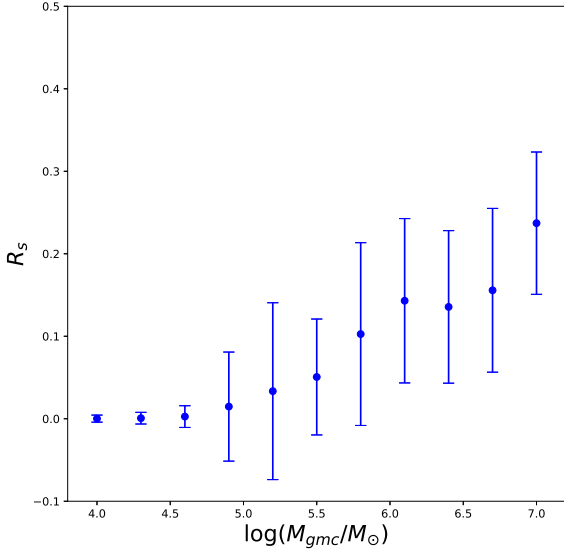


Figure A2. R_s ($M_{\text{ns}}/M_{\text{gmc}}$) as a function of M_{gmc} in the selected five models. The error bar indicates the 1σ dispersion of R_s in each M_{gmc} bin. This plot is based on R_s for GMCs selected from the models at different time steps.

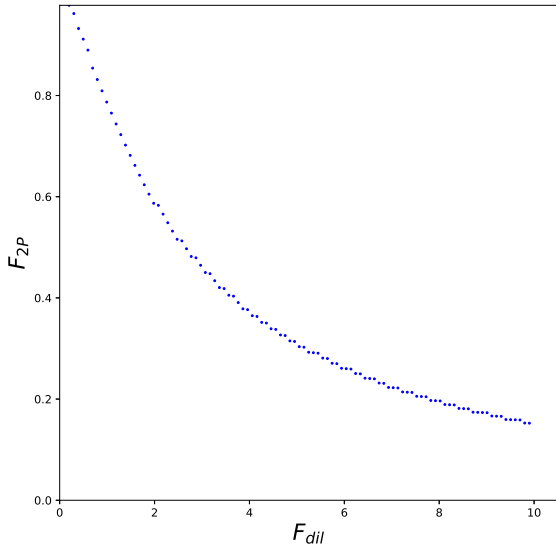


Figure B1. F_{2P} as a function of F_{dil} in a simple one-zone model of chemical enrichment in GC formation. Data points at different 100 time steps are plotted in this figure. The anticorrelation between F_{dil} and F_{2P} is a universal trend in the adopted one-zone models, which enables this study to develop a mathematical formula for $F_{\text{dil}}-F_{2P}$ relations adopted in the models for the observed $M_{\text{gc}}-F_{1P}$ relation (see the main text).

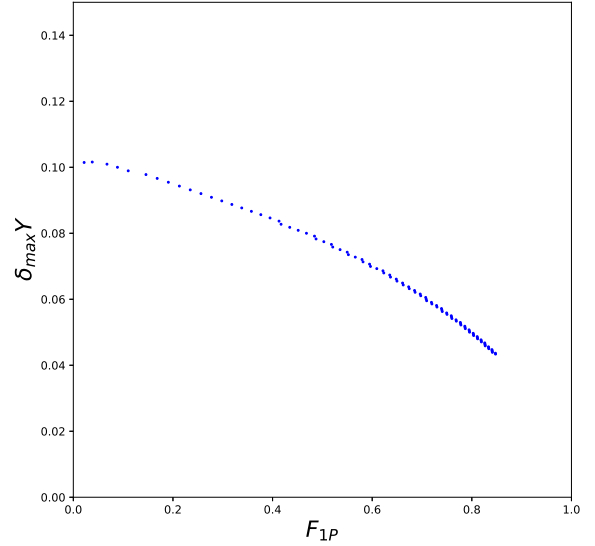


Figure B2. Differences in Y between new stars with minimum and maximum Y ($\delta_{\text{max}}Y$) as a function of F_{1P} in the one-zone chemical enrichment model for GCs with MPs. This $F_{1P}-\delta_{\text{max}}Y$ relation is expected, because F_{1P} and $\delta_{\text{max}}Y$ correlates and anticorrelated with F_{dil} , respectively.

30% of the gas can be expelled from galaxies: the details of the wind model are given in B12. We assume that (i) the initial $[\text{Fe}/\text{H}]$ of the gas is -4, (ii) the gas infall time scale (τ_{inf}) is a free parameter, and (iii) the half-mass radius of a gas-rich dwarf galaxy, R_{h} , is 200 pc. We investigate the time evolution of the SFR, $[\text{Fe}/\text{H}]$, and Σ_{SFR} over 3 Gyr (from $T = 0$ to 3 Gyr) in models with different τ_{inf} in which the final stellar masses are $[3-6] \times 10^8 M_{\odot}$, corresponding to gas-rich dwarf galaxies.

Fig. C1 describes how Σ_{SFR} evolves with $[\text{Fe}/\text{H}]$ in the model with $\tau_{\text{inf}} = 10^8$ yr. As the total gas mass increases with time through gas infall, both $[\text{Fe}/\text{H}]$ and Σ_{SFR} increase with time, which results in a positive correlation between Σ_{SFR} and $[\text{Fe}/\text{H}]$. Then Σ_{SFR} reaches its peak at $[\text{Fe}/\text{H}] \approx -2.1$, when the total gas mass starts to decrease due to gas consumption by star formation. After its peak, Σ_{SFR} decreases with increasing $[\text{Fe}/\text{H}]$ almost linearly. Since a lower Σ_{SFR} means a lower F_{2P} , this result implies that F_{2P} can be lower for higher $[\text{Fe}/\text{H}]$ in GCs with $[\text{Fe}/\text{H}] > -2.1$. It is confirmed that this anticorrelation between $[\text{Fe}/\text{H}]$ and Σ_{SFR} can be seen in other models with different τ_{inf} , though the $[\text{Fe}/\text{H}]$ values at the Σ_{SFR} peak are different between these models.

Fig. C2 shows the time (T) evolution of Σ_{SFR} in the model with $\tau_{\text{inf}} = 10^8$ yr. After reaching its peak at $T = 0.3$ Gyr, Σ_{SFR} starts to decrease with increasing T . This means that there should be a positive correlation between ages and F_{2P} of GCs formed after $T \approx 0.2$ Gyr in this model. It is also clear that this age- F_{2P} correlation after the Σ_{SFR} peak can be seen in other models with different τ_{inf} . These results imply that younger GCs are likely to have smaller F_{2P} , because F_{2P} can correlate with Σ_{SFR} . It is possible that GCs cannot be formed due to much smaller gas masses and densities in

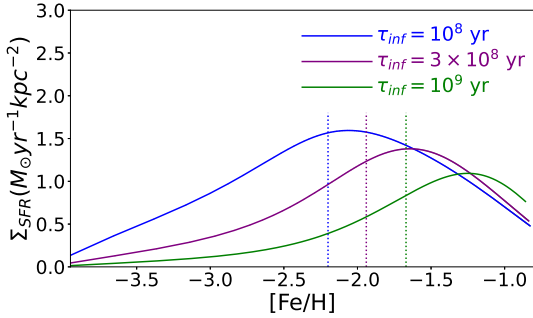


Figure C1. Σ_{SFR} as a function of $[\text{Fe}/\text{H}]$ in one-zone chemical evolution models for a gas-rich dwarf with $\tau_{\text{inf}} = 10^8$ yr (blue), $\tau_{\text{inf}} = 3 \times 10^8$ yr (purple), and 10^9 yr (green). A fixed half-mass radius (200pc) is assumed to calculate Σ_{SFR} at different time steps in these models. The vertical dotted line for each model indicates $[\text{Fe}/\text{H}]$ when the total mass of new stars (M_{ns}) becomes $3 \times 10^7 M_{\odot}$. The result for the dwarf model with $\tau_{\text{inf}} = 10^8$ yr accordingly implies that if GCs are formed only after $M_{\text{ns}} \geq 3 \times 10^7 M_{\odot}$, then the GCs with higher $[\text{Fe}/\text{H}]$ can have lower $F_{2\text{P}}$ due to lower Σ_{SFR} . These results of the adopted idealized models can be used in the physical interpretations of the observed relation between $[\text{Fe}/\text{H}]$ and $F_{2\text{P}}$ and by ME20.

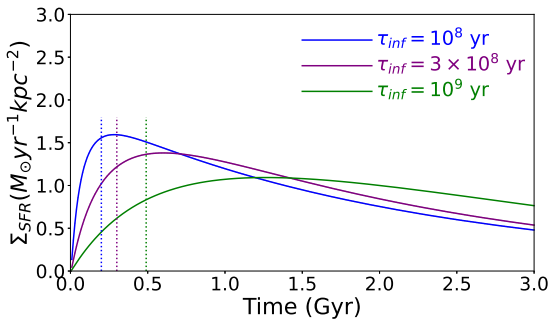


Figure C2. Σ_{SFR} as a function of time (T) in the same models as adopted in Fig. C1. The vertical dotted line for each model indicates T when the total mass of new stars becomes $3 \times 10^7 M_{\odot}$. These results can be used in discussing the observed relation between ages of GCs and $F_{2\text{P}}$ (ME20). For example, if GCs can be formed only after $T = 0.2$ Gyr in dwarfs with $\tau_{\text{inf}} \approx 10^8$ yr, the GCs with older ages are likely to have higher $F_{2\text{P}}$.

the very early phases of galaxy formation before Σ_{SFR} peaks. Although we adopt idealized one-zone models in these discussions, the models can grasp some essential ingredients of the physical processes that can possibly determine $F_{2\text{P}}$ in GC formation within galaxies. It is doubtlessly our future work to investigate the origins of the possible correlation and anticorrelation of $F_{2\text{P}}$ with the ages and metallicities of GCs using more sophisticated models of GC formation, ideally numerical simulations of GCs within high- z galaxies.

APPENDIX D: A SWEET SPOT FOR CHEMICAL ENRICHMENT BY MASSIVE AGB STARS

In the SCI scenario, only massive AGB stars ($4 \leq m_{\text{agb}}/M_{\odot} \leq 10$) must chemically pollute pristine gas to form MPs that exhibit correlations and anticorrelations (e.g., O-Na) between various elements. This implies that GCs with MPs cannot form during the later phases of galaxy formation, when low-mass AGB stars—which outnumber high-mass ones—begin to pollute GMCs. Therefore, the present study predicts a “sweet spot” where only massive AGB stars pollute GMCs within their host dwarf galaxies. Using the one-zone chemical evolution models adopted by BT12, we investigate the total mass of stars (M_{T0}) that have just left the main sequence at a given time step (T) as a function of the turn-off mass (m_{T0}) in our galaxy models.

Fig. D1 shows M_{T0} as a function of m_{T0} in models with $C_{\text{SF}} = 0.1$ for IMF slopes of $\alpha = 2.35$ (Salpeter) and 1.5 (top-heavy) at $T = 100, 300,$ and 800 Myr. Here, M_{T0} is normalized to the total mass of infalling gas (which is set to unity) in each model, and M_{T0} is calculated every Myr. Obviously, m_{T0} decreases as T increases, meaning that stars with lower masses can chemically enrich GMCs during later phases of galaxy evolution.

Although GMCs are polluted exclusively by massive AGB stars ($m_{\text{agb}} \geq 4.5 M_{\odot}$) at $T = 100$ Myr, they can be polluted by all AGB stars with $m_{\text{agb}} \geq 3 M_{\odot}$ at $T = 300$ Myr. At $T = 800$ Myr, the dominant stellar population polluting GMCs consists of $m_{\text{agb}} \approx 2 M_{\odot}$ AGB stars. This implies that 2P stars formed in these GMCs would have enhanced C+N+O abundances, which is a feature not observed in most 2P stars. These results suggest that GCs with MPs can form well before $T = 800$ Myr in steadily star-forming galaxies. Since AGB stars with low m_{agb} begin to pollute GMCs after $T = 800$ Myr, it is unlikely that GCs with MPs can form ≈ 800 Myr after the onset of star formation in steadily star-forming galaxies.

These results are independent of α across all six models. However, models with a top-heavy IMF yield a larger M_{T0} for massive AGB stars, implying that GMCs can be more heavily polluted by massive AGB stars, ultimately leading to a larger $F_{2\text{P}}$. If a secondary starburst occurs a few to several Gyr after the onset of star formation in a galaxy, a sharp peak in M_{T0} could emerge around $m_{\text{T0}} \approx 5 M_{\odot}$ tens of Myr after the starburst. Depending on the strength of this starburst, massive SCs formed during the event could potentially host MPs.

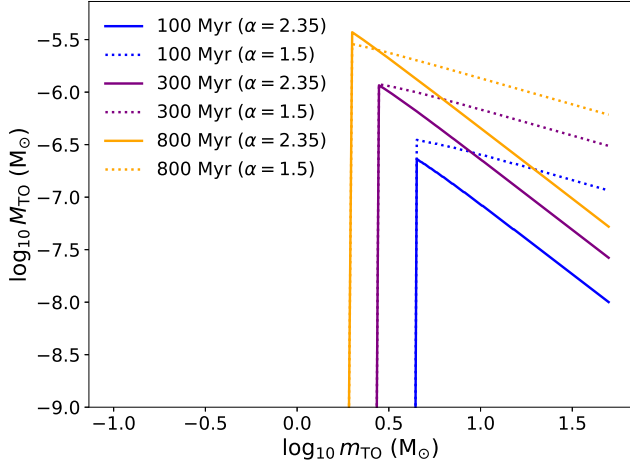


Figure D1. M_{TO} as a function of the turn-off mass (m_{TO}) at $T = 100$ Myr (blue), 300 Myr (purple), and 800 Myr (orange) for the six models with $\alpha = 2.35$ (solid lines) and 1.5 (dotted lines). The total mass of stars that have just left the main sequence (M_{TO}) at a given time step is calculated every Myr in these models.